BTR-103

GENERIC CHANNEL SIMULATOR

Phillip A. Bello

Prepared under Contract MDA904-95-C-2078

Reporting Period: 10 February 1995 - 10 February 1997

BELLO, Inc. 80 Gary Rd. Needham, MA 02194

781-433-0846. pbello@ieee.org

ABSTRACT

This document is the final report under Contract MDA904-95-C-2078. It provides the mathematical channel models and associated ranges of parameters for the most recent radio communication channels implemented by the Generic Channel Simulator (GCS). Specific default scenarios for parameters are provided. The channels examined in this report are: Cellular/PCS Handset-BaseStation (including Indoor and Outdoor channels), VHF/UHF Mobile-Mobile, VHF/UHF Mobile-BaseStation, VHF/UHF Air-Air, VHF/UHF Air-Ground, and Land Mobile Satellite. In addition, special attention is given to channel models characterizing slow fading over the detection interval and/or small amounts of frequency selective distortion over the receiver bandwidth. All these models may be used for analytical evaluation of LPI detection and communication performance. They may also be used as the basis for software and hardware channel simulations and the development of standards for comparative modem performance evaluation. This report includes a summary of the structure of the Generic Channel Simulator. An appendix presents scenarios for the Wideband HF channel including parameters for propagation, atmospheric noise, and narrowband interference.

Acknowledgment

The interest and encouragement of Douglas Rahikka, Dr. Richard Dean, and David Dudich are hereby acknowledged. Their foresight in supporting this effort will accelerate the use of the NSA LPI/D Evaluation Standards and the improvement of existing standards for wireless communications in general.

TABLE OF CONTENTS

1 INTRODUCTION

This report details the work performed by BELLO, Inc. under Contract MDA904-95-C-2078 during the period from 10 February, 1995 to 10 February, 1997. The research and development effort under this contract is divided into two main tasks. The first task was to develop and deliver Appendix B of the NSA LPI/D Evaluation Standard. This Appendix has been provided as a separate document (BELLO, Inc. Technical Report BTR-104).

The second task was to expand the capabilities of the Generic Channel Simulation (GCS) software and obtain the parametric driving tables required to simulate the channels discussed in Section 1.2. Lincoln Laboratory under a separate contract has carried out actual software development and required modifications of the GCS[1]. BELLO, INC has provided the specifications of algorithms and technical direction.

1.1 Background

The NSA LPI/D Evaluation Standard proposes a layered approach for evaluation, using analysis, simulation, and testing under sequentially more complicated and realistic conditions. An integral part of this standard is the specification of representative and repeatable radio channel conditions for performance evaluation. The primary purpose of Appendix B of the LPI/D Evaluation Standard is to provide the user with the necessary mathematical /statistical radio channel models and associated ranges of parameters required to carry out test procedures in the Evaluation Standard. Also, since an integral part of the evaluation procedure is the use of channel simulators, the GCS software being developed is of direct relevance.

[1] C.M.Keller, Generic Channel Simulator Software, MIT Lincoln Lab. Project Memo 44PM-AST-0046, 7 June 1996.

The GCS is an outgrowth of HF Ionospheric modeling and simulation work carried out under Contract DAAB07-93-C-N651. A prior report[2] documents the basis for the HF channel models developed. The tapped delay line and associated statistical models employed were of a generic nature and it was found that much of the software could be employed directly or modified to model other radio channels, particularly the mobile cellular and non-cellular channels in the higher frequency bands.

Thus under Contract DAAB07-94-C-H601 modifications and additions were made to allow the simulation of macrocell and microcell channels[3]. A subset of the software developed has been adopted as a commercial standard by the JTC[4] for testing of PCS/Cellular modems. In addition to the JTC model, a more realistic channel model, called the Mixed Model, was developed. Work under the current contract has made the channel simulations developed in the previous contract more versatile and has increased the types of channels simulated.

There are three broad classes of channel phenomena of interest: path loss, distortion produced by the propagation channel, and additive disturbances. It is intended that the GCS represent each of these phenomena. Thus the work carried out in the original contract (DAAB07-93-C-N651) provided simulations for HF narrowband interference and atmospheric noise. Path loss formulae were not programmed for the HF channel and need to be included at a future date.

Extensive treatment of path loss was provided for the VHF/UHF to PCS/Cellular bands, including propagation loss models for urban environments, in the previous contract (DAAB07-94-C-H601). However, simulation of additive disturbances in these

---

[2] P.A. Bello, Wideband HF Propagation, Narrowband Interference, and Atmospheric Noise Models for Link Perfomance Evaluation, MITRE Technical Report MT 93B0000086, July 1993.

[3] P.A.Bello, C.A.Nissen, andJ.J. Blanchard, Generic Channel Simulator, Draft Final Report on Project 8632L,Mitre Corp., September 30, 1994

[4] The JTC is a cooperative effort between committee T1 (actually technical subcommittee T1P1) sponsored by the Alliance for Telecommunication Industry Solutions (ATIS) and the Telecommunication Industry Association (TR46).

bands was not considered. The current contract partially remedies this omission by including a simulation of automobile ignition noise. At some future date the additive disturbance simulation should be expanded to include other-user interference.

1.2 Summary

In evaluating the performance of detection systems for radio channels, it is useful to define certain limiting conditions on time and frequency selectivity. The initial sections of this report present simplifications of these channel models that apply when there is *slow fading* over the signal observation interval T, or when there is *small distortion* due to frequency selective fading over the signal bandwidth W, or when both slow fading and small distortion are present. The definitions of slow fading and small distortion are made specific. These simplifications frequently allow a more tractable analytical evaluation of LPI/D modem performance.

When the slow fading condition applies a simplified model called the *Quadratic Time Selective Power Series* or just *Quadratically Time Selective Channel Model* can be used. Such a model may be represented by the weighted sum of the outputs of three parallel random time invariant filters in which the three time-variant weights are $\{1, (j2\pi t), (j2\pi t)^2\}$, where t is the time variable. When the small distortion condition applies, a simplified model called the *Quadratic Frequency Selective Power Series* or just *Quadratic Frequency Selective Channel Model* can be used. Such a model may be represented by the weighted sum of the input and the first two derivatives of the input signal in which the three weights are time variant, generally random processes.

When both the slow fading and small distortion conditions apply a combination of the two models results in which the channel is represented by 9 time-invariant complex coefficients. The resulting model is called the *Quadratic Selective ft-Power-Series Channel Model*.

Two additional conditions, *many fade times* (over T) and *many fade frequencies* (over W) are introduced. When one or both of these conditions apply, analytical evaluation of signal detection performance can frequently be simplified by approximating detector decision variables with either normally distributed random variables or variables that are simply related to normally distributed variables.

The following four sets of inequalities define the special channel conditions:

1) $BT \leq 1$, the *slow fading* condition is valid

2) $BT \geq 10$, the *many fade times* condition is valid

3) $WL \leq 1$, the *small distortion* condition is valid

4) $WL \geq 10$, the *many fade frequencies* condition is valid

where B is the total Doppler spread of the channel and L is the total multipath spread of the channel.

Section 2 defines what is meant by limited time and frequency selectivity and presents a brief review of some canonical input-output relations for time variant channels needed to develop the channel models presented in this report. Section 3 presents the covariance functions for the system functions of interest assuming the wide sense stationary uncorrelated scattering (WSSUS) channel [1] model which is used extensively in the modeling work presented in this report. These covariance functions lead to a complete statistical description of the WSSUS channel in general and the limited time and frequency selective fading models in particular, when complex Gaussian statistics are assumed for the system functions. Sections 4,5, and 6 present the three canonical models mentioned above that apply to restricted time and frequency selective fading conditions.

In Section 7 we consider channel models and parameters for the Cellular/PCS Handset-BaseStation Channels. The first class of channel models examined (Section 7.1) is the simplified channel model standards proposed by the JTC. The generic model used is a *Discrete Complex Gaussian Factorable WSSUS channel*. Such a model consists of a finite set of independently fluctuating paths with complex Gaussian statistics and the

same Doppler Power Spectrum for the fading of each path. Given the Doppler spectrum, the channel is completely determined statistically by specifying the delays and strengths of the paths. The JTC standards involve a specification of these path delays and strengths for different environments. Section 7.1 includes the parameters for the limited time and frequency selective fading models corresponding to the JTC standard models.

A more accurate class of channel models is presented in Section 7.2, called the M*ixed Discrete/Scatter* or simply the *Mixed Model*. The JTC models were constructed with a primary emphasis on simplicity, and a secondary emphasis on matching channel measurements. The Mixed model is used to achieve a higher level of realism with a modest increase in complexity. A review of the measured multipath characteristics and the references mentioned therein, reveals a common pattern: the impulse responses for urban paths consist of a mixture of unresolved paths plus discrete resolved paths with the latter caused by reflections from large objects. The unresolved paths arrive early due to reflections in the vicinity of the mobile antenna. Sometimes there is a later group of weaker unresolved paths due to a very strong reflector that is visible from the base antenna but not visible to the mobile antenna. Usually, however, there is only one unresolved group of paths. The number of strong discrete paths is usually not large, and some may be delayed considerably. This mixed continuous discrete structure can exist with or without a significant direct path, depending upon the geometry.

To represent the observed behavior of the impulse responses, separate models are adopted for each unresolved group of paths and for the discrete paths. The *Discrete Non-Fading Paths Model* is used to represent the discrete paths. Such a model consists of a set or random phased and Doppler shifted paths with fixed amplitudes.

We call each unresolved group of paths a "scatter" path, or scatter propagation mode. Assuming a large number of unresolved paths and utilizing the Central Limit Theorem, a scatter path can be modeled in the short term as a Complex Gaussian WSSUS channel. As in the JTC models, in the interests of simplicity, and, it is felt, no loss in utility for the LPI/D Evaluation Standard purposes, a factorable Delay Doppler Scatter Function is proposed. With such a model the Doppler Spectrum associated with fading at different path delays is the same. The scatter path is realized with a uniformly tapped delay line with taps spaced closer than the bandwidth of the input signal.

Generally speaking, the observed Mixed Model behavior exists for both the elevated base antennas of macrocellular channels and for the low base antennas of microcellular channels, with the primary difference being in the delay spread of the scatter path which is considerably smaller for the microcellular channel. The literature on both macro and microcellular channel measurements is reviewed to obtain ranges of measured parameters for the Mixed Model representation of the macro and microcellular channels. In addition parameters are derived from the Mixed Model channel parameters to represent the corresponding limited time and frequency selective fading channel models.

Section 8 and 9 present models and parameters appropriate to the communications between two airborne platforms or between an airborne platform and ground, respectively. Due to the paucity of appropriate experimental results, the results presented are based in part upon theoretical models of reflection and scattering from surfaces having two dimensional Gaussian statistics.

Generally speaking, the VHF/UHF Air-Air and Air-Ground Channel in the 100-500 MHz band may represented by a Mixed Model. Specifically, over water, there are two discrete paths: a direct LOS path from the transmitting to receiving platform, and a possible specular reflection path. In addition there is a possible scatter path due to scatter from surface irregularities. Over land it is possible to have tilted, relatively flat surfaces, that can produce more than one specular reflection. As will be quantified, for the theoretical model, the relative strengths of the specular and scatter paths depend upon the statistics of the surface irregularities and the operating frequency, and the combined strengths of the specular and scatter paths relative to the direct path depends upon the antenna patterns and the surface reflection coefficient.

An extensive literature search was conducted to find models and experimental data for overland communications. Unfortunately, only a single reference was found containing Air-Air channel measurements over land (and sea) and these were at 1 GHz. Two references were found for Air-Ground channel measurements and these were at 1 GHz and above. Consequently it was necessary to use the theoretical model even though it is more appropriate for a sea surface than a land surface. The available overland Air-Air and Air-Ground measurements were used to obtain parameters for the overland channel.

The physical aspects of the VHF/UHF Mobile channels discussed in Section 10 are similar to those of the cellular/PCS channels discussed in Section 7 . Both of these channels partition into two classes: those in which one of the terminals is at the ground mobile level and the other is elevated above the roof line and those in which both terminals are at the ground mobile level. From a channel modeling viewpoint, the lower operating frequency band and the mobility of both ground terminals distinguish the VHF/UHF Mobile channels from the cellular/PCS channels. Unfortunately there exist no measurement campaigns dedicated to estimating the multipath characteristics of the VHF/UHF Mobile channel as there were for the Cellular/PCS channels.

While propagation effects do vary with operating frequency, the multipath delays are strongly affected by the physical location of reflecting and scattering objects. Moreover, there are considerable variations in observed multipath delay profiles at a *fixed* operating frequency as the location of terminals changes within urban and suburban environments. Thus we assume that the multipath spreads and structures observed for Cellular/PCS channels may be used for the VHF/UHF channels. While the absence of measurements force us to use the Cellular/PCS channel multipath models and parameters for the VHF/UHF Mobile channel, we do not believe that gross errors will be committed thereby. Consequently the Mixed Model is used for the VHF/UHF Mobile channels also but with an adjustment of Doppler spread and shifts appropriate to the lower frequency band. In addition, in the case of Mobile-Mobile channels we consider the possible effect of having both terminals mobile on the shape of the Doppler power spectrum. A theoretical Doppler spectrum appropriate to two moving terminals is derived.

The VHF/UHF mobile communicator must operate in an environment containing additive electromagnetic (EM) disturbances. The EM disturbances arise from a variety of sources. For purposes of classification and identification**,** it can be subdivided in a number of ways. A particularly simple and important distinction is that between natural and man made disturbances. It is generally agreed that the disturbances dominating the performance of UHF/VHF mobile communication systems do not arise from natural causes. Hence, we have concentrated entirely on man-made disturbances.

Man-made disturbances can be divided into two categories: interference from other communicators, called other-user interference, and interference from all other radiators, e.g., civilian, industrial, scientific, and medical devices. Since the dominant source of the latter interference is automobile ignition noise (aside from locating the receiver very near other sources, e.g., under a power line at frequencies of 100 MHz or lower), we have confined our attention to modeling this non-user interference. Other-user interference statistics are dependent upon the specific communication system. Thus the interference produced in CDMA systems will be quite different from that in TDMA systems. To first order, CDMA communications interference, at least, can be modeled by additive Gaussian noise if one assumes that power control is working reasonably well. Modeling of other-user interference is not covered in this report. Section 11 discusses the modeling of ignition noise as a random pulse train. Experimental data supporting statistical models of pulse amplitudes and arrival times is presented in addition to measurements of noise power level as a function of frequency.

Section 12 discusses models for Land Mobile Satellite Channels. Low Earth Orbit (LEO) and Medium Earth Orbit (MEO satellite systems are in the process of development [56][57] for the purpose of implementing land mobile communications. The Land Mobile Satellite (LMS) systems are proposed primarily as a complement to existing and proposed terrestrial cellular systems, since the latter are most cost-effective in urban areas, while the former are more cost-effective in underpopulated regions. However, the LMS system has also been considered for use in urban areas when a compatible cellular standard is not available.

Modeling of the LMS channel is a topic of current investigation. Except for Section 12.4 , where the single paper found on wideband LMS channel modeling is discussed, we have found it necessary to confine our attention to narrowband LMS channel modeling where flat fading is appropriate. In modeling the LMS channel three propagation categories or states are used: *clear* or *open, shadowed*, and *blocked*. The relative importance of these categories depends upon the environment. The *clear* state is

epitomized by open areas with a clear line-of-sight and a minimal amount of multipath and scatter. This state will occur frequently in rural environments.

On the other hand the *blocked* state is characteristic of a heavily built-up urban environment, particularly if the satellite is at a low elevation angle. In such a state impenetrable objects block the line-of-sight between the satellite and mobile and reception occurs via diffraction and reflections. Considerable attenuation and multipath will usually exist and the strength of the multipath signal varies slowly with approximate lognormal statistics. Such a channel state is typical of terrestrial land-mobile cellular channels in urban environments when no direct path or large resolvable reflected paths exist.

The *shadowed* state is exemplified by a line-of-sight path through vegetation, for example transmission to a mobile traveling along a tree-lined street. In this case an attenuated, time variant, line-of-sight signal and a scatter multipath signal exist. The line-of-sight signal fluctuates slowly compared to the multipath signal and has been modeled by lognormal statistics.

In Section 12.1 we consider models for the individual states. These models are essentially special cases of models already presented except that lognormal statistics are introduced to model certain slow variations in the power of the direct path signal and/or the multipath signal. These slow variations are appropriate for the previous models also but were not introduced because the amount of multipath in these models increases the time for simulation so much that it was not feasible to introduce the slow lognormal time variations. For the non-urban LMS channel models only flat fading models are needed because the multipath spread is small compared to the reciprocal bandwidths of interest. In such a case it is feasible to introduce the lognormal fluctuations in the simulations. If the channel bandwidth is small enough it would be practical to introduce lognormal fluctuations in the urban environment also.

Since the ground terminal is mobile, the individual propagation states persist only for a finite time and there are random transitions from one state to another due to the changing propagation path. Markov Chain models have been used to represent the flat fading LMS channel as a stochastic process involving two or more states. These models are reviewed in Section 12.2. Section 12.3 specifies the Markov Chain model simulation approach to be used.

We have reviewed frequently mentioned papers on Indoor channel measurements and statistical modeling[72]-[76] and others [77]-[80] presenting only measurements on path loss and/or rms multipath spread. As a result of this review we conclude that the Mixed Discrete/Scatter model employed for the Outdoor radio mobile channels in the GCS is suitable for the short term or small-scale fluctuations of the Indoor channel and the Indoor-Outdoor Microcell channel. The scatter portion of the model is primarily due to the myriad of multiple reflection paths in the rooms containing the transmitter and the receiver, while the discrete portion is due to the direct path and large reflecting surfaces in the building (or even outside). An exponential Delay Power Spectrum is appropriate for the scatter portions of the channels. Usually one scatter channel is appropriate but occasionally two are needed. As for Outdoor radio channels, long term or large-scale fluctuations in signal strength of Indoor radio channels are best modeled by the lognormal distribution.

Section 13.1 presents the channel model standards proposed by the JTC for the Indoor channel. These are similar to the JTC models for the outdoor channel briefly discussed in Section 7.1 of this report and in detail in [2]. They employ the Discrete Complex Gaussian Factorable WSSUS channel model presented in Section 7.1. While this model is simpler, the Mixed Discrete/Scatter model is more realistic.

Section 13.2 proposes a Mixed Discrete/Scatter model for the Indoor and Indoor-Outdoor channels. Section 13.2.1 reviews past channel modeling and measurements

efforts in references [72] - [80] and Section 13.2.2 presents default scenarios for the Mixed model based upon these measurements.

The Generic Channel Simulator (GCS) is a companion software package designed to implement the channel models developed under the present contract and two prior related contracts, DAAB07-93-C-N651 and DAAB07-94-C-H601. The modeling and simulation carried out in contract DAAB07-93-C-N651, dealt only with the HF Ionosphere channel. The tapped delay line models and associated statistical channel models employed were of a generic nature and it was found that much of the software could be employed directly or modified slightly to model other radio channels, particularly the mobile cellular and non-cellular channels in the higher frequency bands. Thus under subsequent contracts the repertoire of simulated channels has expanded considerably. Section 14 presents tree diagrams showing the directory structure of the program and the names of individual programs. A brief discussion of the individual programs and input parameter is presented. To reduce the burden to a GCS user in having to select from a large range of parameters, optional default scenarios identical to those discussed in the body of this report have been introduced. An Appendix has been provided to this report supplying default scenarios for the WBHF channel, since they had not previously been supplied. The GCS software is under current development by Lincoln Laboratories.

For each channel separate programs are provided which simulate distortion (e.g. time variant multipath), and additive disturbances (e.g., interference) in addition to programs that allow estimation of path loss. Channel model and additive disturbance programs are normalized so any desired SNR can be achieved by adjustment of scale factors after simulator output files have been generated. The software has been programmed in ANSI C and developed in a Unix environment on a SUN workstation. Both Motif Windows and command -line scripts can be used for entry of parameters.

2 SPECIFICATIONS FOR LIMITED TIME AND FREQUENCY SELECTIVITY

In evaluating the performance of detection systems for radio channels, it is useful to define certain limiting conditions on time and frequency selectivity. This section defines mathematically what is meant by limited time and frequency selectivity and presents a brief review of some canonical input-output relations for time variant channels needed to develop associated channel models useful for detection analyses.

If z(t) and w(t) represent complex envelopes of the channel input and output, respectively, then

$$w(t) = \int Z(f)T(f,t)e^{j2\pi ft}\,df \tag{2.1}$$

$$w(t) = \int z(t-\xi)g(t,\xi)d\xi \tag{2.2}$$

where $Z(f)$ is the spectrum of z(t), T(f,t) is called the *Time-Variant Transfer Function*, and $g(t,\xi)$ is called here the *Time Variant Impulse Response* of the channel. T(f,t) and $g(t,\xi)$ are Fourier transform pairs on the (f, ξ) variables, i.e.,

$$g(t,\xi) = \int T(f,t)\exp(j2\pi f\xi)d\xi \tag{2.3}$$

$$T(f,t) = \int g(t,\xi)\exp(-j2\pi f\xi)\,df \tag{2.4}$$

To simplify notation in the subsequent development we assume a "center" frequency of f=0, consistent with complex envelope notation, and a time origin of t=0 for

the detector observation interval. The analysis is readily generalized for frequency and time offsets. Thus in our subsequent discussions an observation interval of duration T should be assumed to be centered at t=0 and a signal of bandwidth W should be assumed to be centered at f=0.

The presence of a "mean" path delay ξ_0 produces a linear variation of phase with frequency and the presence of a "mean" Doppler shift ν_0 produces a linear variation of phase with time on the time-variant transfer function. In analyzing the behavior of the time-variant transfer function, particularly when power series expansions in time and frequency are used, it is best to include these variations as separate operators providing a delay of ξ_0 on the input signal and a Doppler shift of ν_0 on the output signal. Precise definitions of ξ_0 and ν_0 will be given in Section 4.

We now introduce two necessary channel parameters for the definition of limiting conditions on time and frequency selectivity: the "total" multipath spread L, and the "total" Doppler spread B. L denotes the duration of the impulse response $g(t,\xi)$ along the delay or "age" variable, ξ, while B denotes the spectral width of T(f,t) vs t, i.e., the spectral width of a received carrier. Four limiting conditions are of interest for WSSUS models of radio channels,

1) 2π BT <<1, called the *slow fading* condition,

2) 2π BT>>1, called the *many fade times* condition,

3) 2π WL << 1, called the *small distortion* condition, and

4) 2π WL >> 1, called the *many fade frequencies* condition.

The phenomenological descriptions used for these inequalities should be interpreted in a statistical sense. Thus, when 2π BT<<1, with high probability there will

be only a partial fade in the observation interval, while when $2\pi BT >>1$ with high probability there will be many fades in the observation interval. In an analogous fashion, for the dual cases, when $2\pi WL << 1$, with high probability, there will be small distortion over a frequency band of width W, while when $2\pi WL >> 1$, with high probability there will be many fades (i.e., dips, notches, or nulls) over a frequency band of width W.

Depending upon the duration of the observation time and the signal bandwidth these conditions can occur in four distinct combinations:

- slow fading/ small distortion

- slow fading/ many fade frequencies

- many fade times/ small distortion

- many fade times/ many fade frequencies

For the first three cases some simplifications in the mathematical representation of the system functions is possible, as described in [1], based upon power series expansions of the time-variant transfer function T(f,t) in t or f or both, depending upon whether the first , second, or third combination of inequalities is valid, respectively. The terminology's, *t-power series*, *f-power series*, and *tf(*or *ft)-power series*, channel models are used in [1] to describe the channel models implied by these mathematical representations. In the subsequent three sections we will review these special channel models.

From an engineering point of view, it is desirable to have numerical values for the products BT and WL to define thresholds for which the conditions 1) - 4) are applicable. The rationale for obtaining such threshold values may be found in [1], Section VI-B Eq.(202) (and the time frequency dual argument). Specifically, consider inequality

3) which corresponds to small distortion due to frequency selectivity. The 3-term quadratically frequency selective f-power series model of the transfer function is used below to model the distortion in this case. The results in Section VI-B of [1] allow one to compute the strength of the mean squared error in the output signal incurred by using this model.

We shall arbitrarily select the value of WL for which the mean squared error is 20 dB below the output signal from the exact channel as the maximum value of WL for which the inequality 3) applies. To apply Eq.(202) of [1] it is necessary to assume a shape for the power spectrum of the input signal and a shape for the density of scattered power versus path delay for the channel (the delay power spectrum defined below). For simplicity we assume a rectangular power spectrum of width W Hz for the input signal and a rectangular delay power density spectrum of width L sec for the channel. Then it may be shown that when $WL \cong 1$, the mean squared error in the quadratically frequency selective fading model is 20 dB below the desired signal.

By using time-frequency duality, and dealing with the slow fading condition 1), one may conclude that when $BT \cong 1$ the mean squared error incurred by using the quadratic time selective fading model is 20 dB below the output power of the exact channel. Here T is the duration of observation of the input signal and B is the width of an assumed Doppler power spectrum for the channel.

The many fade times condition 4) can be quantified by assuming a rectangular Doppler power spectrum of B Hz bandwidth and determining the number of linearly independent samples that exist in an observation time T. Assuming BT is much larger than unity the number of independent complex samples is close to BT . A value of BT equal or greater than ten is then a reasonable choice for satisfaction of the many fade frequencies condition 4). Applying time-frequency duality, a value of WL equal or greater than ten is a reasonable choice for satisfaction of the many fade frequencies condition 2). A uniform delay power spectrum of width L is assumed. Thus, to summarize, for

1) $BT \leq 1$, the *slow fading* condition is valid

2) $BT \geq 10$, the *many fade times* condition is valid

3) $WL \leq 1$, the *small distortion* condition is valid

4) $WL \geq 10$, the *many fade frequencies* condition is valid

It should be understood that the arguments leading to 1') to 4') above are heuristic and the parameters B, W are *total* bandwidth measures and the parameters T, L are *total* time duration measures.

We conclude this section with a review of some properties of the complex Gaussian WSSUS channel which are needed in the sequel. In the subsequent channel model development two additional system functions need to be introduced, $U(\xi, \nu)$, the *Delay-Doppler Spread Function* and $G(f,\nu)$[5] , the *Doppler Spread Function.* The four system functions can be related by single or double Fourier transforms as discussed in [1]. The input-output relationship corresponding to the former system function is

$$w(t) = \int \int z(t-\xi)e^{j2\pi\nu t}U(\xi,\nu)d\nu d\xi \qquad (2.5)$$

This equation may be regarded as representing the output signal as a continuum of delayed and Doppler shifted replicas of the input signal, where the replica delayed by ξ sec. and Doppler shifted by ν Hz has the differential amplitude $U(\xi,\nu)d\nu d\xi$. $T(f,t)$ and $U(\xi,\nu)$ are related by double Fourier Transforms,

$$T(f,t) = \int\int U(\xi,\nu) e^{-j2\pi\xi f} e^{j2\pi\nu t} d\nu d\xi \tag{2.6}$$

$$U(\xi,\nu) = \int\int T(f,t) e^{j2\pi\xi f} e^{-j2\pi\nu t} df dt \tag{2.7}$$

From their definition, it may be seen that L, the total multipath spread, is the width of $U(\xi,\nu)$ along the ξ direction, while B, the total Doppler spread, is the width of $U(\xi,\nu)$ along the ν direction.

The input-output relation corresponding to $G(f,\nu)$ is

$$W(f) = \int Z(f-\nu) G(f-\nu,\nu) d\nu \tag{2.8}$$

where W(f),Z(f) are the spectra of w(t) and z(t), respectively. Eq.(8) represents the output spectrum as a convolution of the input spectrum with the Doppler Spread Function. As mentioned previously, $G(f,\nu)$ can be related to the other three system functions by Fourier transforms. In particular we note that $G(f,\nu)$ is the Fourier transform of T(f,t) along the t direction, i.e.,

$$G(f,\nu) = \int T(f,t) e^{-j2\pi\nu t} dt \tag{2.9}$$

It is readily seen that the width of $G(f,\nu)$ along the ν direction is equal to the total Doppler spread parameter B.

---

[5] In [1] this system function was called the Output Doppler Spread Function. The additional terminology was needed in order to accommodate the larger number of system functions introduced

3 COVARIANCE FUNCTIONS FOR THE SYSTEM FUNCTIONS

This section presents the covariance functions for the system functions of interest assuming a wide sense stationary uncorrelated scattering (WSSUS) channel[1]. These covariance functions lead to a complete statistical description of the WSSUS channel in general and to the limited time and frequency selective fading models in particular, when complex Gaussian statistics are assumed for the system functions.

For the complex Gaussian WSSUS channel model each one of the system functions is a two dimensional complex Gaussian process. As a result the covariance functions of a system function are sufficient to provide a complete statistical description of that system function. The covariance function of these system functions and others and the relation between these covariance functions has been developed in [1] for both WSSUS and non-WSSUS channels. For the WSSUS channel T(f,t) is a wide sense stationary process in time and frequency with covariance function,

$$\overline{T^*(f,t)T(f+\Omega,t+\tau)} = R(\Omega,\tau) \tag{3.1}$$

where $R(\Omega,\tau)$ is called the *Time-Frequency Correlation Function* of the channel.

For the WSSUS channel the covariance function of the impulse response g(t,ξ) is given by

$$\overline{g^*(t,\xi)g(t+\tau,\eta)} = Q(\tau,\xi)\delta(\eta-\xi) \tag{3.2}$$

where $\delta(\bullet)$ is the unit impulse function and we call $Q(\tau,\xi)$[6] *the Tap Gain Correlation Function.* $Q(\tau,\xi)$ and $R(\Omega,\tau)$ are related by Fourier transforms

$$Q(\tau,\xi) = \int R(\tau,\Omega)e^{j2\pi\Omega\xi}d\Omega \tag{3.3}$$

$Q(\tau,\xi)$ may be interpreted as the autocorrelation function for fluctuations in path complex amplitude at path delay ξ. Eq.(9) states that the fluctuations are uncorrelated for different delays and for complex Gaussian statistics the fluctuations are independent.

The covariance function of the Delay -Doppler Spread Function $U(\xi,\nu)$ is given by

$$\overline{U^*(\xi,\nu)U(\eta,\mu)} = S(\xi,\nu)\delta(\eta-\xi)\delta(\mu-\nu) \tag{3.4}$$

where $S(\xi,\nu)$ is called the *Delay- Doppler Scatter Function* or just the *Scatter Function*. Eq.(3.3) states that the contributions to the received signal from "scattering" elements at different delays and Doppler shifts are uncorrelated and for the complex Gaussian channel are statistically independent. $S(\xi,\nu)$ and $R(\Omega,\tau)$ are related by double Fourier transforms,

$$S(\xi,\nu) = \int\int R(\Omega,\tau)e^{j2\pi\Omega\xi}e^{-j2\pi\tau\nu}d\Omega d\tau \tag{3.5}$$

$$R(\Omega,\tau) = \int\int S(\xi,\nu)e^{-j2\pi\Omega\xi}e^{j2\pi\tau\nu}d\xi d\nu \tag{3.6}$$

It is worth noting that $S(\xi,\nu)$ is the two-dimensional power density spectrum of T(f,t).

[6] A different terminology was used in [1]. The terminology used here is conforms better with accepted usage.

The covariance function for the Doppler Spread Function is given by

$$\overline{G^*(f,\nu)G(f+\Omega,\nu+\mu)} = P(\Omega,\nu)\delta(\mu-\nu) \tag{3.7}$$

where $P(\Omega,\nu)$ is called the Doppler Cross Power Density Spectrum. The four functions $Q(\tau,\xi)$, $S(\xi,\nu)$, $R(\Omega,\tau)$, and $P(\Omega,\nu)$ are related by single and double Fourier transforms as diagrammed in Fig.9 of [1].

Two power spectra, $Q(\xi)$, the Delay Power Spectrum and $P(\nu)$, the Doppler power spectrum, and their transforms $q(\Omega)$, the Frequency Correlation Function and $p(\tau)$, the Time Correlation Function, respectively, are of frequent use. These are defined as follows,

$$Q(\xi) = Q(0,\xi) = \int S(\xi,\nu)d\nu \tag{3.8}$$

$$P(\nu) = P(0,\nu) = \int S(\xi,\nu)d\xi \tag{3.9}$$

$$q(\Omega) = \int Q(\xi)e^{-j2\pi\Omega\xi}d\xi \tag{3.10}$$

$$p(\tau) = \int P(\nu)e^{j2\pi\tau\nu}d\nu \tag{3.11}$$

$Q(\xi)$ describes the intensity of scattered power versus path delay ξ and $q(\Omega)$ may be interpreted as the complex crosscorrelation function between the complex amplitudes of received tones as a function of the frequency spacing Ω. $Q(\xi)$ is also the power spectrum of T(f,t) versus f with t fixed. $P(\nu)$ describes the intensity of scattered power versus path Doppler shift ν and $p(\tau)$ may be interpreted as the autocorrelation function of the

complex envelope of a received tone. $P(\nu)$ is also the power spectrum of $T(f,t)$ versus t with f fixed.

Simplified representations of the covariance functions occur for a *factorable* WSSUS channel. For the factorable channel the Scatter Function factors into a term dependent on delay alone and a term dependent on Doppler alone. From Eq.'s (3.8) and (3.9) this factorization must be given by

$$S(\xi, \nu) = Q(\xi)P(\nu) \tag{3.12}$$

Factorization of the other covariance terms follows from (3.12),

$$R(\Omega,\tau) = q(\Omega)p(\tau) \tag{3.13}$$

$$Q(\tau,\xi) = p(\tau)Q(\xi) \tag{3.14}$$

$$P(\Omega,\nu) = q(\Omega)P(\nu) \tag{3.15}$$

4 CHANNEL MODEL FOR SLOW FADING/SMALL DISTORTION CASE

A channel model appropriate to both slow fading and small distortion can be obtained by approximating T(f,t) with several terms in a Taylor series expansion in f and t. This representation has been investigated in [1] where it is called the ft-Power-Series Model. We limit the expansion to terms no higher than quadratic in f and t and call the resulting model a Quadratic Selective ft Power Series Channel Model,

$$T(f,t) = \sum_{m=0}^{2}\sum_{n=0}^{2} T_{mn}(2\pi j)^{m+n} f^m t^n \tag{4.1}$$

where

$$T_{mn} = \frac{1}{m!n!(2\pi j)^{m+n}}\left[\frac{\partial^{m+n} T(f,t)}{\partial f^m \partial t^n}\right]_{f=0,t=0} \tag{4.2}$$

Using Eq.(6),

$$T_{mn} = \frac{1}{m!n!}\int\int (-\xi)^m \nu^n U(\xi,\nu)d\xi d\nu \tag{4.3}$$

This channel model is completely specified by the 9 parameters, $\{T_{mn}; m = 0,1,2, n = 0,1,2\}$.For a complex Gaussian WSSUS channel, this is a set of nine correlated complex Gaussian variables which are completely specified statistically by the corresponding covariance matrix. We now evaluate the generic element of this matrix

$$\overline{T_{mn}^* T_{pq}} = \frac{1}{m!\,n!\,p!\,q!}\int\int\int\int (-\xi)^m \nu^n (-\eta)^p \mu^q \overline{U^*(\xi,\nu)U(\eta,\mu)}d\xi d\nu d\eta d\mu \tag{4.4}$$

The average in the integrand is given by Eq.(3.4). Thus we find that

$$\overline{T^*_{mn} T_{pq}} = \frac{1}{m!\, n!\, p!\, q!} \int\int \xi^{m+p} \nu^{n+q} S(\xi, \nu) d\xi d\nu \tag{4.5}$$

which can be recognized as a moment of the Scatter Function. For the case of a factorable Scatter Function Eq.(4.5) simplifies to

$$\overline{T^*_{mn} T_{pq}} = \frac{1}{m!\, p!} \int \xi^{m+p} Q(\xi) d\xi \frac{1}{n! q!} \int \nu^{n+q} P(\nu) d\nu \tag{4.6}$$

which are products of moments of the Delay and Doppler Power Spectra. In any case note that the correlations are real positive numbers.

We now define specific values for the mean path delay ξ_0 and mean Doppler shift ν_0 as centroids of the corresponding power spectra, i.e.,

$$\xi_0 = \frac{\int \xi Q(\xi) d\xi}{\int Q(\xi) d\xi} \tag{4.7}$$

$$\nu_0 = \frac{\int \nu P(\nu) d\nu}{\int P(\nu) d\nu} \tag{4.8}$$

As discussed previously, we assume that mean path delay and Doppler shift are modeled separately by providing a delay on the input signal and a Doppler shift on the output signal. For the resulting normalized channel we shall assume that the centroids ξ_0 and ν_0 vanish.

This choice causes many terms in the covariance matrix to vanish for the factorable Scatter Function case. Note that

$$\int P(\nu)d\nu = \int Q(\xi)d\xi = \int\int S(\xi,\nu)d\xi d\nu = \overline{|T(f,t)|^2} \equiv p_0 \tag{4.9}$$

where we have defined p_0 as the mean squared absolute value of the time variant transfer function $\overline{|T(f,t)|^2}$.

To simplify the presentation of the covariance matrix we use the following notation for the normalized moments of the Delay and Doppler Power Spectra,

$$\eta_n = \frac{1}{p_0}\int \xi^n Q(\xi)d\xi \tag{4.10}$$

$$\mu_n = \frac{1}{p_0}\int \nu^n P(\nu)d\nu \tag{4.11}$$

Note that, by hypothesis, $\eta_l = \mu_1 = 0$ and $\eta_0 = \mu_0 = 1$. With these definitions,

$$\overline{T^*_{mn}T_{pq}} = p_0\frac{1}{m!\,p!}\eta_{m+p}\frac{1}{n!q!}\mu_{n+q} \tag{4.12}$$

We redefine the nine parameters with single rather than double subscripts as follows,

$$g_1 = T_{00}; g_2 = T_{10}; g_3 = T_{01}; g_4 = T_{11}; g_5 = T_{20}; g_6 = T_{02}; g_7 = T_{21}; g_8 = T_{12}; g_9 = T_{22} \tag{4.13}$$

The covariance matrix of the parameters, C, is then given by the average of the matrix product

$$\mathbf{C} = \overline{\mathbf{G}^{*\mathrm{T}}\mathbf{G}} \tag{4.14}$$

where G is the row vector of coefficients,

$$\mathbf{G} = \begin{bmatrix} g_1 & g_2 & g_3 & g_4 & g_5 & g_6 & g_7 & g_8 & g_9 \end{bmatrix} \tag{4.15}$$

and $\mathbf{G}^{\mathbf{T}}$ is the transpose of G. The element in the m'th row and n'th column of C is given by the average $\overline{g_m^* g_n}$. Carrying out the averages we find that for the factorable Scatter Function

$$\mathbf{C} = p_0 \begin{bmatrix} 1 & 0 & 0 & 0 & \eta_2/2 & \mu_2/2 & 0 & 0 & \eta_2\mu_2/4 \\ 0 & \eta_2 & 0 & 0 & \eta_3/2 & 0 & 0 & \eta_2\mu_2/2 & \eta_3\mu_2/4 \\ 0 & 0 & \mu_2 & 0 & 0 & \mu_3/2 & \eta_2\mu_2/2 & 0 & \eta_2\mu_3/4 \\ 0 & 0 & 0 & \eta_2\mu_2 & 0 & 0 & \eta_3\mu_2/2 & \eta_2\mu_3/2 & \eta_3\mu_3/4 \\ \eta_2/2 & \eta_3/2 & 0 & 0 & \eta_4/4 & \eta_2\mu_2/4 & 0 & \eta_3\mu_2/4 & \eta_4\mu_2/8 \\ \mu_2/2 & 0 & \mu_3/2 & 0 & \eta_2\mu_2/4 & \mu_4/4 & \eta_2\mu_3/4 & 0 & \eta_2\mu_4/8 \\ 0 & 0 & \eta_2\mu_2/2 & \eta_3\mu_2/2 & 0 & \eta_2\mu_3/4 & \eta_4\mu_2/4 & \eta_3\mu_3/4 & \eta_4\mu_3/8 \\ 0 & \eta_2\mu_2/2 & 0 & \eta_2\mu_3/2 & \eta_3\mu_2/4 & 0 & \eta_3\mu_3/4 & \eta_2\mu_4/4 & \eta_3\mu_4/8 \\ \eta_2\mu_2/4 & \eta_3\mu_2/4 & \eta_2\mu_3/4 & \eta_3\mu_3/4 & \eta_4\mu_2/8 & \eta_2\mu_4/8 & \eta_4\mu_3/8 & \eta_3\mu_4/8 & \eta_4\mu_4/16 \end{bmatrix} \tag{4.16}$$

Examination of Eq.(4.16) shows that the essential channel parameters needed to specify the covariance matrix of the parameters and thus the channel model statistics are $\eta_2, \eta_3, \eta_4, \mu_2, \mu_3, \mu_4$. The parameters $\sqrt{\eta_2}$ and $\sqrt{\mu_2}$ (and sometimes twice their values) have been called the *rms multipath spread* and *rms Doppler spread*, respectively, in the literature.

As a final point we note that the input/output relationship, corresponding to the Quadratically Selective ft-Power-Series Channel Model, Eq.(4.1), is given by

$$w(t) = \sum_{n=0}^{2} \sum_{m=0}^{2} T_{mn} (2\pi jt)^n \frac{d^m z(t)}{dt^m} \tag{4.17}$$

When the mean path delay and Doppler shift are included the input/output relationship becomes

$$w(t) = e^{j2\pi\nu_0 t} \sum_{n=0}^{2} \sum_{m=0}^{2} T_{mn} (2\pi jt)^n \frac{d^m z(t-\xi_0)}{dt^m} \tag{4.18}$$

Eq. (4.18) could be used to model channel input-output behavior in the detection analyses when the fading is slow over the detection time interval and the degree of frequency selectivity is small over the signal bandwidth as evidenced by satisfaction of the inequalities $BT \leq 1$, and $WL \leq 1$. Assuming complex Gaussian statistics the covariance matrix of the parameters $\{T_{mn}; m = 0,1,2, n = 0,1,2\}$ given above leads to a complete statistical description of the received signal w(t).

5 CHANNEL MODEL FOR SLOW FADING/MANY FADE FREQUENCIES CASE

A channel model appropriate to slow fading but with no constraint on frequency selective fading distortion can be obtained by representing T(f,t) by several terms in a Taylor series expansion in t. This representation has been investigated in [1] where it is called the t-Power-Series Model. We limit the expansion to terms no higher than quadratic in t and, as in [1], call the resulting model a Quadratically Time Selective Power Series Channel Model,

$$T(f,t) = \sum_{n=0}^{2} T_n(f)(2\pi jt)^n \tag{5.1}$$

where

$$T_n(f) = \frac{1}{n!(2\pi j)^n}\left[\frac{\partial^n T(f,t)}{\partial t^n}\right]_{t=0} \tag{5.2}$$

An alternate expression for $T_n(f)$ is given by

$$T_n(f) = \frac{1}{n!}\int \nu^n G(f,\nu)d\nu \tag{5.3}$$

Because T(f,t) is a complex Gaussian wide sense stationary process in f, the filters, although time-invariant, have transfer functions that are complex Gaussian wide sense stationary random processes in the frequency variable. As a consequence the joint statistical properties of these filters are completely determined from the crosscovariance functions

$$q_{mn}(\Omega) = \overline{T_m^*(f)T_n(f+\Omega)} \tag{5.4}$$

With the aid of Eq.'s (5.3) and (3.5) it is readily determined that

$$q_{mn}(\Omega) = \frac{1}{n!\,m!}\int \nu^{n+m} P(\Omega,\nu)\,d\nu \tag{5.5}$$

When the channel has a factorable Scatter Function, Eq.(3.15) shows that Eq.(5.5) may be simplified to

$$q_{mn}(\Omega) = p_0 \frac{\mu_{n+m}}{n!\,m!} q(\Omega) \tag{5.6}$$

where the coefficient μ_n has been defined in Eq.(4.11). Eq.(5.6) shows that, apart from a constant multiplier, all the crosscovariance(and covariance) functions of the model filters have the same shape, namely, $q(\Omega)$,the Frequency Correlation Function of the channel. Knowledge of $q(\Omega)$ (or $Q(\xi)$ since these functions are related by Fourier Transforms) and the three coefficients μ_2,μ_3,μ_4 provide a complete statistical description for the factorable channel.

From Eq.'s (5.1) and(2.1) we deduce that the input/output relationship corresponding to the Quadratically Time Selective Power Series Channel Model can be expressed in the form

$$w(t) = \sum_{n=0}^{2} (j2\pi t)^n \int Z(f)T_n(f)e^{j2\pi ft}\,df \tag{5.7}$$

When the mean path delay and mean Doppler shift are included, this relationship changes to

$$w(t) = e^{j2\pi\nu_0 t}\sum_{n=0}^{2} (j2\pi t)^n \int Z(f)T_n(f)e^{j2\pi f(t-\xi_0)}\,df \tag{5.8}$$

Eq.(5.8) could be used to model channel input-output behavior in the detection analyses when the fading is slow over the detection time interval and no constraint is placed upon the degree of frequency selectivity. When the degree of frequency selectivity as considerable, as indicated by satisfaction of the inequality $WL \geq 10$, there will be many fluctuations of $T_n(f)$ over the band occupied by Z(f), which is of width W. In any case, assuming complex Gaussian statistics, the crosscovariance(and autocovariance) functions of the $\{T_n(f); n = 0,1,2\}$ given above lead to a complete statistical description of the received signal.

6 CHANNEL MODEL FOR MANY FADE TIMES/SMALL DISTORTION CASE

A channel model appropriate to small frequency selective fading distortion over the signal bandwidth of interest, but with no constraint on the rapidity of fading over the detector observation interval, can be obtained by representing T(f,t) by several terms in a Taylor series expansion in f. This representation has been investigated in [1] where it is called the f-Power-Series Model. We limit the expansion to terms no higher than quadratic in f and, as in [1], call the resulting model a Quadratically Frequency Selective Power Series Channel Model,

$$T(f,t) = \sum_{n=0}^{2} G_n(t)(2\pi jf)^n \tag{6.1}$$

where the complex gain

$$G_n(t) = \frac{1}{n!(2\pi j)^n}\left[\frac{\partial^n T(f,t)}{\partial f^n}\right]_{f=0} \tag{6.2}$$

An alternate expression for $G_n(t)$ is given by

$$G_n(t) = \frac{1}{n!}\int (-\xi)^n g(t,\xi)d\xi \tag{6.3}$$

Because T(f,t) is a complex Gaussian wide sense stationary process, the gains $\{G_n(t); n=0,1,2\}$ are complex Gaussian wide sense stationary random processes. As a

consequence the joint statistical properties of these complex gains are completely determined from the crosscovariance functions

$$p_{mn}(\tau) = \overline{G_m^*(t)G_n(t+\tau)} \tag{6.4}$$

With the aid of Eq.'s (6.2) and (3.2) it is readily determined that

$$p_{mn}(\tau) = \frac{1}{n!m!}\int \xi^{n+m} Q(\tau,\xi)d\xi \tag{6.5}$$

When the channel has a factorable Scatter Function, Eq.(6.5) may be simplified to

$$p_{mn}(\tau) = p_0 \frac{\eta_{n+m}}{n!m!} p(\tau) \tag{6.6}$$

where the coefficient η_n has been defined in Eq.(4.10). Eq.(6.6) shows that, apart from a constant multiplier, all the cross and autocovariance functions of the complex gain processes have the same shape, namely, $p(\tau)$,the Time Correlation Function of the channel. Knowledge of $p(\tau)$ (or equivalently $P(\nu)$, since they are related by Fourier Transforms) and the three coefficients η_2, η_3, η_4 provide a complete statistical description for the factorable channel.

From Eq.'s(6.1) and(2.1) we deduce that the input/output relationship corresponding to the Quadratically Frequency Selective Power Series Channel Model can be expressed in the form

$$w(t) = \sum_{n=0}^{2} G_n(t)\frac{d^n z(t)}{dt^n} \tag{6.7}$$

When the mean path delay and mean Doppler shift are included, this relationship changes to

$$w(t) = e^{j2\pi\nu_0 t}\sum_{n=0}^{2} G_n(t)\frac{d^n z(t-\xi_0)}{dt^n} \tag{6.8}$$

Eq.(6.8) could be used to model channel input-output behavior in the detection analyses when the frequency selective distortion is small over the input signal bandwidth and no constraint is placed upon the rapidity of fading in the detection interval. When the fading is rapid, as indicated by satisfaction of the inequality $BT \geq 10$, there will be many fluctuations of $G_n(t)$ over the detection interval T_0 . In any case, assuming complex Gaussian statistics, the crosscovariance(and autocovariance) functions of the $\{G_n(t); n = 0,1,2\}$ given above lead to a complete statistical description of the received signal.

7 CELLULAR/PCS HANDSET-BASESTATION CHANNELS

In this section we consider channel models and parameters for the Cellular/PCS Handset-Basestation Channels. These radio channel models employ one or more of three canonical mathematical channel models either singly or in combination, namely the *Complex Gaussian Factorable WSSUS* model, the *Discrete Complex Gaussian Factorable WSSUS* model, and the *Discrete Non-Fading-Paths* model.

A recent report [2] reviewed the literature on urban mobile cellular radio channel measurements in order to model these channels. Two classes of models were given detailed consideration and corresponding software simulators were developed. The first class of channel models studied were the simplified channel model standards proposed by the Joint Technical Committee (JTC)[7]. A more accurate class of channel models was then developed, called the *Mixed Discrete/Scatter* or simply *Mixed Channel Model*. We consider these in order.

7.1 JTC Models

The JTC propagation channel models may be called *Discrete Complex Gaussian Factorable WSSUS Channel Models*. The Delay Power Spectrum for the discrete WSSUS model has the form

$$Q(\xi) = \sum_{n=1}^{N} p_n \delta(\xi - \tau_n) \qquad (7.1)$$

corresponding to N complex Gaussian fading paths, with $\{p_n, \tau_n\}$ equal to the strength and delay of the n'th path, respectively. The set of values $\{p_n, \tau_n\}$ for n=1 to N is sometimes called the *tap weight profile*. To simplify notation we normalize the mean absolute squared value of the transfer function , p_0, to unity, i.e.,

[7] The JTC is a cooperative effort between committee T1 (actually technical subcommittee T1P1) sponsored by the Alliance for Telecommunication Industry Solutions (ATIS) and the Telecommunication Industry Association (TR46).

$$p_0 = \int Q(\xi)d\xi = \sum_{n=1}^{N} p_n \equiv 1 \tag{7.2}$$

Each path fluctuates independently but with a power spectrum of the same shape due to the assumption of a factorable scatter function. The Doppler power spectrum chosen in the model is that due to Clarke [3] and Jakes [4]

$$P(\nu) = \frac{1}{\pi} \frac{1}{\sqrt{(V/\lambda)^2 - \nu^2}}; |\nu| < \frac{V}{\lambda} \tag{7.3}$$

where V is the velocity of the mobile andλ is the wavelength at the carrier frequency. The input-output relationship corresponding to the JTC model is

$$w(t) = \sum_{n=0}^{N} \sqrt{p_n} h_n(t) z(t - \tau_n) \tag{7.4}$$

where the complex tap weight, $h_n(t)$, with power spectrum given by the Doppler Power Spectrum (Eq. (7.2)), has been normalized to unit power. ν_0 vanishes because of the even symmetry of the Doppler Power Spectrum .

Section 4 showed that the parameters ξ_0, ν_0 and the normalized moments $\eta_2, \eta_3, \eta_4, \mu_2, \mu_3, \mu_4$ are the essential data to provide a complete statistical description of the slow fading/small distortion factorable complex Gaussian WSSUS channel. Because of the symmetry in the Doppler Power Spectrum, μ_3=0. In addition, by integration, one may determine that

$$\mu_2 = \frac{1}{2}\left(\frac{V}{\lambda}\right)^2 \tag{7.5}$$

$$\mu_4 = \frac{3}{8}\left(\frac{V}{\lambda}\right)^4 \tag{7.6}$$

The mean path delay ξ_0 is given by

$$\xi_0 = \sum_{n=1}^{N} p_n \tau_n \tag{7.7}$$

Normalizing the Delay Power Spectrum to zero mean path delay, the generic multipath parameter η_m is found to be given by

$$\eta_m = \sum_{n=1}^{N} (\tau_n - \xi_0)^m p_n \tag{7.8}$$

Instead of presenting values for channel parameters η_3, η_4 we consider related, well- known, dimensionless "shape" parameters used in modeling probability distributions, namely, the "skewness" β and the "excess", γ, given by

$$\beta = -\frac{\eta_3}{\eta_2^{3/2}} \qquad \gamma = \frac{\eta_4}{\eta_2^2} - 3 \tag{7.9}$$

In addition, instead of η_2 we present the related *rms multipath spread* parameter

$$s = \sqrt{\eta_2} \tag{7.10}$$

For the JTC models different tap weight profiles were assigned to different environments. Initially, the profiles had a maximum of 10 taps but this was reduced to 6 taps. For each environment the statistical variation of parameters was handled by specifying three tap weight profiles to represent mild(channel A), worse(channel B), and severe(channel C) multipath conditions. Channels A and B occur relatively frequently, while channel C is rare. Six different environments were considered for outdoor channels:

1) urban-high-rise low-antenna
2) urban-suburban low-rise low-antenna
3) residential low-antenna
4) urban-high-rise high-antenna
5) urban-suburban low-rise high-antenna
6) residential low-antenna

Table 7.1 lists the parameters s, β, and γ, with appropriate subscripts for channels A, B, and C, for each of the six environments.

As discussed in Section 5, the channel parameters needed for the slow fading/many fade frequency case are the Doppler parameters $(\nu_0, \mu_2, \mu_3, \mu_4)$ already presented above

Table 7.1

Multipath and Doppler Parameters for JTC Mild, Worse, and Severe Channel Conditions for Each of Six Different Outdoor Environments

	Channel A (Mild)			Channel B (Worse)			Channel C (Severe)		
ENVIRONMENT	s_A(ns)	β_A	γ_A	s_B(ns)	β_B	γ_B	s_C(ns)	β_C	γ_C
urban-high-rise low-antenna	99	-1.9	5.1	630	-2.1	3.9	1600	-3.1	11
urban-suburban low-rise low-antenna	99	-1.9	5.1	630	-2.1	3.9	2400	-2.8	7
residential low-antenna	62	-2.1	4	450	-0.86	0.66	900	-2.3	4
urban-high-rise high-antenna	500	-2.8	10	3100	-2.9	8.5	8000	-1.8	3.6
urban-suburban low-rise high-antenna	99	-1.9	5.1	630	-2.1	3.9	2400	-2.8	7
residential high-antenna	350	-0.59	-1.1	2300	-1	-0.26	6500	-0.66	-0.091

plus the Delay Power Spectra for each of 6 environments and channels A, B, C. For the six-tap case, the latter are given by the tap weight profiles in [2], Fig's 3.22-3.27.

As discussed in Section 6, the channel parameters needed for the many fade times/small distortion case are the multipath parameters $(\xi_0, \eta_2, \eta_3, \eta_4)$ plus the Doppler Power Spectrum (given in Eq.(7.2) A set equivalent to (η_2, η_3, η_4), namely, (s,β,γ), has already been presented above for the eighteen cases of interest.

7.2 Mixed Discrete/Scatter Model

In Section 7.2.1 we consider the case of base antennas above the roof line, which is characteristic of macrocellular channels, while in Section 7.2.2 we consider the case of base antennas below the roof line, which is characteristic of microcellular channels.

7.2.1 Base-Antenna Above Roof Line

The discussion in this section is divided into two parts. Section 7.2.1.1 presents the analytical basis for the proposed channel models and Section 7.2.1.2 reviews channel measurements in an attempt to extract parameters for the models.

7.2.1.1 Mathematical Model

A review of the measured multipath characteristics [2] and the references mentioned therein, reveals a common pattern: the impulse responses for paths with base antennas above-the-roof lines consist of a mixture of unresolved paths plus discrete resolved paths. When the environment producing the multipath is urban, the unresolved paths arrive early due to reflections in the vicinity of the mobile antenna. Sometimes there is a later group of weaker unresolved paths due to a very strong reflector that is visible from the base antenna but not visible to the mobile antenna. Usually, however, there is only one unresolved group of paths. The number of strong discrete paths is usually not large, and some may be delayed considerably -- 10 microseconds or, rarely even greater .When the reflecting environment contains mountains and high urban "cores", a relatively unusual combination, more than one unresolved groups of paths can occur. This mixed continuous discrete structure can exist with or without a significant direct path, depending upon the geometry.

The propagation channel simulation procedure for the base antenna above-the-roofs uses separate models for each unresolved group of paths and for the discrete paths. We call each unresolved group of paths a "scatter" path, or scatter propagation mode. Assuming a large number of unresolved paths and utilizing the Central Limit Theorem, a scatter path can be modeled, as far as complex envelopes are concerned, as a quasi-stationary complex Gaussian (WSSUS) channel. Assuming a factorable Scatter Function,

a complete statistical description of the channel requires selection of $Q(\xi)$ and $P(\upsilon)$. Based upon an inspection of measurements and an appeal to physical considerations, it was decided in [2] to adopt an exponential delay power spectrum shape. Thus we assume that the delay power spectrum of the *k*-th scatter path, with the mean path delay normalized to zero, is given by

$$Q_k(\xi) = \frac{1}{\tau_k} \exp\left(-\frac{\xi + \tau_k}{\tau_k} \right) \quad ; \quad \xi \geq -\tau_k \tag{7.11}$$

where τ_k is the "delay constant", i.e., the value of ξ at which $\exp(-\xi/\tau_k)$ reduces to 1/e. The delay power spectrum in Eq.(7.11) has been normalized to unit area, so that the mean absolute squared value of the corresponding transfer function is unity. It is readily determined that

$$\eta_2 = \tau_k^2; \eta_3 = 2\tau_k^3; \eta_4 = 9\tau_k^4 \tag{7.12}$$

so that

$$s = \tau_k; \beta = -2; \gamma = 6 \tag{7.13}$$

for the exponential shaped Delay Power Spectrum.

Theoretical derivations for $P(\upsilon)$ have been carried out by several authors, e.g., Clarke [3], and Jakes [4]. Under the assumption of a continuum of paths arriving uniformly distributed in azimuth and at zero elevation angle, Clarke (and Jakes) showed that $P(\upsilon)$ is given by Eq.(7.2). Since the incoming rays due to the multipath components will not be arriving at the zero elevations assumed in the Clarke/Jakes model, because the energy must come from above as well as from below due to reflections from the surface, the Clarke/Jakes power spectrum is not justified. A better model is the uniform Doppler spectrum:

$$P(\upsilon) = \frac{\lambda}{2V} \quad ; \quad |\upsilon| < \frac{V}{\lambda} \tag{7.14}$$

For this power spectrum,

$$\mu_2 = \frac{1}{3}\left(\frac{V}{\lambda}\right)^2; \mu_3 = 0; \mu_4 = \frac{1}{5}\left(\frac{V}{\lambda}\right)^4 \tag{7.15}$$

The Scatter Function for a set of N scatter paths can then be expressed as

$$S(\xi, \nu) = P(\nu)\sum_{n=1}^{N} p_n Q_n(\xi - d_n) \tag{7.16}$$

where d_n is the mean path delay of the n'th scatter path and $p_n P(\nu) Q_n(\xi - d_n)$ is the Scatter Function of the n'th scatter path. p_n is the mean absolute magnitude squared of the n'th scatter path transfer function.

The input-output relationship for the scatter paths is

$$w_s(t) = \sum_{n=1}^{N} p_k \int z(t - d_k) g_k(t, \xi) d\xi \tag{7.17}$$

where $w_s(t)$ is the output signal due to the scatter paths alone and $g_k(t, \xi)$ is the time variant impulse response of the k'th scatter path in which the mean path delay has been normalized to zero. The mean Doppler shift is zero because of the assumed symmetrical shape of the Doppler Power Spectrum. The transfer functions of each of these scatter paths may be expanded in a power series in time and/or frequency, with associated multipath and Doppler parameters, to produce the canonical quadratic selective models discussed in Sections 4, 5, and 6.

In addition to the scatter paths there are usually a few discrete paths representing reflections from large objects plus a possible direct path. The input- output relationship for these discrete paths is given by

$$w_d(t) = \sum_{k=1}^{K} e^{j2\pi \upsilon_k t} e^{j\theta_k} \sqrt{h_k}\, z(t - \xi_k) \tag{7.18}$$

where $w_d(t)$ is the received signal due to K discrete paths, $\sqrt{h_k}$, ξ_k $(\xi_1 < \xi_2 \cdot \cdot < \xi_K)$, υ_k, and θ_k are the amplitude, delay, Doppler shift, and phase shift, respectively, of the k-th path. The model (7.18) is called the *Discrete Non-Fading Paths Model*.

The Doppler shifts in (7.18) can be expressed as

$$\nu_k = \frac{V}{\lambda} \mathrm{Cos}(\alpha_k) \tag{7.19}$$

where α_k is the angle between the velocity vector of the mobile and the line-of-sight to the reflecting object.

The time-variant transfer function of the Discrete Non-Fading Paths Model can be expanded in power series in time and/or frequency to produce models to characterize the three cases: slow fading/small distortion, slow fading/many fade frequencies, and many fade times/small distortion. However, the statistics of the parameters will not be complex Gaussian as for the case of the scatter channel. From (7.18) it may be seen that the Time Variant System Function and the Delay-Doppler Spread Function of the Discrete Non-Fading Paths channel are given by,

$$T(f,t) = \sum_{k=1}^{K} \sqrt{h_k} e^{j2\pi\theta_k} e^{-j2\pi\xi_k f} e^{j2\pi\nu_k t} \tag{7.20}$$

$$U(\xi,\nu) = \sum_{k=1}^{K} \sqrt{h_k} e^{j\theta_k} \delta(\xi - \xi_k)\delta(\nu - \nu_k) \tag{7.21}$$

Using Eq. (4.3) the channel coefficients in the quadratic selective tf power series model for the slow-fading/small-distortion case are found to be

$$T_{mn} = \frac{1}{m!n!} \sum_{k=1}^{K} (-\xi_k)^m (\nu_k)^n \sqrt{h_k} e^{j\theta_k} \tag{7.22}$$

The coefficients T_{mn} should be used in Eq.(4.18) to provide the input-output relationship for the slow-fading/small-distortion case. Suitable values for the mean path delay and Doppler shift (ξ_0, ν_0) may readily be determined.

For the slow-fading/many-fade-frequency case the filter $T_n(f)$ used in the t power series model , Eq.(5.2), is found to be

$$T_n(f) = \frac{1}{n!}\sum_{k=1}^{K} \nu_k^n \sqrt{h_k}\, e^{j\theta_k}\, e^{-j2\pi\xi_k f} \tag{7.23}$$

for the Discrete Non-Fading Paths channel. $T_n(f)$ should be used in Eq.(5.8) to define the input -output relationship for the discrete channel for the slow-fading/many-fade-frequency case.

Finally, for the many-time-fades/small-distortion case the complex gain $G_n(t)$ used in the f power series model, Eq.(6.1), is found to be

$$G_n(t) = \frac{1}{n!}\sum_{k=1}^{K} (-\xi_k)^n \sqrt{h_k}\, e^{j\theta_k} e^{j2\pi\nu_k t} \tag{7.24}$$

for the Discrete Non-Fading Paths channel. $G_n(t)$ should be used in Eq.(6.8) to define the input-output relationship for the discrete channel for the many-fade-time/small-distortion case. The statistics of $G_n(t)$ are those of the sum of K random phased cissoids. They have been analytically evaluated only for up to three cissoids.

The output signal is given by the superposition of the signals from the scatter modes and the discrete paths

$$w(t) = w_s(t) + w_d(t) \tag{7.25}$$

For each special selective fading model one must sum the corresponding models for the scatter and discrete paths.

The coefficients T_{mn} and the functions $T_n(f), G_n(t)$ are random due primarily to the phases $\{\theta_k\}$ which may be assumed to be independent and uniformly distributed over a range of 2π. In principle this allows the determination of the statistics for the discrete channel fluctuations. Values for the parameters $\{h_k, \nu_k, \xi_k, K\}$ remain to be determined.

7.2.1.2 Measurements

Extensive measurement campaigns for the high base station case extend over more than a 20-year range [5]-[17]. The experimental data, summarized in [2], has been examined to find appropriate ranges of parameter values. This has proven difficult due to the fact that no channel measurement campaigns have attempted to separate the discrete and the scatter modes. The rms multipath spread, s, is the parameter most frequently estimated. Or rather a parameter we shall call s_x is estimated. This is the rms multipath spread computed on a truncated estimated Delay Power Spectrum(or path delay profile, as it is sometimes called) which eliminates all power in the tail of the spectrum which is x dB below the peak of the delay power spectrum. In addition, a parameter we shall call L_x is frequently, but less often estimated. L_x is the "excess delay" (i.e. the delay beyond the earliest arriving path delay) at which the Delay Power Density Spectrum drops to a value x dB below the maximum. For the exponential delay power spectrum it is readily determined that

$$L_x = .23sx \tag{7.26}$$

and

$$s_x = \sqrt{1 - \frac{(.23x)^2 e^{-.23x}}{(1 - e^{-.23x})^2}}\, s \tag{7.27}$$

so that

$$L_x = .23x s_x \sqrt{1 - \frac{(.23x)^2 e^{-.23x}}{(1 - e^{-.23x})^2}} \tag{7.28}$$

Thus s and L_x are linearly related as are s_x and L_x. In the cases wherein both s_x and L_x are measured it is interesting to note that even though the parameters were measured on the composite impulse response, the relationship between the measured parameters s and L_x appears to roughly follow Eq.(7.28) . Values of x that appear frequently are 10 and 20 dB. From Eq.'s (7.26) and (7.27), we find that

$$L_{20} = 4.6s, \;\; L_{10} = 2.3s, \;\; s_{20} = .88s, \;\; s_{10} = .59s \tag{7.29}$$

The most recent measurements were carried out by Wepman, et al [5][6]. In [5] measurements were taken in the 1850-1990 MHz band for three environment categories: flat rural, hilly rural, and urban high rise, all in the Denver, Colorado area. The entries in Table 7.2 (identical to Table 2.6 of [2]) present 90, 50 and 10 percentiles for s_{20} and L_{20} for three environments, using the curves in [5].

Table 7.2
Percentiles for Three Environments

	L_{20} (in μs)			s_{20} (in μs)		
Environment	90%	50%	10%	90%	50%	10%
Flat Rural	0.2	0.6	5.5	*	0.06	0.3
Hilly Rural	*	0.4	11.2	*	0.1	1.5
Urban High-Rise	1.6	3.8	7.2	0.3	0.7	1.2

*not readable from curves in [5]

Eq.'s (7.29) show that, for the exponential Delay Power Spectrum, the ratio of L_{20} to s_{20} is 5.2. Examining the Urban High Rise environment row in Table 2 we find that the ratios are 5.3,5.4, and 6.0 for the 90, 50 and 10 percentiles, respectively. However the correspondence is worse in the Hilly Rural case (4 and 7.5 for the 50 and 10 percentiles, respectively) and particularly poor in the Flat Rural case (10 and 18.3 for the 50 and 10 percentiles, respectively). In both these cases large discrete paths occur at long delays. Moreover the rationale for a scatter path, the presence of many nearby reflecting and scattering mechanisms producing closely delayed components, as in the city, is more likely to be absent in the Flat Rural than the Hilly Rural environments. Consequently it is not surprising that the exponential Delay Power Spectrum would be inappropriate in the Flat Rural case.

In [6] simultaneous measurements were taken at 950 and 1920 MHz for four environment categories: urban high rise, urban, suburban, and semi-rural, all in the

Philadelphia, Pennsylvania area. Unfortunately, only s_{20} measurements were taken. These are shown in Table 7.2 below (identical to Table 2.7 in [2]). The Urban High Rise results in

Table 7.2
s_{20} percentiles for Four Environments

Environment	s_{20} (in μs) 90%	50%	10%
Semi-Rural	0.05*	0.14	0.50
Suburban	0.05*	0.12	0.35
Urban	0.06	0.14	0.41
Urban High-Rise	0.20	0.65	1.20

* reading value from curves in [6] is difficult.

Table 3 are close to the values in Table 2 for the Urban High-Rise case.

Seidel et al [7] have carried out multipath and path loss measurements at 900 MHz in Hamburg, Stuttgart, Dusseldorf, and Frankfurt, Germany. These measurements concentrated on environment scenarios which produced worst case multipath conditions. Detailed cumulative distributions of multipath parameters for each city and environment were not given. Rather, overall cumulative distributions of L_{10} and s_{20} were provided for all environments combined (macrocells and microcells). Some discussion was presented of worst case measurements of each environment. It is evident that the worst of their normally worst case measurements, i.e., largest L_{10} and s_{20} values are produced by discrete reflections from large, distant objects (e.g., city skyscrapers and mountains).

A measurement campaign similar to [7] was conducted earlier by Rappaport, Seidel, and Singh in four United States cities [8] using the same equipment. These cities were Washington, DC.; Greenbelt, Maryland; Oakland, California; and San Francisco, California. As in [7] the measurements focused on revealing worst case power delay profiles where car usage was high. Major thoroughfares, business districts, interstate highways, bridges, and residential areas were selected for measurements. Table 7.3 presents results from [7]and [8] given in [2].

Table 7.3
Percentiles for L_{10} and s_{20} for US and German Cities

	$L_{10}(\mu s)$		$s_{20}(\mu s)$	
Environment	50%	10%	50%	10%
German Cities [7]	1	3	.3	1.2
US Cities[8]	5	18	2	6.0

From Eq.(7.29) the ratio of L_{10}/s_{20} for the exponential Delay Power Spectrum is 2.6. From Table 7.3 we see that for the German cities the ratio of the estimated values are 3.3, and 2.5, for the 50 and 10 percentiles, respectively, and for the US cities the ratios are 2.5, and 3, for the 50 and 10 percentiles, respectively. These results are remarkably close to the theoretical value for an exponential Delay Power Spectrum. It should be noted that the L_{10}, s_{20} values for the US cities are considerably larger (a factor of the order of 5 to 6) than for the German cities and the latter results, although biased towards worst case values by the measurement procedure, are comparable to the unbiased US city measurements shown in Tables 7.1 and 7.2.

Bultitude and Bedal [18] compare high base station antenna multipath measurements from [9] with low base station antenna multipath measurements at 910 MHz. These measurements were conducted in downtown Ottawa, Canada. Table 7.4 presents the minimum, mean and maximum values of s_{25}, s_{20}, L_{10} and L_{20} for the high base

station antennas. Since the statistics in this table are different from the statistics in the previous

Table 7.4
Minimum, Mean, and Maximum Values of s_{25}, s_{20}, L_{10} and L_{20} for the Urban High Rise Measurements Discussed in [18] .

	Minimum	Mean	Maximum
s_{25}	0.07	0.46	1.26
s_{20}	0.1	0.59	1.27
L_{10}	0.2	1.09	3.00
L_{20}	0.5	3.7	7.2

tables, i.e., 90th, 50th and 10th percentile values of the cumulative distributions, a strict comparison is not possible. To the extent that the distributions are approximately symmetric, the means can be compared to the 50th percentile or median value. When this is done, it is found that median values given in [5] and [6] (shown in Tables 2 and 3 above) for the high rise urban environment are comparable to the mean values for L_{20}, s_{20} in [18]. It is interesting to compare various ratios of the estimated parameters in Table 5 with the theoretical values for the exponential Delay Power Spectrum. Thus from this Table we find that L_{10}/s_{20} has the values 2,1.8, 2.4 for the minimum, mean, and maximum columns, respectively. This may be compared to the theoretical value of 2.6 for the exponential Delay Power Spectrum. The ratio L_{20}/s_{20} has the values 5, 6.3, 5.7 for the minimum, mean, and maximum columns, respectively. This compares favorably with the theoretical value of 5.2.

An extensive series of multipath measurements were carried out by Cox and Leck in New York [10][11] at 910 MHz. The parameters s_{30} and m_{30} were estimated. m is the centroid of the Delay Power Spectrum and m_{30} is the centroid for a Delay Power Spectrum which has been truncated 30 dB down from the peak of the spectrum. For the exponential spectrum s=m and s_{30} is very nearly equal to m_{30}. They scatter-plotted their estimated values of s_{30} vs m_{30} and the points were close (within a factor of two), but above the $s_{30} = m_{30}$ line. This behavior is no doubt due to the presence of strong discrete

paths in some of the cases. From their data we determine that the 90th, 50th and 10th percentiles of s_{30} are given by 0.4, 1.2, and 2.7 μsec, respectively. These results are larger than the urban high rise data in [5] and [6] even when it is considered that s_{30} is being compared to s_{20} ($s_{30} / s_{20} = 1.1$ for the exponential Delay Power Spectrum).

One important feature of the papers [10][11] is that they give selected plots of estimated Delay Power Spectra (called profiles) and the scatter and discrete paths can be clearly seen. To quote from [11], p.210, " Some profiles, Fig.3 for example, exhibit a relatively smooth decrease in scattered power with increasing excess delay, while others, Fig.'s 6(a) and 6(d) for example, are quite "spikey". Also, low to moderate d[8] and s[9] are more often associated with smooth profiles, while large values of d and s are usually produced by one or more intense reflections (spikes in the profile) at large excess delay (see Fig. 6(d))." Because the figures in [10] and[11] depicting profiles are small it is difficult to obtain estimates of s for the scatter modes. Moreover it is not clear that profile examples presented were typical or just presented to prove a point. However , in the absence of other profile data, it was decided to extract parameters for a discrete/scatter model for each of the profiles presented in [10] and [11].

Since the profiles are plotted in dB vs. excess delay time, an exponential profile will show up as a straight line with a negative slope. The figures showed only a single scatter mode of significant strength. Straight line "eyeball" approximations to the continuous part of the spectrum yielded the parameter s for the scatter path in each profile. The discrete components were generally easily identified as to relative power and delay. Unfortunately, determination of the power in the scatter component relative to the discrete components required an extensive analysis to model the measurement process in [10] and [11] for an assumed discrete/scatter model.

Table 7.5 presents the parameters of the discrete/ scatter models obtained as described above for the 9 figures in [10] and[11] that contained measured path profiles. Using each of these models and the theory developed, it is possible to estimate what the rms multipath spread would be if the model were probed by the equipment in [10] and [11] and path profiles were measured. The last two columns in Table 7.5 compare the actual measured s_{30} parameters for each of the 9 cases with predicted s parameters based upon the models for each case as defined by the parameters in Table 7.5. The predicted

[8] our m_{30}

[9] our s_{30}

and measured parameters are close indicating a certain degree of consistency for the models.

In the event that additional measured path profile data does not become available, it will be necessary to draw upon the data in Table 7.5 to provide parameters for the mixed discrete/scatter channel models. Thus, using the data from column 3 of Table 7.5, one may determine that the 90, 50, and 10 percentiles of the delay constant τ for the scatter mode (inferred by linear interpolation of the data entries) are .77,1.24, and 2.2 μs. It is interesting to note that the 50 and 10 percentiles are close to those of the estimated rms multipath spreads of the measured path profiles of the complete 100-profile data base, namely, 1.2 and 2.5 μs, respectively.

With the small data base it is even more difficult to deduce meaningful statistics for the discrete paths. We note that in 5 out of the 9 path profiles, a direct path of significant strength existed. In 2 cases there were no significant resolvable direct paths at all, i.e., essentially a pure scatter model; in 2 there were only direct paths plus a scatter path. and one of these (profile 3 in Table 6) was a direct path with a weak scatter path ; in 2 cases

Table 7.5

Parameters for mixed discrete/scatter channel model obtained from measured path profiles in references [10] and [11]

	Scatter Path Parameters		Discrete Paths' Parameters								Model Spread	Meas. Spread
Profile	p*	$\tau(\mu s)$	h_1	$\xi_1(\mu s)$	h_2	$\xi_2(\mu s)$	h_3	$\xi_3(\mu s)$	h_4	$\xi_4(\mu s)$	$s(\mu s)$	$s_{30}(\mu s)$
1.(Fig.3a[10])	.628	.81	.372	0							.75	.77
2.(Fig.6a[10])	.859	.74	.009	3	.005	6	.116	7	.011	9.5	3.0	3.0
3.(Fig.7a[10])	.044	1.44	.956	0							.42	.39
4.(Fig.8a[10])	1.0	1.24									1.24	1.22
5.(Fig.9a[10]	.247	2.08	.374	0	.374	4	.006	6			2.0	2.1
6.(Fig.3[11])	1.0	1.1									1.1	1.2
7.(Fig.6a[11])	.262	1.4	.586	0	.114	4.5	.037	7.5			2.0	2.0
8.(Fig.6b[11])	.181	1	.239	0	.573	1	.004	4	.004	7	.73	.6
9.(Fig.6d[11])	.47	2.3	.205	1.5	.129	3	.032	5	.162	9	3.3	3.3

* the sum of the powers in the scatter path and the discrete paths has been normalized to unity ,i.e., $p + \sum h_k = 1$.

there were three discrete paths; and the remaining three profiles contained 4 paths, although for one of these profiles (No. 8 in Table 6), the two longest paths were quite weak. The largest path strength was the first or second path in 4 out of the 5 cases in which there was more than 1 discrete path. For purposes of detection analyses, it is probably sufficient to select several or even all of the path profiles in Table 6.

7.2.2 Base-Antenna Below Roof Line

The previous discussion in section 7.2.1 has focused on channels in which the base-station antenna is at or above the roof, the macrocell configuration for wireless communication. Here we consider the case of channels in which the base-station antenna is below the roof level, the microcell configuration for wireless communication.

In contrast to the case of a high base-station antenna, there can be found relatively little in the way of comprehensive measurements of impulse response characteristics for the low base-station antenna in the literature. One can infer such data exists from reading the recent papers reporting the extensive measurement campaigns by Feuerstein, et al [24], and Xia, et al [25].

A default approach we can use for modeling is to adopt the JTC models already presented for the low base-station cases in Section 7.1. However we believe a better approach is to follow the ideas presented in Section 3.2.2 of [2]. In this latter approach separate consideration is given to the *lineal microcell channel* in which the transmitter and receiver are in sight of one another along a street and the *nonlineal microcell channel* in which the transmitter and receiver are on different streets and the line-of -sight between transmitter and receiver is blocked. The *lineal microcell channel* itself can be subdivided into the *urban-canyon channel* and *non urban-canyon channel* . The urban-canyon lineal microcell channel attempts to characterize communication along urban streets with very high buildings that essentially confine reflections to the building sides and the road along the street between the transmitter and receiver. The non urban-canyon

model applies to the other lineal microcell cases: urban, suburban, and rural environments in which additional reflections may occur due to large outlying objects, e.g., bridges, buildings, and mountains. Analogously, the nonlineal microcell channel can be subdivided into urban- canyon and non urban-canyon classes.

Some theoretical work on the urban-canyon lineal microcell channel (from [26]) was discussed in Section 2.1.1.2. of [2]. We call this model the *urban-canyon dielectric building model* for lineal microcells. Fig.7.1 shows the idealized street layout assumed in the x,y ground plane. The origin of coordinates is assumed to be on one corner, marked 0, while the y axis is along one side of the main street on which the base and mobile antennas are positioned. Thus the x axis is parallel to the cross streets. The distance between corresponding points on adjacent streets is W while the width of a cross street is S and the width the main street is W. All buildings are assumed composed of the same material and to extend indefinitely higher than the antennas.

The appropriate input/output relation for this channel is

$$w(t) = \sum_{n=-N}^{N} \varepsilon_n \left(g_n e^{-j2\pi d_n/\lambda} z(t - d_n/c) + h_n e^{-j2\pi d'_n/\lambda} z(t - d'_n/c) \right) \qquad (7.30)$$

The first term in parentheses in Eq. (7.30) is the contribution due to a wall reflected path reflecting from the walls $|n|$ times without hitting the ground. The second term is the contribution due the same number of wall reflections but also a ground reflection. As proven in [26] the projection of these two paths onto the ground are identical and for large separations between base and mobile antennas, they tend to cancel, producing the 40 dB/decade reduction in signal strength with increasing separation discussed in Section 2.1.1.2. of [2]. Positive and negative values for *n* are used to distinguish between the two possible sets of paths having $|n|$ wall reflections. A geometric-optics based analytical solution for the parameters of this model are given in [26] for arbitrary

antenna patterns and polarization and arbitrary constitutive parameters for the walls and ground.

For simulation purposes one may precompute finely sampled values for the amplitudes $(g_n(t), h_n(t))$ and corresponding path lengths $(d_n(t), d'_n(t))$ as a function of mobile position for a desired trajectory of the mobile, e.g., travel down the center of the street. The parameter $\varepsilon_n(t)$ is zero or one, depending upon whether a path-pair is trapped by a cross street or not. While $\varepsilon_n(t)$ changes instantaneously in the model, in reality, diffraction effects will prevent the abrupt loss and reappearance of a reflected wave due to cross street trapping effects. This smooth transition can be incorporated at some future date.

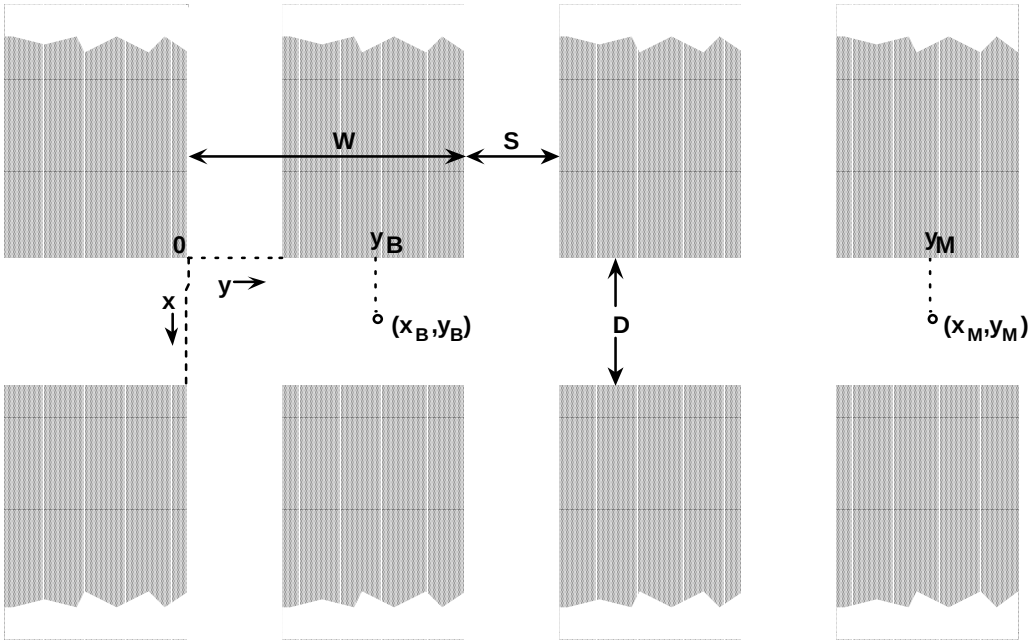

Figure 1 Layout of Main Street Containing Base and Mobile Antennas and Cross Streets for Urban Canyon Dielectric Building Model

Once the mobile position is expressed as a function of time, a table lookup plus interpolation allows computation of $g_n(t), h_n(t), d_n(t)$ and $d_n'(t)$.

For the purposes of Appendix B of the LPI Evaluation Standard the model in Eq.(7.30) is a discrete channel model with transfer function

$$T(f,t) = \sum_{n=-N}^{N} \varepsilon_n(t)\left(g_n(t)e^{-j2\pi d_n(t)/\lambda}\, e^{-j2\pi f d_n(t)/c} + h_n(t)e^{-j2\pi d_n'(t)/\lambda}e^{-j2\pi d_n'(t)f/c}\right) \qquad (7.31)$$

Due to the abrupt change of $\varepsilon_n(t)$ between 0 and 1, the quadratic selective tf power series model for the slow-fading/mild-distortion model and the quadratic selective t power series model for the slow-fading/many fade frequency case are not convergent. However the many-fade-times/small-distortion quadratic selective f power series model is convergent. In fact since the multipath spread for the urban canyon lineal microcell channel is small, this latter model will be particularly appropriate.

To obtain the non urban-canyon lineal microcell channel model it is necessary to add another discrete multipath channel to characterize reflection from large objects, usually at much longer delays. This discrete model is not only identical in form to the discrete channel model employed in the discrete/scatter model for base-station antennas elevated above the roof line, but also appears to have comparable values of excess delays for the discrete paths

For the urban-canyon nonlineal microcell case, as discussed in Section 2.1.2 of [2], propagation may occur via road-guided waves involving both reflections from walls and ground and diffraction around corners, in addition to diffraction over roof edges. The few relevant measurements discussed in Section 2.2.2 of [2] and the theoretical work of

Rossi and Levy [28] suggest that the loss of the direct path by corner turning, causes many hitherto unimportant small multipath components to suddenly become relevant with a consequent increase of multipath spread. The farther the mobile from the base, the larger the number of relevant paths is likely to be. Thus the multipath structure will likely vary from a modest number of discrete resolvable paths near the first corner turn to a virtual continuum of unresolvable paths for large enough separations. To obtain the model for the non urban-canyon nonlineal microcell case we add the same type of discrete model to the urban-canyon case as we did in the corresponding case of the lineal microcell channel.

To the extent that the multipath of the wall reflections are unresolvable, it may make sense to simplify the modeling and employ a scatter model with exponential delay power spectrum for the wall reflections. Then the only difference between the macro and microcell models is that in the latter case the multipath of the scatter component is considerably less than the former case. The presence or absence of the urban-canyon attribute of the microcell channel is then reflected in the absence or presence, respectively, of the discrete channel model for the outlying multipath components.

We now present numerical values for parameters that may be determined from measurements using the review of measurements in [2]. The earliest paper we have found reporting the results of a comprehensive measurement campaign for a low base station antennas is by Bultitude and Bedal [18] at 910 MHz in downtown Ottawa. They actually reported on both high and low base station antenna experiments and the former results were summarized in Section 7.2.1 Each antenna run was over a 5 m length of street during which 128 impulse response estimates were recorded at 3.81 cm intervals. Only LOS paths were measured for the low base station antennas. The paper presents average, mean, and maximum rms multipath spreads and mean L_x values for $x = 10, 15, 20$ and 25 dB. A threshold of 30 dB below the peak was used in computation of the rms delay spreads.

Due to the existence of weak discrete paths with long delays out to the measurable limit of 12.7 μs, the rms multipath spreads for the LOS low base station channels were comparable to those of the high base station antenna channel. Thus the minimum, average, and maximum rms delay spreads for the high base station antenna were 0.098,

0.59, and 1.27 μs, while the corresponding results for the LOS low base station antenna were 0.061, 0.48, and 2.94 μs. (No statistically significant variations with antenna height were found so we have averaged in values for the different antenna heights.)

A visual comparison of some path delay profiles in [18] for the LOS low and non-LOS high base antenna cases(Fig's 2 and 3 of [18]) reveals clearly that the early group of paths in the impulse response was much smaller in width for the LOS low antenna than the non-LOS high antenna case but in both cases there was a number of low level discrete multipath components. This phenomenon is clearly evidenced by comparing mean L_x values for the two situations. Thus mean L_{10} and L_{20} values for the LOS low base station case are 0.24 and 0.73 μs, respectively as opposed to 1.05 and 3.724 μs, respectively, for the non-LOS high base station case. Table 7.6 (Table IV from [18]) presents mean L_{10}, L_{15}, L_{20} and L_{25} values for three city blocks and the four transmit antenna heights from a subset of measured paths in which there were significant multipath components for long delays.

Table 7.6

Widths of Worst-Case Microcellular Channel Average Impulse Response Envelopes

Block	Antenna Height	Widths (μs) at Indicated Power Levels (dB) Below the Envelope Peak			
		−10	−15	−20	−25
1					
	L0	0.20	0.44	0.62	1.10
	M1	0.20	0.44	0.56	1.40
	M2	0.40	0.60	1.05	1.40
	HI	0.2	0.82	1.04	1.08
2					
	L0	0.24	0.52	0.60	0.80
	M1	0.24	0.40	0.56	0.74
	M2	0.20	0.28	0.50	0.64
	HI	0.44	0.82	1.12	7.16
3					
	L0	0.20	0.22	0.38	0.78
	M1	0.20	0.44	0.90	2.84
	M2	0.20	0.30	0.50	0.60
	HI	0.20	0.26	0.96	1.00

Using a high threshold, e.g., L_{15}, should eliminate much of the low level discrete multipath and yield a value much nearer to the L_{15} value that would have occurred in the absence of the discrete multipath. Then, if a mixed discrete/scatter model is assumed with an exponential delay power spectrum for the scatter component, the theoretical relationship between L_{15} and s, Eq. (7.26), may be used to estimate the delay constant of the scatter component which is identical to s in the absence of discrete components. The resulting values of s are sufficiently small sometimes to question whether these numbers should be adjusted to account for the artificial increase in spread caused by the non-zero width of the sounding signal autocorrelation function. For a WSSUS channel one may readily correct the measured value of s.[10] Using Eq.(7.26) and the L_{15} values in Table 7.6 we can construct the set of delay constant estimates in Table 7.7. The last column shows that the corrections are usually negligible and small in any case, for these measurements.

Table 7.7

Estimated Values of Delay Constant for Scatter Component Using L_{15} Values from Table 7.6

Block	Antenna Height	L_{15} μs	τ μs	corrected τ μs
1				
	L0	0.44	.128	.124
	M1	0.44	.174	.171
	M2	0.60	.128	.124
	HI	0.82	.209	.206
2				
	L0	0.52	.150	.146
	M1	0.40	.115	.110
	M2	0.28	.081	.074
	HI	0.82	.238	.236
3				
	L0	0.22	.063	.054
	M1	0.44	.128	.124
	M2	0.30	.087	.080
	HI	0.26	.075	.067

[10] The corrected value of s is given by $\sqrt{s^2 - s_p^2}$ where s_p is the rms delay spread of the probing signal. The measured rms delay spread of the probing signal was .033 microsecond[18], which is close to the theoretical value of .0316 for the prober chip pulse duration of.1 microsecond.

Although the approach used to obtain Table 7.7 is admittedly crude and over-estimates τ due to contamination by the discrete paths, this is all that can be done with the published data. Undoubtedly good data bases exist. It will be necessary to obtain these to produce more accurate estimates of mixed channel parameters. One may obtain the following percentiles from the limited data in the last column in Table 7.7: {.063,.124,.215} microseconds for the 90,50, and 10 percentiles, respectively.

8 VHF/UHF AIR-AIR CHANNEL

Generally speaking, the VHF/UHF Air-Air Channel in the 100-500 MHz band may be modeled by a discrete/scatter channel model. Specifically, over water , there are two discrete paths: a direct LOS path from the transmitting to receiving platform, and a possible specular reflection path. In addition there is a possible scatter path due to scatter from surface irregularities. Over land it is possible to have tilted, relatively flat surfaces, that can produce more than one specular reflection. As will be quantified below, for the theoretical models available, the relative strengths of the specular and scatter paths depend upon the statistics of the surface irregularities and the operating frequency, and the combined strengths of the specular and scatter paths relative to the direct path depends upon the antenna patterns and the surface reflection coefficient.

A simplified modeling of the Air-Satellite channel was carried out by Bello in [19], following along the work of Mallinckrodt[20] and Durrani and Staras[21], which, in turn, are based upon the theory of scattering from rough surfaces presented by Beckman and Spizzichino[22]. In the portion of this theory used in [19]-[21] the assumption is made that the surface height can be modeled as a two dimensional Gaussian process. Such a surface model has been found to be reasonable for the ocean. An extensive literature search was conducted to find models and experimental data for overland communications. Unfortunately, only a single reference was found containing Air-Air channel measurements over land (and sea) and these were at 1 GHz[30]. This report will be discussed at the end of this section.

In [19] it was found that the scatter channel for the ocean surface could be modeled approximately as a complex Gaussian WSSUS channel. A theoretical scattering function was derived for the scatter channel with parameters determined as a function of the surface characteristics, operating frequency, and the relative velocity of the platforms. To obtain models for the Air-Air Channel it was necessary to generalize the approach

used in [19] for the Air-Satellite channel to the Air-Air channel. In this section we summarize the results obtained from this modeling analysis. To simplify the presentation here we assume aircraft are traveling at level flight, a flat earth, and a factorable Scattering Function. The following definitions are used:

λ = wavelength corresponding to carrier frequency.

d = the distance between the aircraft projections on the earth's surface.

h_1, h_2 = altitudes of two aircraft normalized to d.

P_{sp} = power received over the specular path

P_{sc} = power received over the scatter path

P_d = power received over the direct path

P_m = total multipath power $(P_{sp} + P_{sc})$

P = transmitted power

G = product of power gains of the aircraft antennas in the direction of the specular reflection point relative to corresponding product of power gains in the LOS direction.

G_s = product of power gains of the aircraft antennas in the direction of the specular reflection point .

G_d = product of power gains of the aircraft antennas in the LOS direction

Γ = Fresnel reflection coefficient for ideal flat earth surface at specular point. Depends upon polarization.

σ = rms value of height of surface fluctuations.

α = rms value of slope of surface fluctuations.

v_{i_1}, v_{i_2} = components of the velocity vectors of the two aircraft in the vertical plane containing the aircraft.

v_{p_1}, v_{p_2} = components of the velocity vectors of the two aircraft perpendicular to the vertical plane containing the aircraft.

The Doppler Power Spectrum of the scatter path, normalized to unit area, and zero mean Doppler shift, is found to be Gaussian shaped, i.e.,

$$P(\nu) = \frac{1}{\sigma_\nu \sqrt{2\pi}} \exp\left(-\frac{\nu^2}{2\sigma_\nu^2} \right) \tag{8.1}$$

where

$$\sigma_\nu = \frac{2\alpha h_1 h_2}{\lambda \sqrt{1 + (h_1 + h_2)^2}} \sqrt{\left(\frac{v_{p_1}}{h_1} + \frac{v_{p_2}}{h_2} \right)^2 + \frac{1}{1 + (h_1 + h_2)^2} \left(\frac{v_{i_1}}{h_1} + \frac{v_{i_2}}{h_2} \right)^2} \tag{8.2}$$

The actual mean Doppler shift is the same as the Doppler shift of the specular reflection, ν_s, given by

$$\nu_s = \frac{v_{i_2} - v_{i_1}}{\lambda \sqrt{1 + (h_1 + h_2)^2}} , \tag{8.3}$$

while the Doppler shift of the direct path, ν_d, is given by

$$\nu_d = \frac{v_{i_2} - v_{i_1}}{\lambda \sqrt{1 + (h_1 - h_2)^2}} . \tag{8.4}$$

It may also be shown that the Delay Power Spectrum of the scatter path is given approximately by

$$Q(\xi + \xi_s) = \frac{1}{2\sigma_i \sigma_p \, d/c} \exp\left(-\frac{(\sigma_i^2 + \sigma_p^2)}{4\sigma_i^2 \sigma_p^2} \left(\frac{\xi}{d/c} \right) \right) I_0\left(\frac{\left| \sigma_i^2 - \sigma_p^2 \right|}{4\sigma_i^2 \sigma_p^2} \left(\frac{\xi}{d/c} \right) \right) \quad ;\xi \geq 0 \tag{8.5}$$

where ξ_s is the delay of the specular path,

$$\xi_s = \frac{d}{c}\sqrt{1+(h_1+h_2)^2} \tag{8.6}$$

and

$$\sigma_i^2 = 2\alpha^2 \frac{h_1 h_2}{(h_1+h_2)^2} \frac{1}{\left(1+(h_1+h_2)^2\right)^{3/2}} \tag{8.7}$$

$$\sigma_p^2 = 2\alpha^2 \frac{h_1 h_2}{\sqrt{1+(h_1+h_2)^2}} \tag{8.8}$$

I_0 is the modified Bessel Function of the first kind and order 0. Since c is the velocity of light, the factor d/c appearing in the above expressions is the time to propagate over a distance d. The path delay for the direct path is

$$\xi_d = \frac{d}{c}\sqrt{1+(h_1-h_2)^2} \tag{8.9}$$

To a first approximation the sum of the powers received over the specular and scatter paths, called the multipath power, P_m, is constant and given by

$$P_m = P\left(\frac{\lambda}{4\pi d}\right)^2 \left(\frac{1}{1+(h_1+h_2)^2}\right) G_s |\Gamma|^2 \tag{8.10}$$

while the power received over the direct path is given by

$$P_d = P\left(\frac{\lambda}{4\pi d}\right)^2 \left(\frac{1}{1+(h_1-h_2)^2}\right) G_d \tag{8.11}$$

and the ratio of the multipath power to the direct path power is given by

$$\frac{P_m}{P_d} = \frac{1+(h_2-h_1)^2}{1+(h_2+h_1)^2} G|\Gamma|^2 \tag{8.12}$$

P is the transmitted power, i.e., the power fed into the transmitting antenna.

The relative amount of power in the specular and scatter paths depend upon the roughness of the surface in relation to the wavelength and the angle of incidence of the reflection at the specular point. Specifically, the powers received over the specular path and scatter paths, P_{sp} and P_{sc}, respectively, are given by,

$$P_{sp} = P_m \exp\left(-\left(\frac{4\pi\sigma}{\lambda}\right)^2 \frac{(h_1+h_2)^2}{1+(h_1+h_2)^2}\right) \tag{8.13}$$

$$P_{sc} = P_m\left(1-\exp\left(-\left(\frac{4\pi\sigma}{\lambda}\right)^2 \frac{(h_1+h_2)^2}{1+(h_1+h_2)^2}\right)\right) \tag{8.14}$$

There are some experimental results that indicate the scattered power is somewhat less that (8.14) but due to the approximate nature of our analysis we have not introduced this refinement.

The reflection coefficient is given by (see [3] pg. 81)

$$\Gamma = \frac{\sin\theta - z}{\sin\theta + z} \tag{8.15}$$

where

$$z = \begin{cases} \sqrt{\varepsilon_o - \cos^2\theta}\,/\varepsilon_o & ;\ \text{vertical polarization} \\ \sqrt{\varepsilon_o - \cos^2\theta} & ;\ \text{horizontal polarization} \end{cases} \tag{8.16}$$

$$\varepsilon_0 = \varepsilon - j60\sigma_c\lambda \tag{8.17}$$

in which θ is the incidence angle,ε is the dielectric constant of the ground relative to unity in free space, and σ_c is the conductivity of the surface in mhos per meter. For ground and microwave frequencies, it is usually the dielectric constant ε which has the dominant effect on propagation. Table 8.1 (identical to Table 1 of [3]) gives values of typical ground constants.

The previous sections showed that the parameters ξ_0, ν_0, the mean delay and Doppler shift of the scatter path, respectively, and the central moments $(\eta_2, \eta_3, \eta_4), (\mu_2, \mu_3, \mu_4)$ of the Delay and Doppler Spectra, respectively, are the essential data to provide a complete statistical description of the slow fading/small distortion factorable complex Gaussian WSSUS channel. For the small distortion/many fade times case the parameters (η_2, η_3, η_4) are needed in addition to $P(\nu)$ while for the many fade frequencies/slow fading case the parameters (μ_2, μ_3, μ_4) are needed in addition to $Q(\xi)$.

Table 8.1 Typical Ground Constants

Type of Surface	σ_c (mho/m)	ε
Poor Ground	0.001	4
Average Ground	0.005	15
Good Ground	0.02	25
Sea Water	5	81
Fresh Water	0.01	81

Because of the symmetry in the Doppler Power Spectrum, μ_3=0 and $\nu_0 = \nu_s$. In addition, by integration, one may determine that

$$\mu_2 = \sigma_v^2 \tag{8.18}$$

$$\mu_4 = 3\sigma_v^4 \tag{8.19}$$

By integration over the Delay Power Spectrum (8.5) one may show that

$$\xi_0 = (\sigma_i^2 + \sigma_p^2)\frac{d}{c} + \xi_s \tag{8.20}$$

$$\eta_2 = 2\left(\sigma_i^4 + \sigma_p^4\right)\left(\frac{d}{c}\right)^2 \tag{8.21}$$

$$\eta_3 = 8\left(\sigma_i^6 + \sigma_p^6\right)\left(\frac{d}{c}\right)^3 \tag{8.22}$$

$$\eta_4 = 12\left(5\sigma_i^8 + 2\sigma_i^4\sigma_p^4 + 5\sigma_p^8\right)\left(\frac{d}{c}\right)^4 \tag{8.23}$$

The related rms multipath spread, skewness, and excess parameters s, β, and γ defined in Eq's (7.9)-(7.12) are given by

$$s = \sqrt{2}\,\frac{d}{c}\sqrt{\sigma_i^4 + \sigma_p^4} \tag{8.24}$$

$$\beta = -\sqrt{8}\,\frac{1 + b^3}{\left(1 + b^2\right)^{3/2}} \tag{8.25}$$

$$\gamma = 12\,\frac{1 + b^4}{\left(1 + b^2\right)^2} \tag{8.26}$$

where

$$b = \frac{\sigma_p^2}{\sigma_i^2} = \left(h_1 + h_2\right)^2\left(1 + \left(h_1 + h_2\right)^2\right) \tag{8.27}$$

Note that for small h_1 and h_2,b may be neglected in comparison to 1 and $s \approx \sqrt{2}\frac{d}{c}\sigma_i^2,\ \beta \approx -\sqrt{8},\ \gamma \approx 12.$

For simulation purposes it should be sufficient to consider a quasi-stationary model in which over the simulation interval path variation effects are accounted for by the Doppler shifts and Doppler spread. In addition it should be adequate to reference the multipath components to the direct path, i.e., the direct path is normalized to unity. The time variant transfer function of this mixed discrete/scatter channel can then be represented in the form

$$T(f,t) = 1 + e^{j2\pi\xi_\Delta f} e^{j2\pi\nu_\Delta t}\left(g_{sp}e^{j\phi} + g_{sc}T_{sc}(f,t)\right) \tag{8.28}$$

where ϕ is a random phase angle uniformly distributed over 2π,

$$\xi_\Delta = \frac{d}{c}\left(\sqrt{1+(h_1+h_2)^2} - \sqrt{1+(h_1-h_2)^2}\right) \tag{8.29}$$

$$\nu_\Delta = \frac{\nu_{i_2} - \nu_{i_1}}{\lambda}\left(\frac{1}{\sqrt{1+(h_1+h_2)^2}} - \frac{1}{\sqrt{1+(h_1-h_2)^2}}\right) \tag{8.30}$$

$$g_{sp} = |\Gamma|\sqrt{G\frac{1+(h_2-h_1)^2}{1+(h_2+h_1)^2}\exp\left(-\left(\frac{4\pi\sigma}{\lambda}\right)^2\frac{(h_2+h_1)^2}{1+(h_2+h_1)^2}\right)} \tag{8.31}$$

$$g_{sc} = |\Gamma|\sqrt{G\frac{1+(h_2-h_1)^2}{1+(h_2+h_1)^2}\left[1-\exp\left(-\left(\frac{4\pi\sigma}{\lambda}\right)^2\frac{(h_2+h_1)^2}{1+(h_2+h_1)^2}\right)\right]} \tag{8.32}$$

The time-variant transfer function of the scatter channel, $T_{sc}(f,t)$, has been normalized to unit average magnitude squared value and is assumed to have a factorable scatter function with Delay Power Spectrum given by Eq.(8.5) and Doppler Spectrum given Eq.(8.11).

It should be noted that the multipath will usually be significant only when values of h_1 and h_2 are small compared to 1, since otherwise there will normally be sufficient antenna discrimination (i.e., G<<1) to reduce the reflections and/or scattering to negligible values, assuming top-mounted antennas. Moreover, when h_1 and h_2 are small

compared to unity , θ ($\approx h_1 + h_2$) will be small and $|\Gamma|$ will be close to unity , at least for vertical polarization. Then the multipath power P_m becomes nearly equal to the direct path power P_d (see eq(99)). Of course, in the special situation wherein it is decided to receive from a nearby platform at a lower altitude and the antenna beam is adjusted to look down, h_1 and h_2 can be large and θ can be close to 90°.

The power in the specular component relative to the power in the scatter component is given by the ratio

$$\rho = \frac{\exp(-g^2)}{1 - \exp(-g^2)} \tag{8.33}$$

where

$$g = \frac{4\pi\sigma}{\lambda} \frac{h_1 + h_2}{\sqrt{1 + (h_1 + h_2)^2}} = \frac{4\pi\sigma}{\lambda} \sin\theta \tag{8.34}$$

When g becomes small compared with 1 most of the power is in the specular component, while when g becomes large compared to 1, most of the power is in the scatter component. Table 8.2 presents approximate values of σ versus % of occurrence in the North Atlantic. These results are from [20] where the data was stated to be from [23]. To take a numerical example, assume θ ($\approx h_1 + h_2$) is .1 or 5.7 degrees. Table 8.3 shows

Table 8.2
Measured Values of σ

% of Occurrence in North Atlantic	RMS Roughness σ in feet
80	.74
60	1.0
40	3.0
15	6.6

calculations of the specular/scatter power ratio, Eq.(120), as a function of carrier frequency for each of the four values of σ in Table 8.2. Note that for the calm seas, σ=.74, the multipath is almost purely specular over the whole band from 100 to 500 MHz, while for rough seas, σ=6.6, the reverse is true.

As θ increases the specular component decreases in strength relative to the scatter component. Table 8.2 shows calculations of the specular/scatter power ratio as a function of carrier frequency for each of the four values of σ in Table 8.2 for θ= 90°. Only frequencies from 100 to 300 MHz are shown because the specular component is negligible at higher frequencies

The Doppler spread, multipath spread, and various central moment parameters depend upon the rms surface slope parameter α. For the sea, at least, a value of .1 is regarded as extreme by Mallinckrodt[20] , but Cox and Munk[31] show values extending up to .28 for wind velocities up to 30 knots. Values to use over ground need to be established.

We consider further numerical examples for the small θ case to illustrate the theory. Assume the aircraft are at the same height h, and one is following the other with velocity vectors in the vertical plane containing the aircraft. Then, the rms Doppler spread is given by

$$\sigma_\nu = 2\alpha h \frac{v_\Sigma}{\lambda} \tag{8.35}$$

Table 8.3

Specular/Scatter Power Ratios Versus Frequency and RMS Surface Height for Incidence Angle = 5.7°

Carrier Freq. in MHz.	σ=.74 ft	σ=1.0 ft	σ=3.0 ft	σ=6.6 ft
100	111.017	60.5679	6.29745	0.96084
150	49.0646	26.6438	2.54321	0.251401
200	27.3822	14.7721	1.24514	0.0611823
250	17.3473	9.27917	0.661324	0.0117183
300	11.8975	6.29745	0.361332	0.0016315
350	8.61255	4.50173	0.196755	0.00016037
400	6.48174	3.33847	0.104486	1.105E-05
450	5.02212	2.54321	0.0532606	5.33E-07
500	3.97933	1.97668	0.0257563	1.80E-08

Table 8.4

Specular/Scatter Power Ratios Versus Frequency and RMS Surface Height for Incidence Angle = 90°

Carrier Freq. in MHz.	σ=.74 ft	σ=1.0 ft	σ=3.0 ft	σ=6.6 ft
100	1.12749	0.45696	2.9369E-05	0
150	0.31516	0.0794653	0	0
200	0.085638	0.00977114	0	0
250	0.0192673	0.00071285	0	0
300	0.00330859	2.9369E-05	0	0

where v_Σ is the sum of the velocities of the two aircraft,

$$v_\Sigma = v_{i_1} + v_{i2} \tag{8.36}$$

At 733 ft/sec (500 mph), 500 MHz(λ=2 ft), and h=α=.1, the rms Doppler spread becomes 7.3 Hz. At 100 MHz, the rms Doppler spread reduces to 1.5 Hz. Smaller values of α and h will cause these spread values to reduce proportionately. The difference between the Doppler shift of the specular path and the direct path is given approximately by

$$\nu_s - \nu_d = 2h^2\left(\frac{v_\Delta}{\lambda}\right) \tag{8.37}$$

where

$$v_\Delta = v_{i_2} - v_{i_1} \tag{8.38}$$

With the above approximations the rms multipath spread, s, simplifies to

$$s = \frac{\alpha^2}{\sqrt{2}}\frac{d}{c} \tag{8.39}$$

or, for α=.1, s = .0071 d/c. Thus at d=50,000 ft. the rms multipath spread is approximately 350 ns for α=.1. The difference between the delay at the specular point and the direct path delay is given by

$$\xi_s - \xi_d = 2h^2\frac{d}{c} \tag{8.40}$$

which for h=.1 and d=50,000 ft. yields a value of 1 μs for the difference.

There are a large number of parameters needed to specify this Air-Air channel model: aircraft positions and velocities, antenna discrimination(G) and polarization, surface constitutive parameters(dielectric constant and conductivity), rms surface slope and height, and operating frequency. For the purposes of Appendix B of the LPI

Evaluation Standard, it makes sense to consider a restricted set of scenarios, especially due to the lack of statistics for parameters and the approximate nature of the channel model. We now consider such a restricted set.

We consider then a selection of positions and velocity vectors for the aircraft .In the PCS models the user selects the mobile velocity. However, in the Air-Air channel there are, in general, three velocity components for each vehicle. We assume level flight to reduced these to two for each vehicle, which is still a lot for the user to specify. The aircraft

motion will be constrained so that velocity vectors are in-plane which corresponds to one aircraft directly following or approaching the other. Then only two velocities need to be selected.

With regard to positions, we select *near*, *medium*, and *far* relative positions for the aircraft, say d= 5000, 50,000, and 500,000 feet. For the medium and far configurations the aircraft have the same height, say 25,000 feet, while for the near configuration one aircraft is at 25, 000 feet while the other is at a much lower altitude, say 5000 feet, with the higher aircraft antenna focused down towards the low altitude aircraft. Table 8.5 presents three geometry/velocity configurations.

For the readers interest, Table 8.6 presents example calculations of various black box model parameters for 48 scenarios corresponding to α =.1. For other values of α only the rms multipath and Doppler spread columns need be changed. Since the multipath spread varies as α^2 and the Doppler spread varies as α, the scaling is simple. From Cox and Munk [31], it seems reasonable to select two values of α corresponding to *low* wind speed (α=.1) and *high* wind speed (α=.25) . With regard to the rms surface slope, from Table 8.2 it may be seen that we can select three values to cover a range of sea roughness: *smooth*(σ=.74 ft*), medium*(σ=2 ft*),* and *rough*(σ= 6.6 ft). The antenna power gain in the specular direction relative to the direct path direction can vary widely. We arbitrarily select three values: *low* (G=.1), *medium* (G=.5), *high* (G=.9).

It should be reiterated that the above model is based upon a two dimensional Gaussian distribution for surface heights which has only been validated for the ocean. As mentioned at the beginning of this section, one report presenting Air-Air channel measurements was located [30] which presented results for land and sea over-flight. The experiments were conducted to evaluate the effect of multipath on an aircraft collision avoidance system. .5 microsec pulses were transmitted at 1030 MHz between two aircraft flying at the same altitude (9500 - 12000 ft.) but at diverging paths so that for each run impulse response envelopes could be collected at grazing angles θ from around 5 to 75 degrees. Both top and bottom mounted antennas were used. The details of the antenna patterns were not given but it seems reasonable to assume that they were designed to be uniform in azimuth. Most of the data analysis was concerned with quantifying the strength of the multipath signal relative to the direct path signal and determining the utility of using top mounted antennas to reduce multipath. However some qualitative information on multipath spread and Doppler spread could be inferred.

Over the ocean, a frozen lake, and smooth land (desert, flat plain) the multipath was quoted to be a " slightly distorted pulse-like replica of the direct pulse signal followed by a low level noise-like waveform lasting ten's of microseconds" with the earliest multipath having the delay corresponding to reflection from the specular reflection point. Over rough land (mountains, forested areas, and suburban areas) the pulse-like component vanished and only the noise-like component was present, but at a low-level. Details on the computation of multipath power are not presented so the numbers given will have to be accepted on faith. The median multipath-to-signal ratio for the bottom-to-bottom antenna configuration with a 30 degree grazing angle (i.e.,$\theta = 30°$), was quoted to be as high as 0 dB for the over ocean paths, -5 dB over a frozen lake, -15 dB over smooth land, and -20 dB over rough land.

Table 8.5

Three Geometry/Velocity Configurations for Air-Air Channel

CONFIG	AIRCRAFT GEOMETRY					AIRCRAFT VELOCITIES			
	D feet	H1 feet	H2 feet	h1= H1/D	h2= H2/D	Vi1 fps	Vi2 fps	Vp1 fps	Vp2 fps
near	5,000	25,000	5,000	5	1	550	660	0	0
medium	50,000	25,000	25,000	.5	.5	550	660	0	0
far	500,000	25,000	25,000	.05	.05	550	660	0	0

Table 8.6
Black Box Channel Parameters for Different Air-Air Scenario's Assuming α=.1

SCENARIO SPECIFICATION					BLACK BOX CHANNEL PARAMETERS							
config	freq MHz	multipath power (dB rel. direct)	rel. scatt pwr	rel. spec pwr	rms Dop sprd (Hz)	rms mult sprd (ns)	b	k	rel spec del (μs)	rel spec Dop (Hz)	specular power (dB rel. direct)	scatter power (dB rel. direct)
near	100	0,-5,-10,-15	1(0)	0(1)	1.84	1162	1332	.023	9.8	.86	-∞(0,-5,-10,-15)	0,-5,-10,-15(-∞)
near	500	0,-5,-10,-15	1(0)	0(1)	9.22	1162	1332	.023	9.8	4.29	-∞(0,-5,-10,-15)	0,-5,-10,-15(-∞)
med.	100	0,-5,-10,-15	1(0)	0(1)	6.05	279	2	.125	20.7	3.22	-∞(0,-5,-10,-15)	0,-5,-10,-15(-∞)
med.	500	0,-5,-10,-15	1(0)	0(1)	30.2	279	2	.125	20.7	16.1	-∞(0,-5,-10,-15)	0,-5,-10,-15(-∞)
far	100	0,-5,-10,-15	1(0)	0(1)	1.2	3483	.01	.025	2.49	.05	-∞(0,-5,-10,-15)	-0,-5,-10,-15(-∞)
far	500	0,-5,-10,-15	1(0)	0(1)	6.0	3483	.01	.025	2.49	.273	-∞(0,-5,-10,-15)	-0,-5,-10,-15(-∞)

.

Since channel pulse responses were evaluated at 20 times /second, variations faster than 20 Hz were not determinable. Except for the case of the frozen lake overflight, it was found that successive multipath samples were "essentially uncorrelated" indicating a fading spectrum for the envelope which extended beyond 20 Hz. Moreover, the statistics of the fluctuations were well approximated by a Rayleigh distribution. These facts indicate that a scatter channel model with a Doppler power spectrum width larger than 20 Hz dominated the multipath.

Using Eq.'s (8.2) and (8.24) we find that for an altitude of 10,000 ft, airplane velocities of 300 ft./sec (this velocity was a guess: no airplane velocities were given), and an rms surface slope of .05, the rms multipath spread is 43.5 nanoseconds and the rms Doppler spread is 13 Hz. Since the rms multipath spread is much less than the 500 ns pulse width, a pulse-like appearance of the multipath will occur even with the scatter channel model. In addition an rms Doppler spread of 13 Hz results in a 52 Hz width of the Doppler spectrum at the ± 2 standard deviation points. Impulse response snapshots occurring at a 20 Hz rate will then show negligible correlation, as has been observed. Thus the experimental results seem to support the theoretical calculations of the Gaussian surface model for α=. 05.

However, from the measurements it became clear that a rough earth surface reduces the strength of the scatter channel to a level that should be harmless to most communication and detection systems. Strictly speaking this conclusion is appropriate only to the 1 GHz operating frequency used in the data collection. If the operating frequency and grazing angles are lowered to the extent that the surface is no longer electrically rough, specular reflection may result. However, even at 100 MHz, with a wavelength of 10 feet, the physically rough surface will probably still be rough electrically at most grazing angles. But the opposite conclusion is likely over smooth land, even though the smooth land appeared to be electrically rough at nonlineal. In addition the resulting specular reflection channel will probably be stronger than the -15 dB level measured for the smooth land multipath relative to the direct path channel at a 30 degree grazing angle. For the frozen lake case the time constant of the fluctuations was of the order of one second and variations in the strength of the multipath were only of the order of 2 dB, which indicates a primarily specular multipath. *It is clear that, for overland channels, depending on the smoothness of the surface and the grazing angle, the*

multipath in the 100 - 500 MHz band can cover the gamut from scatter to specular. Moreover, it appears that the specular case yields higher multipath power than the scatter case.

To compute multipath and Doppler spread for smooth and medium roughness terrain we will use the Gaussian surface model for overland channels with α=.05. This factor of 2 reduction in α causes a decrease of the rms Doppler spread by a factor of 2, and a decrease of the rms Multipath spread by a factor of 4 relative to the values listed in Tables 8.6. Table 8.7 presents the revised spreads corresponding to α=.05. For rough terrain we arbitrarily use α=.5 because it yields multipath spreads of several microseconds in agreement with measurements.

Table 8.7
Black Box Channel Parameters for Different Air-Air Scenario's Assuming α=.05

SCENARIO SPECIFICATION					BLACK BOX CHANNEL PARAMETERS							
config	freq MHz	multipath power (dB rel. direct)	rel. scatt pwr	rel. spec pwr	rms Dop sprd (Hz)	rms mult sprd (ns)	b	k	rel spec del (μs)	rel spec Dop (Hz)	specular power (dB rel. direct)	scatter power (dB rel. direct)
near	100	0,-5,-10,-15	1(0)	0(1)	.92	291	1332	.023	9.8	.86	-∞(0,-5,-10,-15)	0,-5,-10,-15(-∞)
near	500	0,-5,-10,-15	1(0)	0(1)	4.61	291	1332	.023	9.8	4.29	-∞(0,-5,-10,-15)	0,-5,-10,-15(-∞)
med.	100	0,-5,-10,-15	1(0)	0(1)	3.03	70	2	.125	20.7	3.22	-∞(0,-5,-10,-15)	0,-5,-10,-15(-∞)
med.	500	0,-5,-10,-15	1(0)	0(1)	15.1	70	2	.125	20.7	16.1	-∞(0,-5,-10,-15)	0,-5,-10,-15(-∞)
far	100	0,-5,-10,-15	1(0)	0(1)	.6	871	.01	.025	2.49	.05	-∞(0,-5,-10,-15)	-0,-5,-10,-15(-∞)
far	500	0,-5,-10,-15	1(0)	0(1)	3.0	871	.01	.025	2.49	.273	-∞(0,-5,-10,-15)	-0,-5,-10,-15(-∞)

9. VHF/UHF AIR-GROUND CHANNEL

We define the Air-Ground channel, as the special case of the Air-Air channel in which one terminal is stationary and situated so that under normal operating conditions there is a clear line-of-sight from the aircraft antenna to the ground terminal antenna. In terms of the parameters defined in the previous section, $v_{i_2} = v_{p_2} = 0$, and $h_2 << h_1$. The generic forms for the Doppler and Delay Power Spectra, Eq's (8.1) and (8.3), respectively, remain the same. However the parameters simplify when h_2 is neglected in comparison to h_1 and one platform is stationary.

Table 9.1 presents near, medium, and far geometry/velocity configurations for the Air-Ground channel analogous to those chosen in Table 8.5 for the Air-Air channel. In this case we assumed that the ground antenna was at an elevation of 50 ft. Also for the near scenario the aircraft velocity has been reduced to 300 ft/sec. Assuming a two dimensional Gaussian surface, appropriate to an ocean surface, Table 9.2 presents theoretical calculations of Black Box channel parameters for different scenario's assuming α=.1. Notice that the reciprocal rms multipath spread for the scatter channel is large relative to typical channel bandwidth allocations for all the scenario's as is the reciprocal of the differential delay between the direct path and the specular path. This means that for most over-ocean communication applications the channel is subjected to little or no frequency selective fading and may be modeled simply as a complex time varying multiplier, i.e. as a flat fading channel. It is also important to note that since the Doppler spreads of the scatter channel and the differential Doppler shifts between the direct and specular paths are very small, the fading is predicted to be usually very slow, e.g., a time constant of seconds.

As mentioned previously, the use of the Gaussian surface model has not been validated for over-land communication channel modeling. In the previous section on Air-Air channel models we have found the Gaussian surface model with α=.05 yields values

of multipath and Doppler spreads comparable with the crude estimates of multipath and Doppler spread presented in [30] for (non-rough) over-land Air-Air channel measurements of multipath. Table 9.3 presents Black Box parameters for α=.05. These differ from the parameters in Table 9.2 only in a decrease of Doppler spread by a factor of two and a decrease of Delay spread by a factor of 4. These reductions lead to even less frequency selective fading and longer fading time constants.

Table 9.1

Three Geometry/Velocity Configurations for Air-Ground Channel

CONFIG	AIRCRAFT GEOMETRY					AIRCRAFT VELOCITIES			
	D feet	H1 feet	H2 feet	h1= H1/D	h2= H2/D	Vi1 fps	Vi2 fps	Vp1 fps	Vp2 fps
near	5,000	10,000	50	2	.01	300	0	0	0
medium	50,000	15,000	50	.3	.001	550	0	0	0
far	500,000	15,000	50	.03	.0001	550	0	0	0

Table 9.2
Black Box Channel Parameters for Different Air- Ground Scenario's Assuming α=.1

SCENARIO SPECIFICATION					BLACK BOX CHANNEL PARAMETERS							
config	freq MHz	multipath power (dB rel. direct)	rel. scatt pwr	rel. spec pwr	rms Dop spread (Hz)	rms mult spread (ns)	b	k	rel spec del (ns)	rel spec Dop (Hz)	specular power (dB rel. direct)	scatter power (dB rel. direct)
near	100	0,-5,-10,-15	1(0)	0(1)	.027	1.26	20.4	.002	89.4	.11	-∞(0,-5,-10,-15)	0,-5,-10,-15(-∞)
near	500	0,-5,-10,-15	1(0)	0(1)	.133	1.26	20.4	.002	89.4	.54	-∞(0,-5,-10,-15)	0,-5,-10,-15(-∞)
med.	100	0,-5,-10,-15	1(0)	0(1)	.01	4.13	.099	.00091	28.7	.029	-∞(0,-5,-10,-15)	0,-5,-10,-15(-∞)
med.	500	0,-5,-10,-15	1(0)	0(1)	.052	4.13	.099	.00091	28.7	.14	-∞(0,-5,-10,-15)	0,-5,-10,-15(-∞)
far	100	0,-5,-10,-15	1(0)	0(1)	.0011	46.8	.00091	.0001	3.0	.0003	-∞(0,-5,-10,-15)	-0,-5,-10,-15(-∞)
far	500	0,-5,-10,-15	1(0)	0(1)	..0055	46.8	.00091	.0001	3.0	.0016	-∞(0,-5,-10,-15)	-0,-5,-10,-15(-∞)

Table 9.3

Black Box Channel Parameters for Different Air- Ground Scenario's Assuming α=.05

SCENARIO SPECIFICATION					BLACK BOX CHANNEL PARAMETERS							
config	freq MHz	multipath power (dB rel. direct)	rel. scat t pwr	rel. spe c pwr	rms Dop spread (Hz)	rms mult spread (ns)	b	k	rel spec del (ns)	rel spec Dop (Hz)	specular power (dB rel. direct)	scatter power (dB rel. direct)
near	100	0,-5,-10,-15	1(0)	0(1)	.013	.32	20.4	.002	89.4	.11	-∞(0,-5,-10,-15)	0,-5,-10,-15(-∞)
near	500	0,-5,-10,-15	1(0)	0(1)	.067	.32	20.4	.002	89.4	.54	-∞(0,-5,-10,-15)	0,-5,-10,-15(-∞)
med.	100	0,-5,-10,-15	1(0)	0(1)	.005	1.03	.099	.00091	28.7	.029	-∞(0,-5,-10,-15)	0,-5,-10,-15(-∞)
med.	500	0,-5,-10,-15	1(0)	0(1)	.026	1.03	.099	.00091	28.7	.14	-∞(0,-5,-10,-15)	0,-5,-10,-15(-∞)
far	100	0,-5,-10,-15	1(0)	0(1)	.00055	11.7	.00091	.0001	3.0	.0003	-∞(0,-5,-10,-15)	-0,-5,-10,-15(-∞)
far	500	0,-5,-10,-15	1(0)	0(1)	.0027	11.7	.00091	.0001	3.0	.0016	-∞(0,-5,-10,-15)	-0,-5,-10,-15(-∞)

An exhaustive literature search on Air-Ground channel measurements yielded only two reports [32][33]. In [32] propagation experiments were conducted at S band(3.2 GHz) and at L band(1.053 GHz) in order to characterize multipath for IFF systems. Measurements were conducted over forested, open grass, and ocean surfaces. The 3.2 GHz direct sequence pseudo-noise probe used a 5 ns pulse width while the 1.053 MHz probe use a wide pulse of 3.5 microsec.

As for the Air - Air flights only very low level multipath was observed in travel over forested areas, with peak values 20 dB or more below the direct path. The multipath spread was quoted to be 40 to 60 ns. To get the Gaussian surface model to produce multipath spreads of this order with the geometry of the experiments requires a value of α of the order of .5 as for the Air - Air channel. The durations of fades at various levels relative to the median (range-normalized) level were computed for each run. These duration's are clearly inversely proportional to the (helicopter) aircraft speed which was 70 to 100 knots(119 to 170 ft/sec). Most of the fades are smaller than 1 dB and at these velocities can last for many seconds.

Some measurements were taken over grassland. A strong specular reflection occurred which was sometimes slightly distorted and fluctuating. This was thought to be the result of more than one unresolved specular reflection. In addition, there was apparently enough rough surfaces illuminated by the composite antenna patterns, to produce the low level multipath observed in travel over forested areas. During portions of runs, the received signal showed periods of severe fading (20 to 40 dB fade depths), sometimes quasiperiodic in appearance and sometimes not.

The other set of propagation experiments [33] were conducted at L band (around 1 GHz) and at C band (around 5 GHz) for the purpose of measuring multipath that would affect Microwave Landing Systems. Surroundings chosen for the experiments included terrain appropriate for, or in the vicinity of, landing fields and sometimes included

buildings. Multiple specular paths were measured using direction of arrival estimation techniques in conjunction with vertical and horizontal antenna arrays. At L band the peak specular path strengths ranged from -5 dB to 1 dB while at C band the peak strengths varied from -10 dB to -2 dB relative to the direct path strength. No measurements were made of multipath spread or Doppler spread.

The multiple specular paths were found to arrive at nearly the same azimuth angle as the direct path. These paths are due to the existence of fortuitously oriented, flat enough and large enough terrain "facets" and buildings to reflect significant amounts of energy forward. A discrete multipath model is clearly appropriate for this type of channel. The measurements in [15] at L Band (around 1 GHz) which involve low elevation angles for the airplane line of sight (between 2 and 6 degrees) and relatively smooth terrain, indicate that the number of specular paths is rarely greater than 3 and is usually equal to 2, one of which arrives at an angle expected for the normal specular path. An examination of the plots in Fig.'s 5.10 - 5.39 of [15] shows that the 90,50, and 10 percentile values were -10.5, -4, and -.5 dB below the direct path for this normal specular path. For the vast majority of cases the other specular path was weaker and had an arrival angle between the specular path arrival angle and the direct path arrival angle. This angle was usually at around 1 degree lower than the arithmetic mean of the normal specular and the direct path arrival angles.

Calculations of multipath spread for the multiple specular paths indicate small multipath spreads as for the theoretical calculations presented above for the Gaussian surface model. Thus an appropriate first order black box model for the Air-Ground channel is a complex multiplier with a steady component to represent the direct path and a fluctuating component to represent the multipath. Thus if z(t) represents the complex envelope of the input signal and w(t) represents the complex envelope of the output signal, the input-output relation for the simplified model is given by

$$w(t) = z(t)\left(1 + g_m G_0(t)\right) \tag{9.1}$$

where we have normalized the direct path to unity, $G_0(t)$ is a complex time-variant unity-rms factor that represents the net effect of the multipath components, and g_m represents the rms value of the multipath relative to the direct path. $G_0(t)$ may also be recognized as the first term in an f power series model(see Eq.(6.8) of the multipath channel transfer function.

The statistics of $G_0(t)$ will change with the environment. In considering overland flights for the Air-Ground channel it is necessary to introduce the *multifacet* terrain category. This category applies to terrain with multiple reflecting flat surfaces that produces multiple specular paths. When there are multiple specular reflections from the ground corresponding to the multifacet terrain model, we find that

$$G_0(t) = \sum_{k=1}^{K} \sqrt{h_k}\, e^{j\theta_k} e^{j2\pi\nu_k t} \tag{9.2}$$

where h_k, θ_k, and ν_k represent the strength, phase (assumed random and uniformly distributed), and Doppler shift of the k^{th} specular component relative to the direct path. The Doppler shift ν_k is given by

$$\nu_k = \frac{V}{\lambda}\mathrm{Cos}\,\alpha_k - \frac{V}{\lambda}\mathrm{Cos}\,\alpha_0 \tag{9.3}$$

where V is the aircraft velocity , λ is the wavelength at the carrier frequency, α_k {k=1,..K} is the angle between the velocity vector of the aircraft and the ray that corresponds to the k^{th} specular path, and α_0 is the angle between the velocity vector of the aircraft and the direct path. For the models used here, assuming level flight of the aircraft, it is sufficient to replace α_k by the elevation angle of the corresponding ray as it is received at the ground antenna. The elevation angle of the direct path is $\tan^{-1}(h_1 - h_2)$ and of the theoretical specular path is $\tan^{-1}(h_1 + h_2)$, where h_2 is the normalized height of the ground terminal.

The statistics of $G_0(t)$ will approach complex Gaussian if the number of paths K becomes large and if no one path predominates in strength. For a single specular path, appropriate to an electrically smooth surface (terrain or ocean), only the first term in Eq.(9.2) would be used. For a scatter path representation of the multipath, $G_0(t)$ would be a complex Gaussian process with an appropriate Doppler power spectrum. In view of the small number or specular paths found in [15] at 1 GHz, however, it is hard to justify the complex Gaussian approximation at VHF/UHF frequencies, since the surface becomes smoother electrically at the latter frequencies. However at C band where the surface is rougher electrically and more specular paths have been observed, the complex Gaussian model should be useful.

10 VHF/UHF MOBILE-TO-MOBILE AND MOBILE-BASE STATION (30-500 MHZ)

The physical aspects of the VHF/UHF Mobile channels discussed in this section are similar to those of the cellular/PCS channels discussed in Section 7 . Both of these channels partition into two classes: those in which one of the terminals is at the ground mobile level and the other is elevated above the roof line and those in which both terminals are at the ground mobile level. From a channel modeling viewpoint, the lower operating frequency band and the mobility of both ground terminals distinguish the VHF/UHF Mobile channels from the cellular/PCS channels .

Unfortunately there exist no measurement campaigns dedicated to estimating the multipath characteristics of the VHF/UHF Mobile channel as there were for the Cellular/PCS channels. We shall assume that the multipath spreads and structures observed for the latter channels may be used for the VHF/UHF channels. Thus we propose to use the mixed discrete/scatter channel models for these channels also but with an adjustment of Doppler spread and shifts appropriate to the lower frequency band. In addition, in the case of Mobile-Mobile channels we need to consider the possible effect of having both terminals mobile on the shape of the Doppler power spectrum.

While propagation effects do vary with operating frequency, the multipath delays are strongly affected by the physical location of reflecting and scattering objects. Moreover there are considerable variations in observed multipath delay profiles at a *fixed* operating frequency as the location of terminals changes within urban and suburban environments. Thus, while the absence of measurements force us to use the Cellular/PCS channel multipath models and parameters for the VHF/UHF Mobile channel, we do not believe that gross errors will be committed thereby.

In view of the above, we now focus on determining the Doppler spectrum to be used for the mixed discrete/scatter model of the Mobile - Mobile channel. Using a geometrical optics interpretation, the transmitter is assumed to launch a continuum of rays with strengths dependent on the transmitter antenna pattern. Only a fraction of these rays result in rays arriving at the receiver. Assuming, the direct path is blocked, the following mechanisms are involved in transferring energy to the receiver:

1) single or multiple reflections from objects
2) diffraction around obstacles
3) scattering from objects

Let θ, ϕ represent the elevation and azimuth angle coordinates, respectively, for a ray arriving at the receiver, assuming a receiver-centered spherical coordinate system and let α,β represent the elevation and azimuth angle coordinates, respectively, for a ray leaving the transmitter, assuming a transmitter-centered spherical coordinate system. Then it may be shown that the total Doppler shift, ν, on a received ray with angular coordinates θ, ϕ due to energy transmitted by a ray with coordinates α,β , is given by

$$\nu = \frac{v_T}{\lambda}\cos\alpha\cos(\gamma_T - \beta) + \frac{v_R}{\lambda}\cos\theta\cos(\gamma_R - \phi) \tag{10.1}$$

where v_T, γ_T and v_R, γ_R are the speed and azimuth direction, respectively, of the velocity vectors of the transmitter and receiver, respectively.

Due to the comparable heights of the transmitter and receiver the rays leaving the transmitter and arriving at the receiver which are successful in transferring energy have small elevation angles. To simplify the analysis we assume the elevation angles are zero, and modify (10.1) accordingly,

$$\nu = \frac{v_T}{\lambda}\cos(\gamma_T - \beta) + \frac{v_R}{\lambda}\cos(\gamma_R - \phi) \tag{10.2}$$

Assuming azimuthally uniform antenna patterns, the Doppler power spectrum will be proportional to the probability density function (pdf) of ν in Eq.(10.2).

It is customary to assume that the azimuth angles β,ϕ are independent and uniformly distributed over 2π radians. This assumption is reasonable when diffraction and scattering play a significant role in transferring energy from transmitter to receiver. However when the mechanism of energy transfer is via single or multiple reflections, β and ϕ will be related. This may be understood by representing a multiply reflected ray as an equivalent virtual direct path by using images of the transmitter. For Mobile - Mobile communications within line-of sight, it is shown in [26] that

$$\phi = \begin{cases} -\beta & ;\text{odd number of wall reflections} \\ \beta - \pi & ;\text{even number of wall reflections} \end{cases} \tag{10.3}$$

when the coordinate systems at the transmitter and receiver are translated versions of one another .Substitution of (10.3) into (10.2) yields

$$\nu = \begin{cases} \sqrt{\left(\frac{v_T}{\lambda}\right)^2 + \left(\frac{v_R}{\lambda}\right)^2 + \frac{2v_T v_R}{\lambda^2}\cos(\gamma_T + \gamma_R)}\cos(\phi + \alpha_{odd}) & ;\text{odd no. refl.} \\ \sqrt{\left(\frac{v_T}{\lambda}\right)^2 + \left(\frac{v_R}{\lambda}\right)^2 - \frac{2v_T v_R}{\lambda^2}\cos(\gamma_T - \gamma_R)}\cos(\phi + \alpha_{eve}) & ;\text{even no. refl.} \end{cases} \tag{10.4}$$

where α_{odd} and α_{eve} are phases dependent upon the parameters $v_T, v_R, \gamma_T, \gamma_R, \lambda$. If one assumes a uniform distribution of ϕ, then the pdf of ν becomes independent of α_{odd} and α_{eve}. If the mobiles are moving directly at one another or away from one another, corresponding to $\gamma_T = \pm 90^\circ, \gamma_R = \mp 90^\circ$ the factor multiplying the cosine functions in (10.5) reach the maximum value of $(v_T + v_R)/\lambda$. On the other hand if one mobile is directly following the other, the factors reach the minimum value $|v_T - v_R|/\lambda$.

Unfortunately, derivations of such relationships have not been carried out for the non line-of-sight case. As a first order approach we will confine our model to Eq.(10.2) in which ϕ and β are independent and uniformly distributed over 2π. Then the statistics are independent of the vehicles' directions of motion parameters, γ_T, γ_R. Since ν in Eq.(10.2) is the sum of two independent random variables, we may express the pdf of ν as the convolution of the pdf's of each term in Eq.(10.2). These individual pdf's, which correspond to the Doppler spectrum for a land mobile channel with one terminal fixed, have been calculated by Clarke[4] and Jakes[3]. Specifically they are of the form

$$W(\nu) = \frac{\text{Rect}\left(\frac{\nu}{2\nu_0}\right)}{\pi\sqrt{\nu_0^2 - \nu^2}} \tag{10.5}$$

where ν_0 is the maximum Doppler shift corresponding to the vehicle speed and

$$\text{Rect}(x) = \begin{cases} 1 & ;|x| < 1/2 \\ 0 & ;|x| \geq 1/2 \end{cases} \tag{10.6}$$

The corresponding maximum Doppler shifts for the transmitter and receiver are

$$\nu_T = \frac{v_T}{\lambda} \; ; \; \nu_R = \frac{v_R}{\lambda} \tag{10.7}$$

Thus we may express the desired Doppler power spectrum via the following convolution integral

$$P(\nu) = \int \frac{\mathrm{Re\,ct}\left(\frac{u}{2\nu_R}\right)}{\pi\sqrt{\nu_R^2 - u^2}} \frac{\mathrm{Re\,ct}\left(\frac{\nu - u}{2\nu_T}\right)}{\pi\sqrt{\nu_T^2 - (\nu - u)^2}} du \tag{10.8}$$

It is convenient to define normalized Doppler shift variables and power spectra. Thus we define the parameters

$$\nu_{max} = \mathrm{Max}(\nu_T, \nu_R) \quad ; \nu_{min} = \mathrm{Min}(\nu_T, \nu_R) \tag{10.9}$$

and the ratio

$$a = \frac{\nu_{min}}{\nu_{max}} \tag{10.10}$$

The Doppler power spectrum $P(\nu)$ can then be expressed in terms of a normalized Doppler power spectrum $P_0(\nu)$

$$P(\nu) = \frac{1}{\nu_{max}} P_0\left(\frac{\nu}{\nu_{max}}\right) \tag{10.11}$$

where

$$P_0(\nu) = \begin{cases} \displaystyle\int_{y-a}^{y+a} \frac{dy}{\pi^2\sqrt{1-y^2}\sqrt{a^2 - (y - |\nu|)^2}} & ;0 \le |\nu| \le 1 - a \\ \displaystyle\int_{y-a}^{1} \frac{dy}{\pi^2\sqrt{1-y^2}\sqrt{a^2 - (y - |\nu|)^2}} & ;1 - a < |\nu| \le 1 + a \\ 0 & ;|\nu| > 1 + a \end{cases} \tag{10.12}$$

is a function of the single parameter a. At the values of $\nu=\pm(1-a)$ the pdf becomes infinite.

Akki and Haber [34] presented an evaluation of the same Doppler power spectrum for the Mobile-Mobile channel using a different approach. They presented the result in terms of the Complete Elliptic Integral of the First Kind. Unfortunately the result they give appears to be wrong. In the interval $0 \le |\nu| \le 1-a$ their expression yields complex values(even though they show plots with real values). In the interval $1-a < |\nu| \le 1+a$ their results differ from our numerically evaluated results. Reviewing the quoted integral tables [35] for the integral evaluation they used, revealed two facts: the integral relationship used was restricted to imaginary parts of ν not equal to zero, and, even if they could use the integral tables, they should replace their result by the real part. The latter substitution solves the problem of the complexity of their results in the interval $0 \le |\nu| \le 1-a$. However, although for a>.5 their real part results are then close (within around 10%) to our numerical evaluation of $P_0(\nu)$ from the convolution integral in (141), the numerically evaluated area under $P_0(\nu)$ for our approach is very close to unity (within .1%) as it should be, while the numerically evaluated area under their real part exceeds unity by around %10. As a becomes smaller than .5 the errors in their real part become progressively worse. For these reasons we decided to use the direct numerical evaluation of the convolution integral.

Fig. 10.1 presents plots of $P_0(\nu)$ for values of a=.25,.5,.75,1.0, respectively, for $\nu \ge 0$($P_0(\nu)$ is an even function).The case a=0, not shown here, corresponds to the Classic or Jakes/Clarke spectrum, Eq.(10.5). We call the new spectrum the Classic2 Doppler spectrum. It is interesting to note that aside from the vicinity of the infinite spikes the Classic2 spectra are nearly flat and it is likely that uniform spectra would be satisfactory from the point of view of simulation and modeling, considering the assumptions that had to be made in the derivations.

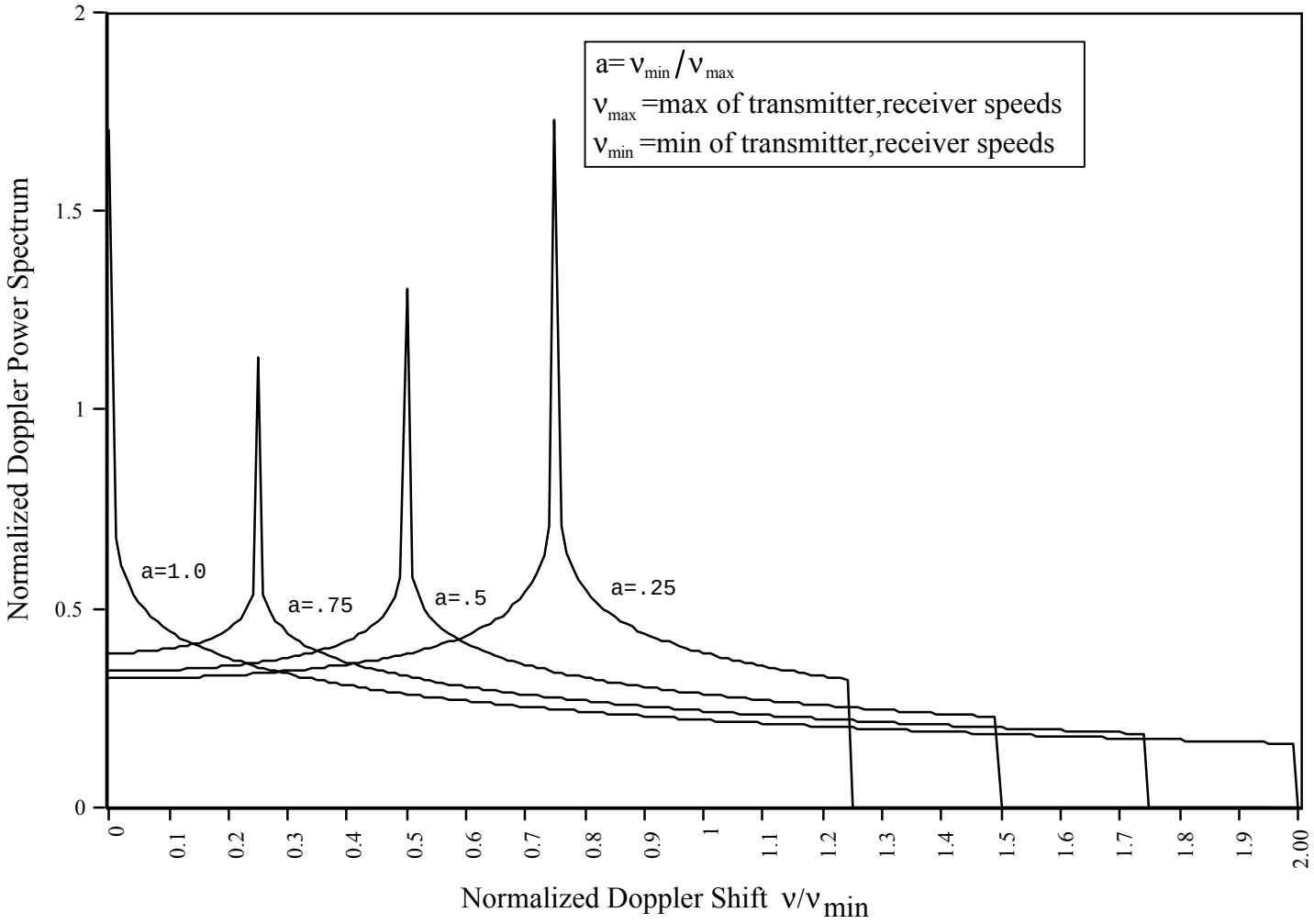

Fig.10.1 Plots of normalized Doppler power spectrum for a=.25,.5,.75,1.0

11 VHF/UHF RADIO CHANNEL ADDITIVE DISTURBANCES

The VHF/UHF mobile communicator must operate in an environment containing additive electromagnetic (EM) disturbances. The EM disturbances arise from a variety of sources. For purposes of classification and identification**,** it can be subdivided in a number of ways. A particularly simple and important distinction is that between natural and man made disturbances. It is generally agreed [36], [37] that the disturbances dominating the performance of UHF/VHF mobile communication systems do not arise from natural causes. Hence, we will concentrate entirely on man-made disturbances.

Man-made disturbances can be divided into two categories: interference from other communicators, called other-user interference, and interference from all other radiators, e.g., civilian, industrial, scientific, and medical devices. Since the dominant source of the latter interference is automobile ignition noise (aside from siting the receiver very near other sources, e.g., under a power line at frequencies of 100 MHz or lower), we will confine our attention to modeling this non-user interference. Other-user interference statistics are dependent upon the specific communication system . Thus the interference produced in CDMA systems will be quite different from that in TDMA systems. To first order, CDMA communications interference, at least , can be modeled by additive Gaussian noise if one assumes that power control is working reasonably well. Modeling of other-user interference is not covered in this report. The following discussion is thus confined to modeling automotive ignition noise.

Section 11.1 discusses the modeling of ignition noise as a random pulse train. Experimental data supporting statistical models of pulse amplitudes and arrival times is presented in addition to measurements of noise power level. Section 11.2 considers application to the Generic Channel Simulator and presents a brief summary with recommended parameter values.

11.1 Automotive Ignition Noise

To understand the structure of ignition noise**,** one must start at the microscopic level, i.e.. at the source of the noise. It is important, in this regard, to be able to correlate the radiated noise with individual spark events in the automotive ignition system. A technique for doing this is described in [4]. The author shows that the interference occurs in impulsive bursts of different strengths at equally spaced intervals of time when the engine is running at constant speed. However, the strengths of the impulses and their spacing differ greatly from vehicle type to vehicle type and from vehicle to vehicle within a given class.

Other factors determining the character of ignition noise are vehicle age and the parts used in vehicle repair. For a detailed discussion-of the vehicle-dependent factors affecting automotive ignition noise, see Shepard and Gaddie [5]. One can identify such events as arc initiation in distributor caps, spark plug arc initiation, arc termination in spark plugs, etc. Their effects differ, to an extreme degree, from car to car. The tightly-controlled experimental setup leading to the measurements in [5] should be described. The car and receiver are both stationary; the receiving antenna is placed about 10 feet away from the open hood (to one side of the car). Clearly, the relative amplitudes of the pulses will be greatly dependent on the geometry of the situation (shielding by other engine parts, etc.'.). but will remain approximately constant with time because of the constant geometry.

The automotive ignition noise environment experienced by a mobile communicator in traffic is a more complex version of the simple experimental situation described above. First of all, the emitter (hood down) and receiver are often both in motion. This fact, coupled with changes in engine speed (which completely changes the physical character of a given emission event,[6]), both combine in such a way as to randomize the impulse amplitudes and vary the intervals between the pulses. Compounding the above situation by placing the communication receiver in a noise environment created by <u>many</u> emitters, one finds that the amplitudes and arrival times tend to become completely randomized as the number of vehicles increases. This heuristic argument appears to be supported by the experimental data.

The problem of ignition noise interfering with communication systems became evident to automobile manufacturers more than two decades ago. The Motor Vehicle Manufacturing Association commissioned Stanford Research Institute to carry out an extensive study of vehicle ignition radiation in the mid 1970's. Also, in the same time frame, studies to develop methods for additional interference suppression were funded. Apparently the manufacturers have taken the noise problem seriously, since there has been a reduction in the level of ignition noise power with time. Still, as we shall discuss below, at the low end of the VHF/UHF band, ignition noise is far from negligible. In the PCS bands, however, mean ignition noise power appears to have reached levels comparable with thermal noise.

11.1.1 Pulse Amplitude Statistics

The simplest useful model of the complex envelope of automotive ignition noise at the input to a bandpass filter is via a simple sum of complex amplitude-modulated impulses, i.e.,

$$n(t) = \sum_{i=-\infty}^{+\infty} A_i e^{j\phi_i} \delta(t - t_i) \tag{11.1}$$

wherein A_i is the magnitude and ϕ_i is the phase of the i'th impulse located at the random time instant t_i. This model assumes the spectrum of the ignition noise is approximately flat across the receiver filter bandwidth. The phase ϕ_i may be regarded as randomly distributed over a 360° interval because of the independence of the occurrence times of the pulses and the carrier frequency cycles. The simulation of ϕ_i involves simply applying a scale factor to a uniformly distributed variable.

In order to characterize the noise for purposes of simulation, we must have descriptive statistics for both the set of amplitudes and the set of arrival times .This section concentrates on the statistics (first-order) of the amplitudes. One important quantity in this regard is the amplitude probability distribution (APD) which is numerically equal to one minus the distribution

function(df).

Although APD's for the noise emanating from individual cylinders have been documented in [42], this data is of little use in the current context where we are interested in a macroscopic noise model. Primarily, we are interested in determining the amplitude statistics of the noise field experienced by the mobile receiver.

The Weibull APD [43] has been found useful for fitting pulse amplitude data. This distribution contains the Rayleigh and exponential distributions as special cases(the parameter m defined below equals 1 for the exponential distribution and 2 for the Rayleigh distribution). f(x), the probability density function(pdf) corresponding to the Weibull APD is given by

$$f(x) = kmx^{m-1}e^{-kx^m} \qquad ; x \geq 0 \tag{11.2}$$

The APD, G(x), is found by integration,

$$G(x) = e^{-kx^m} \qquad ; x \geq 0 \tag{11.3}$$

It is interesting to note that the APD (144) has also been called the “power Rayleigh” APD and used extensively in the modeling of atmospheric noise at HF frequencies[44][45] .

While there is much APD data in the literature [37], [46], we restrict ourselves to data that has been compared with the Weibull distributions and plotted on appropriately scaled paper so that the Weibull APD plots as a straight line. As a case in point, Nielson presents some data for impulsive noise taken at 1370 MHz with an impulse bandwidth of approximately 16 MHz [47]. Amplitude probability densities (APD's) of the received noise are presented in [47]. This data is reproduced in Fig. 11.1. The figures indicate that there are two slopes: one for thermal components and another for the impulse component. Slopes of the impulse component yield values of m from 2.4 to 3.7. Other data showing this type of behavior has been presented by Spaulding [48].

Data relating strictly to automotive ignition noise has been presented by Southwick and Schulz in [49] where tables of the values of the m and k parameters in have also been presented.

The authors of [49] state that automobile ignition noise in all cases was found to be definable by a single set of m and k parameters. More data, along the same lines, is presented by the same team of authors in [46] but without the breakdown to the m and k parameters.

The random impulse train, Equation (11.1), has a uniform power spectral density given by

$$N_i = E[A^2]\lambda \tag{11.4}$$

where λ is the average number of impulses per sec.(estimates for λ will be presented in the next section). It may be shown that

$$E[A^2] = k^{-\frac{2}{m}}\Gamma\left(1+\frac{2}{m}\right) \tag{11.5}$$

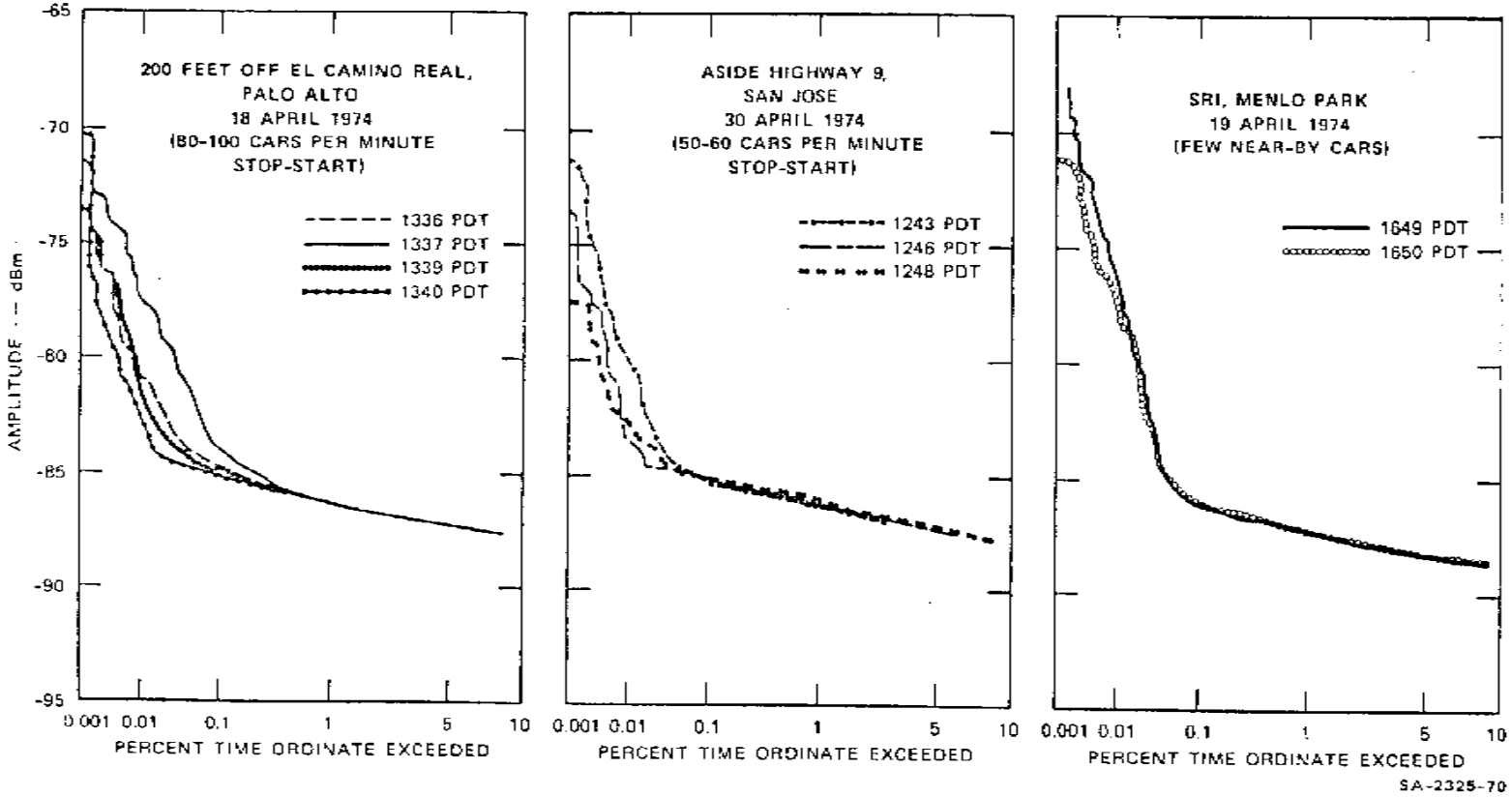

Fig.11.1 Measured Amplitude Probability Densities from [47]

where Γ is the gamma function. Given λ and m, specification of the ignition noise power density determines the parameter k as

$$k = \left[\Gamma\left(1 + \frac{2}{m}\right) \frac{\lambda}{N_i} \right]^{\frac{m}{2}} \tag{11.6}$$

We consider now the generation of impulse magnitudes having a Weibull APD. A random variable (rv) y with an arbitrary continuous APD G(Y) can be generated by performing a nonlinear operation on an rv, u, that is uniformly distributed in the interval (0,1). In particular, if $G^{-1}(\ )$ is the inverse of G( ), then

$$y = G^{-1}(u) \tag{11.7}$$

will generate the desired rv.

In the case of the Weibull APD

$$G^{-1}(u) = \left[\frac{1}{k} \ln\left(\frac{1}{u}\right) \right]^{\frac{1}{m}} \tag{11.8}$$

Thus the nonlinear transformation

$$y = \left[\frac{1}{k} \ln\left(\frac{1}{u}\right) \right]^{\frac{1}{m}} \tag{11.9}$$

will create an rv with the Weibull APD.

11.1.2 Ignition Noise Power Level

Values of the noise power density N_i have been measured in various cities and at various frequencies. A recent summary of power measurements arranged chronologically, is shown in Table 11.1 from [50] covering a span from 1951 to 1989, from 200 to 914 MHz, and a variety of cities and countries (this table was found in recent unpublished work by Spaulding [51]). The power density is presented in dBm/kHz(the power density relative to a watt in a one Hz band, i.e. units of dBW/Hz, is 60 dB less). It is conventional to present the power density in a normalized form, which we call F_a, as the power in a 1 Hz band in dB relative to thermal noise power in a 1 Hz band at a temperature of 290 K. This reference value of power is -204 dBW. The last column labeled F_a has been added here to give the more conventional presentation which is obtained from the second to last column by adding 144 (204-60).

Table 11.1 was an attempt to show that there exists a trend with time of decreasing ignition noise power do to equipment modifications by automotive manufacturers. This trend does appear in the data (aside from the last and most recent entry from Turin, Italy). However the data generally does not compare the same cities at different times for specific frequencies. Only if one assumes that a busy city has the same noise statistics at different localities will this make sense. Also since the data came from several different experimenters some variability can be expected due to different experimental setups.

One comparison is possible for the same city and the same band at two different times. Some power measurements were carried out in Cleveland, Ohio at 480 and 950 MHz in the summer of 1967 by Anzic [52] (these measurements are listed in Table 11.1, although at an incorrect date, 1969) and in 1983 by Lauber . The average F_a found by Anzic at 480 MHz in a noisy urban location was 28 dB while F_a was found to be below 38 dB 90% of the time. For a quiet urban location the average F_a found by Anzic was 11 dB and the 90 percentile was 13 dB. At 950 MHz, the urban noisy location exhibited an average value of F_a of 11 dB and the 90 percentile was 14 dB. The urban quiet noise values were below the noise figure of the receiver and were regarded as unreliable. Comparing the average values of F_a found at 950 MHz by Anzic and

Lauber (assuming noisy urban locations in both cases) we see that the 1967 data is 11 dB higher than the 1983 data, so that the 1983 data shows an average noise power level comparable with thermal noise.

Table 11.1 Power Density Measurements from [15]

City	Source	Freq.	Yr	Population (Millions)	Avg.Pwr. dBm/kHz	F_a dB
New York,NY	Young	300	1951	7.891957	-114	30
New York,NY	Young	400	1951	7.891957	-116	28
New York,NY	Young	200	1951	7.891957	-111	33
New York,NY	Young	500	1951	7.891957	-118	26
New York,NY	Young	250	1951	7.891957	-112	32
Haifa	Simpson	250	1952	0.140000	-116	28
Jerusalem	Simpson	250	1952	0.123000	-119	25
Tel Aviv	Simpson	500	1952	0.335000	-123	21
Tel Aviv	Simpson	250	1952	0.335000	-116	28
Melbourne,Aust.	Ellis	424	1962	1.956400	-125	19
Bendigo,Aust.	Ellis	424	1962	0.040980	-126	18
Ascot Vale,Aust	Ellis	424	1962	1.956400	-126	18
Manhattan, NY	RCA	800	1968	7.891957	-130	14
Phoenix, AZ	Anzic	300	1969	0.584303	-127	17
Cleveland,OH	Anzic	480	1969	0.750879	-116	28
Cleveland,OH	Anzic	950	1969	0.750879	-133	11
Ottawa,Can.	Lauber	400	1976	0.693288	-136	8
Ottawa Can.	Lauber	500	1976	0.693288	-138	6
Ottawa,Can.	Lauber	300	1976	0.693288	-136	8
Ottawa Can.	Lauber	200	1976	0.693288	-132	12
Los Angeles,CA	Flath	510	1977	2.966850	-140	4
Montreal,Can.	Angers	200	1978	2.818300	-136	8
Montreal,Can.	Angers	500	1978	2.818300	-140	4.
Montreal,Can.	Angers	300	1978	2.818300	-137	7
Montreal,Can.	Angers	400	1978	2.818300	-139	5
Ottawa,Can.	Lauber	700	1983	0.743821	-142	2
Ottawa,Can.	Lauber	900	1983	0.743821	-144	0
Cleveland,OH	Lauber	950	1983	0.743821	-144	0
Cleveland,OH	Lauber	600	1983	0.743821	-142	2
Cleveland,OH	Lauber	800	1983	0.743821	-144	0
Turin,Italy	Cost 207	914	1989	1.190688	-127	17

The ignition noise power has been observed to decrease with increasing frequency. Measurements presented by both Spaulding and Disney[53] and Skomal[54] carried out in the seventies show a decrease at the rate of approximately 27.5 dB/decade from below a MHz to 200 MHz.with $F_a \approx 33$ dB at 30 MHz and 18 dB at 100 MHz. The difference between the upper and lower deciles averaged about 14 dB. Above 200 MHz Skomal [54] finds that the noise power decreases at a slower rate with increasing frequency, ≈12.3 dB/decade, with $F_a \approx$ 17 dB at 200 MHz and 9 dB at 900 MHz. Assuming the trend with frequency has not changed, since it is due primarily to the spectral shape of the ignition pulses, we can estimate current values of power by applying a shift of the curves downward a specific number of dB to account for the automotive equipment changes. The single example cited above from Cleveland comparing 1967 and 1983 yielded an 11 dB shift at 950 MHz.

In 1985 Skomal [55] collected all the available published noise power data from 1951 to 1983. The data were separated into an "early" set for 1951 - 1970 and a "late" set for the years 1975 - 1983. We show this data with two sets of dashed trend lines in Fig.11.2 The upper trend line follows the trends discussed above for the Spaulding and Disney [53] and Skomal [54] data. The second trend line is a 10 dB down-shifted version used to approximate the reduced noise power caused by the improved automotive design to reduce noise power. The upper trend line was obtained from data in the 70's and does not match the early data well. However the second trend line is a reasonable approximation for the late measurements and we shall use this trend line to characterize ignition noise. Looking at the data in [53] one may determine that on the average the 90 percentiles are 7 dB above the median trend line and the 10 percentiles are 2.4 dB below the trend lines..

11.1.3 Time Structure of Automotive Ignition Noise

The ignition noise was expressed earlier as a sum of complex amplitude-modulated impulses in Eq.(11.1). In the previous section we addressed the question of determining a statistical description of the impulse magnitudes. In this section we address the question of determining the distribution of the points in time at which the impulses occur.

From the data that has been collected, the consensus of several workers in the field is that there are "no over-riding periodicity's" [36] and that assumption of random arrival time is quite reasonable for modeling the impulsive noise experienced by a mobile communicator in traffic [41].

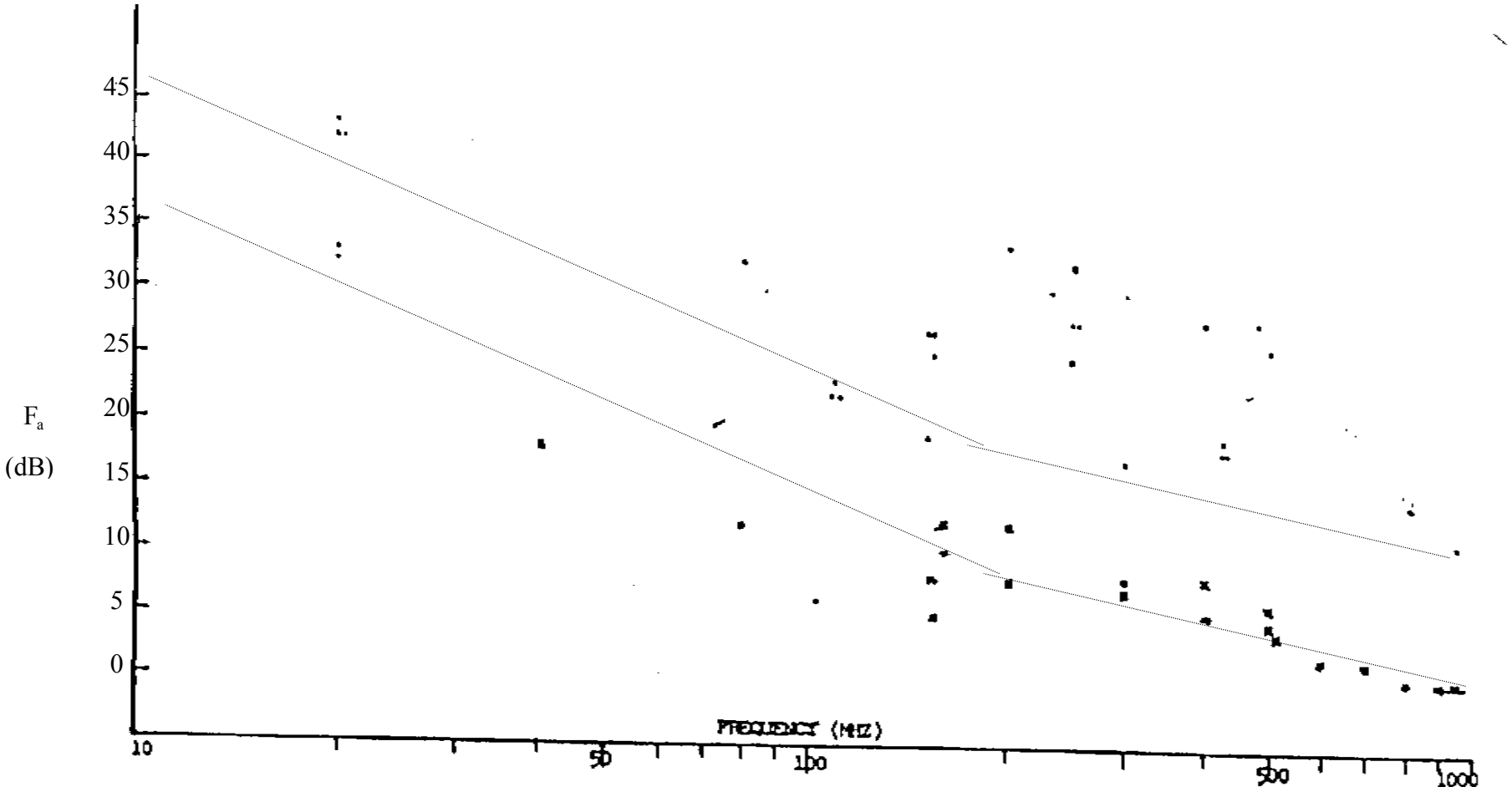

Fig. 11.2 Comparison of Trend Lines Obtained from Spaulding and Disney [53] and Skomal [54] with 1951 - 1970 Noise Power Data Assembled by Skomal [55] and Comparison of 10 dB Downshifted Trend Lines with 1975 - 1983 Noise Power Data.

This has generally been the approach of workers who have attempted to develop theoretical models of the impulsive noise.

When one is willing to make the assumption that the pulse occurrences are completely random, the Poisson process model may be used. This type of process is described by the random sequence of points $\{t_k\}$ along the time axis

$$N(t) = \sum_{k=1}^{\infty} u(t - t_k) \tag{11.9}$$

where N(t) is equal to the number of point occurrences between 0 and t, and u(t) is the unit step function. Under a small set of fundamental conditions, the probability Pr[N(t)= n] is given by

$$\Pr[N(t) = n] = \frac{(\lambda t)^n}{n!} e^{-\lambda t} \qquad ; t \geq 0 \tag{11.10}$$

where λ is called the rate parameter for the process and is the average number of points per unit interval, i.e.,

$$E[N(t + T) - N(t)] = \lambda T \tag{11.11}$$

The average rate parameter λ is the only parameter required to characterize the process, and there is data from which this parameter can be inferred. Fig.11.3 presents measurements of the cumulative distribution of intervals between noise peaks (from [47]). The APD for the interval between events for the Poisson process is an exponential

$$G_p(\tau) = e^{-\lambda \tau} \qquad ; \tau \geq 0 \tag{11.12}$$

One may fit this exponential form to the measurements in Figure 5 in a variety of ways. For example, at the 50 percentile, one may readily determine that

$$\tau_{.5} = \frac{.69}{\lambda} \tag{11.13}$$

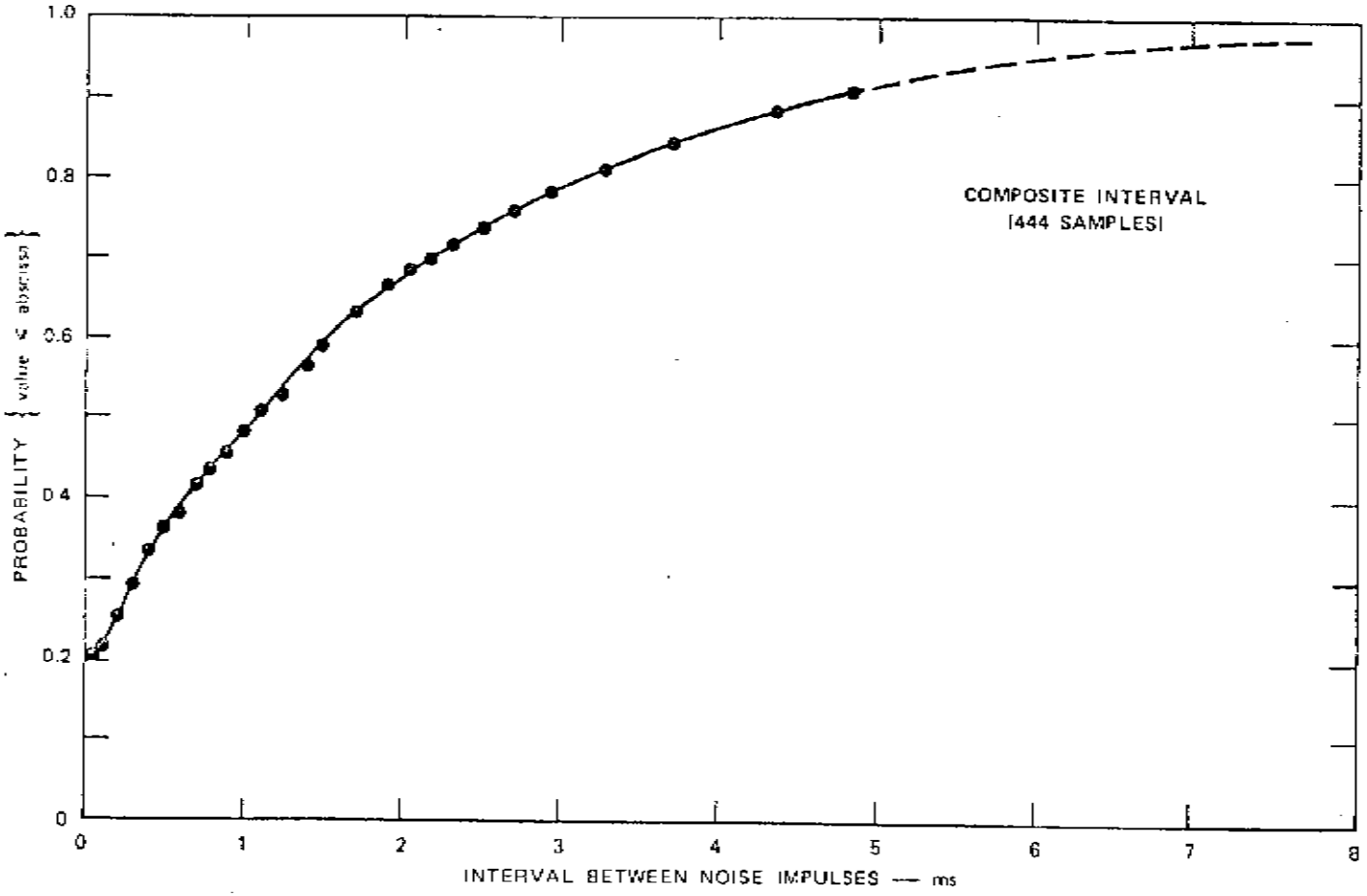

Figure 11.3 Distribution of Intervals between Any Two Peaks (from [47])

From the figure, we estimate that $\tau_{.5} \approx 1.1$ ms, which leads to λ = 630 pulses/sec. Values in the range of 200 to 1000 appear reasonable based upon measured data.

Since

$$G_p^{-1}(u) = \frac{1}{\lambda} \ln \frac{1}{u} \tag{11.14}$$

we may generate successive interarrival intervals by computing the right hand side of (11.14) for successive selections of a variable u uniformly distributed in the interval (0,1). We can simplify the simulation by quantizing each generated interarrival time to integer units of the simulation clock time.

11.2 Application to the Generic Channel Simulator

As of the date of this report, the GCS already includes an impulsive type noise model in it's simulation of HF Atmospheric Noise. Although there are some elements in common, the HF noise model is sufficiently different from the Ignition Noise model to obviate trying to modify the HF noise simulator to provide the Ignition Noise simulator. The generation of a train of independent "impulses" having Poisson arrival statistics with Weibull Amplitude and uniform phase statistics has been discussed in Section 11.1 The parameters needed to specify this impulse train are λ the average pulse arrival rate, m the exponent of the Weibull APD, and F_a the relative ignition noise power density. Table 11.2 presents ranges of values for these parameters.

Table 11.2 Parameter Values for Ignition Noise Simulation

Parameter	Range of Values
λ (pulses/sec)	200 - 1000
m	2.4 - 3.7
Median F_a (30 - 200 MHz)	$36 - 22.3 \log_{10}\frac{f(MHz)}{10}$ *
Median F_a (200 MHz - 2GHz)	$7 - 12.25 \log_{10}\frac{f(MHz)}{200}$ *

*adding 7 dB yields the 90 percentile and subtracting 2.5 dB yields the 10 percentile

Two observations need to be made at this point. As for the impulsive atmospheric noise,

one may expect m to be dependent on bandwidth. However bandwidth dependence does not appear to have been explored . In addition the total non other-user additive disturbances to be used in the simulation must include the ambient receiver thermal noise in addition to the ignition noise. This thermal noise will depend upon the receiver noise figure.

12 LAND MOBILE SATELLITE CHANNELS

Low Earth Orbit (LEO) and Medium Earth Orbit (MEO) satellite systems are in the process of development [56][57] for the purpose of implementing land mobile communications. The Land Mobile Satellite (LMS) systems are proposed primarily as a complement to existing and proposed terrestrial cellular systems, since the latter are most cost-effective in urban areas, while the former are more cost-effective in under populated regions. However , the LMS system has also been considered for use in urban areas when a compatible cellular standard is not available.

Modeling of the LMS channel is a topic of current investigation. An extensive review of propagation effects in LMS systems including experimental results and models was published by Goldhirsh and Vogel [70] in 1992. Although we have brought the review up to the present time, our interest is narrower, being focused on stochastic time series models useful for simulation. Consequently we do not review the large body of experimental measurements and empirical curve fits that are not structured around the development of time series models (e.g. the Empirical Roadside Shadowing models of Goldhirsh and Vogel [59]) In modeling the LMS channel three propagation categories or states are used: *clear* or *open, shadowed*, and *blocked*. The relative importance of these categories depends upon the environment. The *clear* state is epitomized by open areas with a clear line-of-sight and a minimal amount of multipath and scatter. This state will occur frequently in rural environments.

On the other hand the *blocked* state is characteristic of a heavily built-up urban environment, particularly if the satellite is at a low elevation angle. In such a state the line-of-sight between the satellite and mobile is blocked by impenetrable objects and reception occurs via diffraction and reflections. Considerable attenuation and multipath will usually exist and the strength of the multipath signal varies slowly with approximate lognormal statistics(e.g. see [3] Section 2.4). Such a channel state is typical of terrestrial land-mobile cellular channels in urban environments when no direct path or large resolvable reflected paths exist.

The *shadowed* state is exemplified by a line-of-sight path through vegetation, for example transmission to a mobile traveling along a tree-lined street. In this case an

attenuated, time variant, line-of-sight signal and a scatter multipath signal exist. The line-of-sight signal fluctuates slowly compared to the multipath signal and has been modeled by lognormal statistics(e.g. see [60]).

In Section 12.1 we consider models for the individual states. These models are essentially special cases of models already presented except that lognormal statistics are introduced to model certain slow variations in the power of the direct path signal and/or the multipath signal. These slow variations are appropriate for the previous models also but were not introduced because the amount of multipath in these models increases the time for simulation so much that it was not feasible to introduce the slow lognormal time variations. For the non-urban LMS channel models only flat fading models are needed because the multipath spread is small compared to the reciprocal bandwidths of interest. In such a case it is feasible to introduce the lognormal fluctuations in the simulations. If the channel bandwidth is small enough it would be practical to introduce lognormal fluctuations in the urban environment also.

Since the ground terminal is mobile, the individual propagation states persist only for a finite time and there are random transitions from one state to another due to the changing propagation path. Markov Chain models have been used to represent the flat fading LMS channel as a stochastic process involving two or more states. These models are reviewed in Section 12.2. Section 12.3 specifies the Markov Chain model simulation approach to be used. Section 12.4 reviews the single paper found on wideband LMS channel modeling.

12.1 Individual state models

For the case of flat fading over the bandwidths of interest, the channel (excluding additive noise) is represented as a simple complex gain $\gamma(t)$, i.e.,

$$w(t) = z(t)\gamma(t) \tag{12.1}$$

where z(t) is the complex envelope of the input signal, and w(t) is the complex envelope of the output signal.

The complex gains for the three propagation states are special cases of the following generic form for $\gamma(t)$

$$\gamma(t) = \left(d(t) + g(t)G(t)\right) \tag{12.2}$$

where d(t) is the amplitude of the direct or line-of-sight path , and the product g(t)G(t) is the complex gain due to all multipath components referenced to the direct path. As in the models we have presented in the rest of the report, the direct path is used as a reference in the simulation and both phase and Doppler variations of the direct path are removed from $\gamma(t)$. The strength of G(t) has been normalized to unity, so that g(t) is the (ensemble time variant) rms value of the multipath signal. The terms d(t) and g(t) are generally slowly time-varying compared to G(t).

In [58] and [63] the *clear* state is represented with d normalized to unity, i.e.,

$$\gamma(t) = \left(1 + gG(t)\right); \quad \textit{clear} \text{ state} \tag{12.3}$$

For these LMS models $G(t)$ is assumed to be complex Gaussian, so that the magnitude of $\gamma(t)$ has the so-called Ricean statistics [61]. In [67][68], however, d(t) is chosen to be distributed as for the shadowing model, but the variance is chosen very small so that practically speaking the model does not differ from Eq. (12.3).

The *clear* state Rice model does not include specular reflections. The neglect of specular reflections has been justified on the basis of antenna discrimination arguments. For hand-held transceivers these arguments may not always be valid so we have included the option of specular multipath components in addition to the complex Gaussian "scatter multipath" in our proposed clear model . Such inclusion makes this *clear* model identical in form to the Air-Ground channel model discussed in Section 9. Unfortunately there is negligible data on the specular paths and, while we include them in the model, the user

will have to supply the necessary parameters. Alternatively, the user can set the specular path strengths to zero, and join the rest of the LMS channel modeling community.

Another problem, even if the specular paths are neglected, is the specification of the Doppler power spectrum of the scatter multipath. The only measurements of Doppler spectrum for an LMS channel received signal that we have seen are in [58]. These consist of two Doppler power spectra, one for the urban case and one for highway driving. No measurements or statistics of Doppler spread are given. Due to this lack of relevant data, it is necessary to apply theoretical estimates.

Assuming that the scatter multipath for the *clear* channel arises from rough surface scattering, the theory presented in [19]-[21] for the Satellite-Air channel in over-sea propagation yields a Gaussian shaped Doppler Power Spectrum,

$$P(\nu) = \frac{1}{\sigma_\nu \sqrt{2\pi}} \exp\left(-\frac{\nu^2}{2\sigma_\nu^2} \right) \tag{12.4}$$

having an rms Doppler spread σ_ν (one standard deviation) given by

$$\sigma_\nu = 2\alpha \frac{V}{\lambda} \sin\theta \tag{12.5}$$

where V is the mobile velocity, α is the rms slope of the scattering surface, λ is the wavelength at the carrier frequency, and θ is the elevation angle to the satellite.

Eq. (12.5) was derived for a geosynchronous satellite. Strictly speaking the non-GEO satellite movement relative to the earth can be expected to produce some Doppler spread. However one may show that the contribution of the satellite to the Doppler spread is very small and can be neglected.

For overland flights we have used α =.5 in the Air-Air and Air-Ground channel models because this value appeared to match the theoretical multipath spread with the observed values. However the data upon which this conclusion was obtained is crude.

An alternate approach to deriving a Doppler spectrum is to assume, as in the calculations for terrestrial cellular channels that the multipath arrives uniformly in azimuth. This assumption leads to Doppler Power Spectra confined to the band $(-V/\lambda, V/\lambda)$ centered on the mean Doppler shift. When the elevation angles of the arriving waves are confined to 0° the Jakes/Clarke power spectrum shape, Eq.(7.3), results. When waves arrive uniformly distributed in elevation angle, we have already suggested a uniform power spectrum, Eq.(7.14).

The right spectrum choice depends upon the local environment. For the *clear* state in a strictly open area where scatter multipath must come primarily from the surface irregularities, Eq.(12.5) should be reasonable with a fairly large value of α. However, all significant spectral power must be truncated to the band $(-V/\lambda, V/\lambda)$. For *clear* states in suburban and urban environments, where multipath can arrive in less constrained elevation angle directions, it is reasonable to use a the uniform Doppler power spectrum, Eq.(7.14).

The remaining parameter that needs to be selected is g, or equivalently,

$$K = \frac{1}{g^2} \quad , \tag{12.8}$$

the ratio of direct path power to scatter multipath power. One may locate reports which cite measured values for different environments but no statistics have been found. The most extensive listing found is in Table II of [58], and [62] presents a curve showing average values of K (both papers use the symbol c instead of K) vs. elevation angle for an urban environment. The latter reference shows that the value of K increases with increasing elevation angle to the satellite.

The measurements reported in [58] were conducted in areas with different satellite elevation angles to the MARECS satellite at L band (1.54 MHz): Stockholm (13°), Copenhagen (18°), Hamburg (21°), Munich (24°), Barcelona (34°), and Cadiz (43°). Four different azimuth uniform antennas were employed. To quote, " The test

courses were carefully selected to represent different types of environments (city, suburbs, rural roads, highway) and to comprise a mixture of cruising directions." Unfortunately Table II of [58] only lists two environment categories: highway and city . From Table II we have computed interpolated percentiles of K values for the highways and cities as indicated in Table 12.1.

Thus for the highways, which we assume to be rural areas, K is less than 10.8 dB, 10% of the time and 17.8 dB 90% of the time, while for the cities, K is less than 5.2 dB 10% of the time and 11.2 dB 90% of the time.

It is necessary to consider the shadowed and blocked states together, because some papers do not distinguish them. Thus in the models proposed by Lutz et.al. [58] only two states are considered," good" and "bad", where the good state is the *clear* state and the bad state include the *shadowed* and *blocked* states. On the other hand in [60] a single state shadowing model is proposed for the non-urban environment.

Table 12.1

Percentiles for K in dB computed from data in Table II of Lutz et. al. [58]

Environments	**10%**	**50%**	**90%**
Highways	10.8	16.6	17.8
Cities	5.2	6.5	11.2

For the Loo model the channel complex gain is

$$\gamma(t) = \left(d(t) + gG(t)\right) \qquad \text{; Loo model} \tag{12.9}$$

where g is constant, G(t) is complex Gaussian, and d(t) has the lognormal probability distribution. By definition, d(t) is representable as a number raised to a power which is normally distributed. Base e and base 10 are used frequently, i.e.,

$$d(t) = e^{x_1(t)} \tag{12.10}$$

and

$$d(t) = 10^{x_2(t)/20} \tag{12.11}$$

where $\{x_k(t);\ k = 1,2\}$ is a normally distributed random variables with mean and variance (m_k, σ_k) and

$$x_1(t) = \frac{\ln 10}{20} x_2(t) \tag{12.12}$$

Very little parameter information is presented for Loo's model. One set of values for $\{g, m_1, \sigma_1\}$ is given for "infrequent light shadowing" and one set for "frequent heavy shadowing".

Smith and Stutzman [63] proposed the same shadowing model as Loo's but added the *clear* state. Experimental data obtained by Vogel and Goldhirsch [64][65] using helicopters was used to determine parameter values for their model. Table 12.2 presents their quoted ranges of parameters.

Table 12.2

Ranges of Parameter Values for Smith and Stutzman Model [63]

Parameter	Range of Values	Remarks
K	22 to 13 dB	low to high multipath *clear* state
g	-21 to -18 dB	low to high multipath *shadowed* state
m_2	-1 to -10 dB	light to heavy shadowing
σ_2	.5 to 3.5 dB	light to heavy shadowing

As mentioned previously, Lutz et al [58], use a two-state model, where the "good" state is the *clear* state. The "bad" state, which models both *shadowed* and *blocked* states, has no direct path. Thus the channel complex gain is represented by

$$\gamma(t) = g(t)G(t), \tag{12.13}$$

g(t) has a lognormal distribution and G(t) is complex Gaussian. Therefore we can represent $\gamma(t)$ as

$$\gamma(t) = 10^{y(t)/20}\, G(t) \tag{12.14}$$

where y(t) is normally distributed, with mean and rms value (m, σ). Table 12.3 presents interpolated percentiles of (m, σ) obtained from the measurements shown in Table II of [58].

Table 12.3

Percentiles for (m,σ) computed from data in Table II of Lutz et. al. [58]

	10% (dB)	**50% (dB)**	**90% (dB)**
m for highway	-13.8	-8.8	-7.3
σ for highway	2.36	4.8	5.8
m for city	-15.4	-12.2	-10.5
σ for city	2.0	3.8	5.1

The Lutz et al model simplifies the modeling of the LMS channel by defining only two states, *clear* and a *shadowed/blocked* state. The model used for the latter state is most applicable to the blocked state. Thus their sacrifice in accuracy is in the modeling of the shadowed state which appears to be represented better by the Loo model. On the other hand the Loo single state model (which in fact includes the *clear* state as a special case in which σ_1 (or σ_2) is set to zero) and the Smith and Stutzman model (which specifically includes a *clear* state but is the same as the Loo model for shadowing) are deficient in representing the *blocked* state well. It is important to note however that these LMS models are deficient in that the lognormal factors, d(t) and g(t), are not given the time series models necessary for simulation. If the related processes, x(t) and y(t), respectively, are stationary Gaussian processes, then a specification of their power spectra is sufficient to provide a complete statistical model.

12.2 Review of LMS channel Markov chain models

The preceding section reviewed proposed models for the individual LMS channel states. In practice the LMS channel for a moving vehicle will not stay in one state but rather randomly change from state to state depending on the environment. A number of researchers [58][66]-[68] have proposed Markov chain models that produce such changing states. Important parameters of these models are: the number of states, the state transition probabilities, the state probabilities, the state transition interval, and the signal parameters for each state that define the signal as a stochastic process.

Lutz et al [58] present a "good"/"bad" two-state Markov chain model. Table 12.4 presents some data from Table II of [58][11]. The parameters K, m, and σ have already been defined and percentiles presented in Tables 12.1 and12.3 based upon numerical data in Table 12.4. The additional parameters in Table 12.4 are A, D_g, and D_b. A is the fraction of time that the bad or shadowing/blocking state occurs, D_g is the average distance in meters traveled by the mobile wherein the good or clear state occurs, and D_b is the average distance in meters traveled by the mobile wherein shadowing/blocking occurs. The experimental data was obtained via L-Band CW signals received from the MARECS satellite. These latter three parameters are in principle sufficient to define the two state Markov process. There is a point of confusion, however. Eq.(13) of [58] states that A, the probability of the bad state is given by

$$A = \frac{D_b}{D_b + D_g} \tag{12.15}$$

[11] We have omitted some columns and changed some notation to conform to ours.

Table 12.5

Data from Table II of Lutz et al [58}

Environment	A	K	m	σ	D_o	D_b
Highway	0.24	10.2 dB	−8.9 dB	5.1 dB	90 m	29 m
City	0.89	3.9 dB	−11.5 dB	2.0 dB	9 m	70 m
City	0.80	6.4 dB	−11.8 dB	4.0 dB	8 m	32 m
City	0.80	5.5 dB	−10.0 dB	3.7 dB	8 m	33 m
New City	0.57	10.6 dB	−12.3 dB	5.0 dB	45 m	60 m
Highway	0.03	16.6 dB	−7.1 dB	5.5 dB	524 m	15 m
Highway	0.03	18.1 dB	−7.9 dB	4.8 dB	514 m	17 m
Old City	0.66	6.0 dB	−10.8 dB	2.8 dB	27 m	52 m
Old City	0.78	9.3 dB	−12.2 dB	4.4 dB	21 m	76 m
Old City	0.79	11.9 dB	−12.9 dB	5.0 dB	24 m	88 m
Highway	0.25	11.9 dB	−7.7 dB	6.0 dB	188 m	62 m
Highway	0.19	17.4 dB	−8.1 dB	4.2 dB	700 m	160 m
City	0.58	6.0 dB	−10.6 dB	2.6 dB	24 m	33 m
City	0.72	10.0 dB	−11.9 dB	4.9 dB	21 m	55 m
City	0.60	9.5 dB	−12.2 dB	2.0 dB	20 m	31 m
Highway	0.008	11.7 dB	−8.8 dB	3.8 dB	1500 m	12 m
Highway	0.007	16.7 dB	−13.4 dB	5.3 dB	1500 m	11 m
City	0.54	5.5 dB	−13.6 dB	3.8 dB	42 m	49 m
City	0.65	11.0 dB	−15.4 dB	5.4 dB	16 m	29 m
City	0.56	6.5 dB	−15.6 dB	3.8 dB	51 m	65 m
Highway	0.002	14.8 dB	−12.0 dB	2.9 dB	8300 m	17 m
Highway	0.002	17.3 dB	−13.8 dB	2.0 dB	8300 m	17 m

which is not a general relationship provable with the theory of Markov chains. Assuming that A is the steady state probability of the bad state (1-A is then the steady state probability of the good state) then the theory of Markov chains [69] shows that

$$A = \frac{1}{N_b} \tag{12.16}$$

where N_b is the mean recurrent interval for the bad state, i.e., the average number of state transitions between occurrences of the bad state. They actually found that the experimental data did not agree with (12.5) (see discussion below their Eq.(13)) and redefined their measured values of D_g and D_b to ensure conformity with this equation!

Eq.(12.16) states that when the probability of a bad state is small the average time between occurrences of the bad state is large. On the other hand, (12.15) states that when the probability of a bad state is small, the average duration of a bad state is small relative to the average duration of a good state. These are two different statements.

Taken at face value the Markov Chain simulation would involve choosing the first state randomly with the probability A for the bad state and 1-A for the good state. In each state the duration in meters (or seconds using an appropriate vehicle velocity) for which that state persists is an exponentially distributed random variable with mean value equal to the average duration of that state (D_g or D_b as the case may be). When one state ends the other state is chosen and another independent exponentially distributed random variable is chosen with the appropriate average duration for that state.

The signal processes for each state are not completely defined by the other three parameters K, m, and σ. It is necessary also to specify the power spectrum of the complex Gaussian process G(t) and a time series model for the lognormal process g(t).

A uniform power spectrum is chosen for G(t) over the band $(-V/\lambda, V/\lambda)$. The simplest time series model is chosen for the lognormal process g(t): when the bad state occurs, a value of g is chosen randomly from the appropriate lognormal distribution and held constant as long as the bad state is maintained. When the next bad state occurs, an independent selection of g takes place for the duration of the next shadowing interval.

A recent paper [66] by Bischl, Werner, and Lutz extended the above two state models for the LMS channel to include elevation angle dependence and satellite diversity. These are important modifications since there is a significant dependence of state probabilities and signal parameters on elevation angle and the use of diversity is essential for reducing the SNR margin. Due to the satellites transmit power limitation, the shadowed and blocked states generally result in unacceptable communication performance. To include dual diversity a four state Markov chain model is used. Unfortunately, unlike [58], insufficient data is presented from which to construct the Markov chain model.

Lin, Akturan, and Vogel [67] proposed a three state Markov chain model in which each state followed the Loo signal model with different parameters. These parameters were chosen to represent the *clear, shadowed,* and *blocked* states with the Loo model. A major objective of the paper was to justify a data collection method using a fish-eye lens to capture images of the skyline. This data is used to construct parameters for the model. Some validation experiments were conducted using the 2.055 GHz CW transmission from the TDRS satellite to Pasadena CA (21° elevation). The mobile was deployed in four different environments in Pasadena, CA (Urban,Suburban, Rural, Open). Reproducing the data given in [67], Tables 12.6 - 12.9 present state probabilities, transition matrices, and signal parameters (m_d, σ_d, g) for each state, where (m_d, σ_d) are the mean and rms value of d(t). From (m_d, σ_d) one may compute (m_l, σ_l) as follows,

Table 12.6

Urban Pasadena Markov Chain Model Parameters from [67]

	Clear State	Shadowed State	Blocked State
State Probability	.459	.271	.270
Transition Probability Matrix	.968	.029	.003
	.052	.775	.173
	.002	.175	.823
$\mathbf{m}_d$	.9477	.4982	.0824
σ_d	.0767	.2633	.0395
g	.01082	.1650	.0462

Table 12.7

Suburban Pasadena Markov Chain Model Parameters from [67]

	Clear State	Shadowed State	Blocked State
State Probability	.6843	.2879	.0278
Transition Probability Matrix	.97843	.021527	0
	.051158	.942085	.006757
	0	.07	.93
$\mathbf{m}_d$	1.0047	.3234	.0322
σ_d	.2408	.268	.0484
g	.1776	.3338	.1804

Table 12.8

Rural Pasadena Markov Chain Model Parameters from [67]

	Clear State	Shadowed State	Blocked State
State Probability	.7248	.2543	.0208
Transition Probability Matrix	.9776	.0230	.00038
	.063388	.92459	.01202
	.04	.12	.84
$\mathbf{m}_d$	.9633	.3683	.0259
σ_d	.1069	.1220	.0107
g	.1074	.2360	.0873

Table 12.9

Open Pasadena Markov Chain Model Parameters from [67]

	Clear State	Shadowed State	Blocked State
State Probability	.982	.009	.009
Transition Probability Matrix	.999	.001	0
	.097	.71	.194
	.061	.121	.818
$\mathbf{m}_d$	1.0394	.7792	.0315
σ_d	.082	.0655	.0328
g	.0579	.0864	.0539

$$\sigma_l = \frac{1}{2} \ln\left(1 + \frac{\sigma_d^2}{m_d^2}\right) \tag{12.17}$$

$$m_l = \ln m_d - \frac{\sigma_l^2}{2} \tag{12.18}$$

The state transitions occur at 30 times /sec. One piece of information needed to scale the Markov model for different speeds, is the speed at which the mobile was moving. A telephone call to the authors yielded a statement that the average speed was around 35 mph.

Construction of a Markov chain simulation model for each of these environments is possible with the supplied information (reproduced in Tables 12.6 - 12.9) provided the lognormal process d(t) is modeled and the spectrum of G(t) is specified. In [67] it appears that the lognormal process is modeled as in [58], i.e., selected randomly from the correct first order distribution for the current state, held constant while the state is the same, and randomly selected for the next different state. No statement is made about the power spectrum selected for the multipath but a uniform power spectrum may be used as in [58].

Vuketic and Du [68] also propose a Markov chain model similar to that in [67]. Four states are used instead of three. However only one example was presented and the state transition time interval was not given. Consequently we will be unable to use this model.

The data in [58] and [67] appears most useful for simulation purposes. We note that the models are also quite different so it may make sense to implement both. The Lutz model of a quasi-stationary complex Gaussian process with lognormally distributed slowly changing power level is more reasonable for a heavily built up urban environment than the Loo model. On the other hand, in the rural and suburban environments the reverse is true. One common troublesome attribute of these models is the abrupt change

in the signal when the state changes and the static behavior of the lognormal variables when the state is unchanged. Unfortunately, while the data base exists from which to develop stochastic models of the lognormal process, we were unable to find experimentally validated models.

12.3 Markov chain model implementation

We consider here some details of the implementation of the LMS Channel model using the Markov chain model. Assume an N-state Markov model with a matrix **Q** of transition probabilities

$$\mathbf{Q} = \begin{bmatrix} q_{11} & q_{12} & \cdot & \cdot & q_{1N} \\ q_{21} & q_{22} & \cdot & \cdot & q_{2N} \\ \cdot & \cdot & \cdot & \cdot & \cdot \\ \cdot & \cdot & \cdot & \cdot & \cdot \\ q_{N1} & q_{N2} & \cdot & \cdot & q_{NN} \end{bmatrix} \tag{12.17}$$

where q_{mn} is the probability of transition to state n give the system is in state m. Since the system must transition to the same state or to another state, each row of **Q** must sum to unity.

$$\sum_{n=1}^{N} q_{mn} = 1 \tag{12.18}$$

p, the row vector of steady state probabilities of the individual states, can be determined from Q via the equation [69],

$$\mathbf{p} = \mathbf{1}[\mathbf{Q} + \mathbf{E} - \mathbf{1}]^{-1} \tag{12.19}$$

where **1** is an N dimensional row vector of all one's, **E** is an N by N matrix of all one's, and **I** is the identity matrix. The simulation would be started be selecting the initial state randomly according the apriori state probabilities **p.**

Given that the system is in state s, the probability P_r, that it stays in state s for r-1 state transitions, and then exits is given by

$$P_r = q_{ss}^{r-1}(1 - q_{ss}) \tag{12.20}$$

where it should be noted that $(1 - q_{ss})$ is the probability of transition to a state other than s, given that the system is in state s.

Since the Markov chain "remembers" only one state into the past, P_r is the same as the probability that state s has the duration r. Then according to Eq.(12.20), the state duration's are exponentially distributed. The average state duration in units of number of state transitions, is thus

$$N_r = (1 - q_{ss})\sum_{r=1}^{\infty} r q_{ss}^{r-1} = \frac{1}{1 - q_{ss}} \tag{12.21}$$

Assuming that the state transition time is Δ_1, the average time duration of state s, T_s, is

$$T_s = \frac{\Delta_1}{1 - q_{ss}} \tag{12.22}$$

If, during data collection, the mobile was traveling with a velocity of V_1, the average distance traveled by the mobile while in the state s, D_{1s}, is thus

$$D_{1s} = \frac{d_1}{1 - q_{ss}} \tag{12.23}$$

where d_1, the distance the mobile travels in the state transition time, is given by

$$d_1 = V_1 \Delta_1 \tag{12.24}$$

An important question is, given that the experimental data was collected with a mobile traveling at a constant velocity V_1 and state transition distance d_1 how can the Markov chain process, as a time series, be scaled for another mobile velocity, V? Since the time variations of the

channel due to the mobile movement are caused by the spatial pattern of the electromagnetic field, the Markov chain process expressed in terms of distance is the fundamental stochastic process. That is, we may remove the 1 subscript and rewrite Eq.(12.23) as

$$\frac{D_s}{d} = \frac{1}{1 - q_{ss}} \tag{12.25}$$

where D_s is the average distance traveled while the system stays in state s and d is the state transition distance. Eq.(12.25) is invariant to the mobile velocity. If the simulation is to be run with time as the independent variable instead of distance, then one must use

$$\Delta = \frac{d}{V} = \frac{V_1 \Delta_1}{V} \tag{12.26}$$

as the state transition time.

A somewhat simplified Markov chain simulation approach one may use is the "continuous" approximation. In fact this continuous version is needed if the Lutz et al Markov model data [58] are to be used for simulation. For this approximation to be useful, the state transition distance should be small compared to the average state duration's $\{D_s; s = 1, N\}$. It was noted that the state duration probability distribution expressed in terms of the number of state transitions is exponentially distributed. The continuous approximation involves replacing this discrete exponential probability distribution with a continuous exponential distribution,

$$W_s(x) = \frac{1}{D_s} \exp\left(\frac{x}{D_s}\right) \tag{12.27}$$

where x is distance traveled(one may also use the equivalent exponential distribution for time elapsed with average time $T_s = \frac{D_s}{V}$).

The continuous Markov simulation procedure involves the following steps:

1. Select the initial state according to the steady state probabilities **p.**
2. Randomly select the length of the selected state according to the exponential distribution (12.27).
3. Select the next state randomly according to the normalized transition probabilities defined below.

Since the transition process from one state back to itself has been handled with the continuous approximation process, 1. and 2. above, there are only transitions to another state and the transition probabilities have to be renormalized so that they sum to unity excluding the return state transition probability, i.e., the correct transition probability to use in the transition from state m to state n is

$$p'_{mn} = \frac{p_{mn}}{1 - p_{mm}} \tag{12.28}$$

so that

$$\sum_{\substack{n=1 \\ n \neq m}}^{N} p'_{mn} = 1 \tag{12.29}$$

For the two-state examples in [58], there is only one other state and thus the normalized transition probability to the other state is unity.

12.4 Wideband Model

We have obtained only one paper [71] reporting on measurements and modeling of the wideband LMS channel using handheld and roof mounted RHCP antennas. A 30 MHz bandwidth probing signal was used and the magnitude of impulse responses were measured at a rate of 15.6 impulse responses per sec. The measurements were performed for elevation angles of 10 to 80 degrees using a transmitter on a light aircraft. However, channel parameters were given only for 25 degrees elevation angle. Sets of different environments were evaluated, but channel parameters are given only for rural and urban environments. Quoting the paper " Common to all environments is that echoes appear in general with small delays, usually smaller than 600 nsec...." It was also stated that the power of echoes with small delays decreases exponentially versus delay. In a mountainous environment echoes can be found with longer delays and higher power. For elevation angles above 55 degrees the user has line-of-sight conditions most of the time.

The proposed mathematical channel model consists of three separately identified components: the direct path, the "near echoes" which are assumed to be decreasing exponentially in strength with delay, and "far echoes". This model is quite similar to the generic mixed discrete/scatter model used in the GCS. However instead of characterizing the near echoes as unresolved paths, as is done with the mixed model, and using a scatter model with exponential delay power spectrum, there is some attempt to identify the individual near echoes and establish statistics on the number and delays of the near echoes. It seems reasonable to identify the near echoes with the unresolved paths of the mixed model. To this end, we need to obtain the rms delay spread of the near echoes. and the power of the near echoes relative to some reference. Unfortunately, it does not appear possible to obtain statistics on the rms delay spread of the "near echoes" from the reduced data given in Table 1 of [71]. Although they define the near echo power as decreasing exponentially, the meaning of the parameters given in Table 1 defining this echo power are ambiguous. In Table 1 they also give the probability distribution of the near echo delays as exponential in form with a delay constant of 170 nsec. For the urban environment and 320 ns for the rural environment. Additional data will need to be available before we can construct a mixed discrete/scatter model for the wideband LMS channel.

13 THE INDOOR CHANNEL

We have reviewed frequently mentioned papers on Indoor channel measurements and statistical modeling[72]-[76] and others [77]-[80] presenting only measurements on path loss and/or rms multipath spread. As a result of this review we conclude that the Mixed Discrete/Scatter model employed for the Outdoor radio mobile channels in the GCS is suitable for the short term or small scale fluctuations of the Indoor channel and the Indoor-Outdoor Microcell channel. The scatter portion of the model is primarily due to the myriad of multiple reflection paths in the rooms containing the transmitter and the receiver, while the discrete portion is due to the direct path and large reflecting surfaces in the building (or even outside). An exponential Delay Power Spectrum is appropriate for the scatter portions of the channels. Usually one scatter channel is appropriate but occasionally two are needed. As for Outdoor radio channels, long term or large scale fluctuations in signal strength of Indoor radio channels are best modeled by the lognormal distribution.

Section 13.1 presents the channel model standards proposed by the JTC[12] for the Indoor channel. These are similar to the JTC models for the outdoor channel briefly discussed in Section 7.1 of this report and in detail in [2]. They employ the Discrete Complex Gaussian Factorable WSSUS channel model presented in Section 7.1. While this model is simpler, the Mixed Discrete/Scatter model is more realistic.

Section 13.2 proposes a Mixed Discrete/Scatter model for the Indoor and Indoor-Outdoor channels. Section 13.2.1 reviews past channel modeling and measurements efforts in references [72] - [80] and Section 13.2.2 presents default scenarios for the Mixed model based upon these measurements.

[12] The JTC is a cooperative effort between committee T1 (actually technical subcommittee T1P1) sponsored by the Alliance for Telecommunication Industry Solutions (ATIS) and the Telecommunication Industry Association (TR46).

13.1 JTC Model

The channel model used for JTC channel simulation is a discrete WSSUS channel model for which the received signal is represented by the sum of delayed replicas of the input signal weighted by independent zero-mean complex Gaussian time variant processes of identical power spectra. Specifically, the complex low pass representation of the channel output, w(t), is related to the channel input, z(t), by Equation (7.4), repeated below,

$$w(t) = \sum_{n=0}^{N} \sqrt{p_n} h_n(t) z(t - \tau_n) \tag{13.1}$$

where p_n is the strength of the n^{th} weight, and $h_n(t)$ is the complex Gaussian process multiplying the n^{th} delayed replica.

The power spectrum of $h_n(t)$, called the Doppler spectrum of the n^{th} path, controls the rate of fading due to the n^{th} path. To completely define this channel model requires only a specification of the Doppler spectra of the tap weights $\{P(\upsilon)\}$, the tap delays $\{\tau_n ; n = 1,...,N\}$, and the tap weight strengths $\{p_n ; n = 1,...,N\}$. The pairs $\{p_n, \tau_n ; \ n = 1, \ ... \ , N\}$ are sometimes called the tap weight profile of the channel.

No claim is made that this model represents reality. In particular the inclusion of paths containing specular Doppler shifted components, as for the mixed model in Section 7.2 would be more realistic. However in the interests of simplicity and a preference for worst case scenarios, these components have been neglected in this model.

The process $h_n(t)$ is to be regarded as modeling the superposition of unresolved multipath components arriving from different angles and in the vicinity of the delay interval

$$\left(\tau_n - \frac{1}{2W} < \tau < \tau_n + \frac{1}{2W} \right)$$

where W is the bandwidth of the transmitted signal. Each ray, in general, has a different Doppler shift corresponding to a different value of the cosine of the angle between the ray direction and the mobile velocity vector.

In the interests of simplicity, it is assumed by the JTC that for indoor channels a very large number of receive rays arrive uniformly distributed in elevation and azimuth for each delay interval. Also, the antenna is assumed to be either a short or half-wave vertical dipole. These assumptions result in a Doppler spectrum that is nearly flat, and the choice of a flat spectrum has been made, i.e.,

$$P(\upsilon) = \frac{\lambda}{2V} \quad ; \quad |\upsilon| < \frac{V}{\lambda} \tag{13.2}$$

Table 13.1 presents three values of rms multipath spread, SA, SB, and SC for three channels for each of three environments: Indoor Residential, Indoor Office, and Indoor Commercial. For each environment the statistical variation of parameters was handled by specifying three tap weight profiles to represent mild(channel A), worse(channel B), and severe(channel C) multipath conditions. Channels A and B occur relatively frequently, while channel C is rare.

Table 13.1 RMS Multipath Spreads for Three Environments

Environment	SA (ns)	SB (ns)	SC (ns)
Indoor Residential	20	70	150
Indoor Office	35	100	460
Indoor Commercial	55	150	500

The tap weight profiles for channels A, B, and C are presented for the three environments in Tables 13.2, 13.3, and 13.4. These tapped delay line models were meant to apply for channel bandwidths of 10 MHz or lower.

Table 13.2 Indoor Residential Tap Weight Profiles

Tap	Channel A		Channel B		Channel C	
	Rel Delay (nsec)	Avg Power (dB)	Rel Delay (nsec)	Avg Power (dB)	Rel Delay (nsec)	Avg Power (dB)
1	0	0	0	0	0	0
2	100	-13.8	100	-6.0	100	-0.2
3			200	-11.9	200	-5.4
4			300	-17.9	400	-6.9
5					500	-24.5
6					600	-29.7

Table 13.3 Indoor Office Tap Weight Profiles

Tap	Channel A		Channel B		Channel C	
	Rel Delay (nsec)	Avg Power (dB)	Rel Delay (nsec)	Avg Power (dB)	Rel Delay (nsec)	Avg Power (dB)
1	0	0	0	0	0	0
2	100	-8.5	100	-3.6	200	-1.4
3			200	-7.2	500	-2.4
4			300	-10.8	700	-4.8
5			500	-18.0	1100	-1.0
6			700	-25.2	2400	-16.3

Table 13.4 Indoor Commercial Tap Weight Profiles

Tap	Channel A		Channel B		Channel C	
	Rel Delay (nsec)	Avg Power (dB)	Rel Delay (nsec)	Avg Power (dB)	Rel Delay (nsec)	Avg Power (dB)
1	0	0	0	0	0	0
2	100	-5.9	100	-0.2	200	-4.9
3	200	-14.6	200	-5.4	500	-3.8
4			400	-6.9	700	-1.8
5			500	-24.5	2100	-21.7
6			700	-29.7	2700	-11.5

13.2 Mixed Discrete/Scatter Model

This section first reviews prior work on Indoor Channel modeling (Section 13.2.1) and then presents parameters for a mixed model of the Indoor Channel (Section 13.2.2). One paper was found with detailed measurements on an Indoor-Outdoor Microcell channel and the measurements therein served as the basis of an Indoor-Outdoor Microcell channel model.

13.2.1 Review

We first review papers proposing stochastic models of the channels and then papers which focus on measurements of channel parameters. In [72] Dossi,Tartara, and Tallone summarized the results of an indoor channel characterization effort at 2 GHz using a 10 Megachip/sec pseudo random prober. The bandlimited impulse response of the channel was obtained at 160 equally spaced positions $\lambda/8$ apart along a 3 meter linear track to evaluate short term or "local" statistics within an office building and enclosed parking lot. To evaluate global statistics the track location was moved to various positions in the complex. Statistical analyses of these impulse responses were conducted with a view to validating some first and second order statistics.

Specifically, with regard to first order statistics, three distributions were considered for amplitudes of individual multipath components: Rice, Rayleigh, and lognormal. The impulse responses measured contained a direct path and another strong resolvable path plus a large number of unresolved echoes (the words resolved and unresolved are our terminology). Unsurprisingly, it was found that a Rice distribution was valid for the magnitudes of the resolvable paths and a Rayleigh distribution for the unresolved paths. However, when separate 3 meter sections separated large distances were examined, the unresolved paths were found to be modeled better with the lognormal distribution. This type of result is consistent with the measurements observed for outdoor

channels, i.e., short term fluctuations of unresolved paths are Rayleigh while long term fluctuations are lognormally distributed.

With regard to second order statistics, measurements were taken to validate the WSSUS model for the channel. Since the WSSUS model was designed to apply to a scatter channel in which unresolved paths only are involved, this attempt at validation seems ill-advised, considering that resolved paths were present. The impulse responses were processed to obtain correlations along the spatial axis for different path delays in addition to correlation along the path delay axis at different path delays. The results of the former type of correlations showed only that the spatial fluctuation rate of the direct path was less than that of the unresolved paths - a result to be expected apriori. The results of the latter type of correlation showed that the resolved paths were correlated and the unresolved paths decorrelated rapidly. It is important to note, however, that examination of the correlation functions given in their Fig. 5 showed the type of correlation function that one would expect for the impulse response of a WSSUS channel measured with a probe of the bandwidth used. *All in all, the paper serves as a justification for use of the mixed discrete/scatter model to represent the short term fluctuations of the indoor channel.*

Hashemi [73] has developed a stochastic model of the indoor channel based upon measurements in two office buildings. The transfer function of the channel was measured directly by a network analyzer sweeping the band from 900 to 1300 MHz. and the impulse response obtained by the Inverse Fourier Transform. A 3-term Blackman Harris window was used prior to transforming. The delay resolution obtained was quoted as 5 ns. Small scale (called "local") and large scale (called "global") variations of the impulse response were determined. To determine the small scale variations 75 frequency response estimates with spatial displacements of 2 cm were collected in each area. For a linear path the total spatial coverage of the 75 positions would be 5.5 wavelengths at the carrier frequency of 1.1 GHz.

The framework used for modeling the impulse response is what may be called the "bin" model. This model, used by some other researchers (e.g. [74],[75]), divides the time delay axis into small time intervals called "bins" where the duration of a bin is equated to the resolution of the channel probe (5 ns in the present case). Each bin is assumed to contain either one multipath component or no multipath component. No consideration is given to the fact that a bin may contain a superposition of portions of unresolved multipath components. Statistics, such as number of paths, arrival time distributions, and amplitude statistics are then derived for the values in the bins as if they were individual path amplitudes.

As for other researchers, lognormal distributions were found to fit the amplitude statistics data best for large scale variations of paths. Unlike [72], however, where Rayleigh distributions were found to fit the data best for the non LOS paths, lognormal distributions were also found best in [73] for the small scale variations. It should be pointed out, however, that while the local statistics in [73] were derived based upon 75 impulse responses spaced uniformly over 5.5 wavelengths, these responses do not constitute an independent set. Assuming uniformly distributed ray arrival angles, there will be roughly one independent impulse response every half wavelength. Thus there were at most 11 independent responses which is not enough to gather reliable statistics. Under the same assumptions, there were 40 independent responses in the data collection in [72]. On the other hand the resolution of the channel probe in [72] was quoted as 50 ns, which is ten times that of the prober in [73]. Thus the likelihood of unresolved paths is larger in [72] than [73], and, via the Central Limit Theorem, the increase in the number of unresolved paths would tend to produce Rayleigh statistics for the envelope of the impulse response.

Wideband multipath measurements in office buildings at 1300 MHz are presented by Rappaport [74] . 10 ns duration pulses (this duration includes any filters in the system) were sent with a period of 500 ns. The received pulse response was fed to a square law envelope detector and then to a 350 MHz digital storage oscilloscope.

Measurements of the resulting magnitude squared pulse response (frequently called the *power impulse response*) were recorded by digitizing the oscilloscope display and recording the result on flexible disk. As stated by the author "The impulse response measurements have a limited (≈25 dB) dynamic range due to the linear display scale of the oscilloscope". Another problem with the incoherent pulse probing technique relative to the coherent pseudorandom probing is the much higher post detection noise level due to the much larger post-detection bandwidth. Generally the larger noise level requires that channel responses be truncated to shorter delays to obtain adequate SNR's in the measurement. This truncation results in smaller estimated rms multipath spreads.

Multipath measurements were conducted at five fully equipped and operational factory buildings in central Indiana. Four environment classifications were used. The first classification was made based upon whether a Line-of-Sight (LOS) path existed or not. If not, the classification Obstructed Path (OBS) was used. Whether LOS or OBS, the environment was further classified as having Light Surrounding Clutter or Heavy Surrounding Clutter, the distinction being made based upon the number and heights of objects in the building.

Before processing to extract channel parameters, the power impulse response was quantized in delay, into 7.8 ns bins, and the energy of the pulse response in each bin was averaged. Then each bin component was regarded as a "path". Power impulse responses are measured at $\lambda/4$ intervals on a 1 meter path to yield 19 impulse responses. This set of impulse responses is used to examine small scale spatial fading of the individual multipath components. Assuming an independent impulse response every half wavelength, only 9 independent responses were available to estimate small scale statistics. Unfortunately 9 samples is much too small to establish statistical models of any reliability, particularly for long-tailed distributions like the lognormal. Two examples of spatial fluctuations are shown, one for an LOS and one for an OBS environment. In the LOS case (Fig.5 of (74)) a direct path and a specular component can be seen in addition

to smaller unresolved components. In the OBS case the measurements appear like those from a scatter channel with all unresolved components.

Using the power impulse responses, computations of rms delay spread and excess delay were carried out.. A later paper [75] which carries out more statistical analyses of the same data mentions that a threshold of better than 6 dB SNR was used for a bin to exclude noisy portions of the impulse response. In [74], excess delay (first moment or mean) and rms delay (second moment about the mean), are computed on both estimated delay power spectra (average of 19 power impulse responses) and on the power impulse responses. However, cumulative distributions for rms delay are given only for computations based on the power impulse responses. From scatter plots of rms delay spread (in Fig.'s 14 and 15 of [74]), with the rms spread based on estimated delay power spectra, one can see that the rms spreads vary from around 25 to 115 ns except for one isolated measurement in an LOS heavy clutter environment, for which the rms spread was 200 ns. Interestingly, all environments seem to have rms delay spreads scattering over the same range of delay. This is probably due to the discrete reflections usually present in the LOS environments at sufficiently long delays.

Rappaport, Seidel, and Takamizawa [75] utilize 7.8 ns binned power impulse responses obtained from the experiments discussed in [74], to formulate a static statistical model of the indoor communications channel. The author calls each bin that has a power level exceeding a 6 dB SNR threshold a" multipath component", although for unresolved paths this procedure does not actually yield the number of multipath components. Strictly speaking, what he calls the number of multipath components, N_p, provides information only on the total delay time interval, $N_p \cdot 7.8$ ns, that the power impulse response exceeds the 6 dB SNR threshold. The measured probability distribution of N_p was found to be well approximated by a Gaussian distribution.

In addition to N_p, the paper presents estimated values of what they call "the probability of multipath component arrival" as a function of path delay for the LOS and

OBS environments. This parameter represents the fraction of power impulse responses (LOS or OBS) measured for which the bin power at the delay of interest exceeded the threshold.

Using the measurements obtained in the experiments described in [74], estimates of the probability distribution of "large scale" and "small scale" fluctuations of bin power were obtained. As mentioned above, although power impulse responses were measured at $\lambda/4$ intervals on a 1-meter path to yield 19 impulse responses, a maximum of only around 9 independent responses actually exist. This set of impulse responses is used to examine small scale spatial fading of the individual multipath components. There was a collection of 25 1-meter paths that define the large scale fading of the LOS environment and 20 1-meter paths for the OBS environment. They found the lognormal distribution good approximations for both large scale and small scale fluctuations. Unfortunately 9 independent responses is much too small to establish statistical models of any reliability, particularly for long-tailed distributions like the lognormal.

Saleh and Valenzuela [76] present a channel model for indoor propagation based upon measurements of power impulse responses at 1.5 GHz using repetitive 10 ns duration pulse soundings of the first floor in a medium size (14 m by 115 m) office building. The transmitted frequency was swept over a band ± 100 MHz about the carrier frequency at a 100 Hz rate and the squared pulse responses were averaged over these sweeps. The authors give an argument to show that this procedure results in an improved multipath resolution of 4 ns. From our point of view, analysis of their procedure shows that this procedure results in an estimate of the Delay Power Spectrum similar to that provided by averaging different pulse responses over different transmitter or receiver positions.

It is important to note that the data base upon which the model was constructed excluded LOS paths and strong discrete paths with long delays. This makes the results useful for scatter channel modeling. The model arrived at, uses a discrete distribution of

paths arriving in clusters. In this model arrival rates are doubly Poisson: the cluster arrival rate is Poisson as are the arrival rates of the paths in each cluster. Equivalently, the time between cluster arrivals is exponentially distributed as is the time between path arrivals in a cluster. The mean arrival time between paths was found to be 5 ns, essentially the resolution of the system, while the mean arrival time between clusters was stated to be 200 to 300 ns.

For this model the strengths of the paths in each cluster decrease exponentially with delay as do the relative strengths of each cluster. For each room 20 power impulse responses were averaged and decaying exponentials were fitted to each cluster and to the leading peaks of successive clusters. Unfortunately the authors give only the average delay constants over all 8 rooms measured. Over the 8 rooms, an average delay constant of 20 ns was found for the individual clusters and 60 ns for the cluster to cluster delay constant.

Estimates of the statistics of the amplitudes of the individual paths yielded the Rayleigh distribution so that the individual paths could be modeled as Complex Gaussian. As mentioned previously, the data base upon which the model was constructed excluded LOS paths and strong discrete paths with long delays. It was found that for 50% of the cases a single cluster sufficed and only two clusters were required for virtually all measurements. It is clear that this model is very similar to the pure scatter model used in the GCS with either one or two scatter paths having exponentially shaped Delay Power Spectra. In fact there is a discussion comparing this model with the complex Gaussian Wide Sense Stationary Uncorrelated Scattering (GWSSUS) model used in the GCS. They conclude that the latter model is closer to physical reality but felt that the experiments did not provide sufficient resolution to answer definitively which to choose.

We consider now papers devoted to measurements of rms spread (which frequently include path loss also) . Calculations of rms multipath spread were made only on individual power impulse responses by Hashemi [73] as they have been in most other investigations. The use of moments of the Delay Power Spectrum, Doppler Power

spectrum, and Scattering function as gross parameters for modeling WSSUS channels was introduced by Bello [1][81]. These parameters were meant to apply to WSSUS channels only, i.e., channels without any discrete paths.

As mentioned previously in this report, radio channels generally contain a mixture of unresolved multipath components, a possible direct path, and a possible set of discrete paths (resolved reflected components). Only the collection of unresolved paths should be modeled as a WSSUS channel. However for virtually all papers modeling mobile channels, no attempt is made to extract direct and strong reflected components before carrying out computations on estimated Delay Power Spectra. Usually, the Delay Power Spectrum is not estimated at all (by averaging power impulse responses), and computations of rms delay and excess delay are carried out on the individual power impulse responses. The utility of such measurements has not previously been examined. For this reason we now investigate the relationship between rms spreads computed on individual power impulse responses and rms spreads computed on the Delay Power Spectrum via the simulation of a complex Gaussian WSSUS channel with a truncated exponential Delay Power Spectrum.

The mathematical formulation of the simulation is as follows. A rectangular pulse of duration T (>>1) ns is transmitted through a complex Gaussian WSSUS channel which is approximated by a uniformly tapped delay line model with 1 ns spacing in which the tap weights are independent complex Gaussian random variables with strengths following an exponential shape having a delay constant of s (>>1) ns. We have arbitrarily truncated the impulse response at 7 delay constants so that the weakest tap weight is approximately 30 dB below the strongest tap weight. Since we are analyzing only the time delay properties of the channel we can ignore the time variations and confine our evaluations to a random time-invariant channel.

Thus the impulse response of the propagation medium to be simulated for an assumed delay constant of s ns can be represented as

$$g(t) = \sum_{0}^{7s} h_k \delta(t - k) \tag{13.3}$$

where the $\{h_k\}$ are independent complex Gaussian variables and $\delta()$ is a unit impulse. The strength of h_k is given by

$$E\left[\left|h_k\right|^2\right] = \frac{1}{s} e^{-\frac{k}{s}} = Q(k) \; ; \; \{k = 0, 7s\} \tag{13.4}$$

where Q(k) is the Delay Power Spectrum of the channel sampled at a GHz rate. One may compute that the rms delay spread of the impulse response of this channel is given by 97.8 ns for s=100 ns. If the impulse response were not truncated the rms delay spread would be 100 ns.

A probing pulse

$$p(t) = \begin{cases} \frac{1}{\sqrt{T}} & ; \; 0 < t < T \\ 0 & ; \; \text{elsewhere} \end{cases} \tag{13.5}$$

is transmitted through the channel with impulse response (13.3). The measured pulse response w(t) is thus

$$w(t) = \sum_{k=1}^{7s} h_k \, p(t - k) \tag{13.6}$$

It is convenient to represent a 1 GHz sampled and normalized version of the magnitude squared received waveform as a discrete probability distribution

$$\mu(\xi) = \sum_{k=0}^{7s+T-1} P_k \delta(\xi - k) \tag{13.7}$$

where we have assumed that T is an integral number of nanoseconds and the "probability" of the delay value k is given by

$$P_k = \frac{|w(k)^2|}{\sum_{l=0}^{7s+T-1} |w(l)^2|} \tag{13.8}$$

The standard deviation of $\mu(\xi)$, σ_i, is equal to the "instantaneous" rms multipath spread of the measured channel response w(t). This is given by

$$\sigma_i = \sqrt{\sum_{k=0}^{7s+T-1} k^2 P_k - \left(\sum_{k=0}^{7s+T-1} k P_k \right)^2} \tag{13.9}$$

The obvious approach to calculation of the rms multipath spread is to average a large number of magnitude squared channel pulse responses (also called the power delay profile) to obtain an estimate of the Delay Power Spectrum and then to compute the rms multipath spread from this estimated spectrum. From Eq.'s (13.4) and (13.6) it may readily be determined that the average power delay profile is given by the convolution of the true WSSUS channel Delay Power Spectrum with the magnitude squared pulse, i.e.,

$$\tilde{Q}(m) = E\left[|w(m)|^2\right] = \sum_{k=0}^{7s} Q(k)|p(m-k)|^2 \tag{13.10}$$

where $\tilde{Q}(m)$ is the limiting value of the average power delay profile as the number of terms averaged approaches infinity. Because of the convolution property it is readily shown that the rms multipath spread of $\tilde{Q}(m)$, $\tilde{\sigma}$, is given by

$$\tilde{\sigma} = \sqrt{\sigma^2 + \frac{T^2}{12}} \tag{13.11}$$

where σ is the rms multipath spread of the WSSUS channel Delay Power Spectrum Q(m). We have already pointed out that for the example at hand σ=97.8 for our example.

100 independent values of σ_i were generated for T=5,10, 20, 30, 40, 50, 60, 80, 100, and 250 ns and s=100 ns. Table 13.5 presents $\tilde{\sigma}$ and the sample mean and standard deviation (m_{100} ,s_{100}),respectively, of the 100 samples of σ_i for each of the ten values of T, all of which have been normalized to the value of the WSSUS channel rms multipath spread, σ=97.8 ns. These results have been presented in normalized form because they should be valid for any rms multipath spread provided all parameters are >>1 ns.

For values of T/σ less than ≈ 1 the probing pulse spreading causes little increase in $\tilde{\sigma}$, the rms multipath spread based upon the average power delay profile. Note that the sample mean m_{100} is very close to $\tilde{\sigma}$ indicating that for the range of T/σ values considered, σ_i is essentially an unbiased estimator of rms multipath spread. Note also that for small T/σ values s_{100} is a relatively small fraction of $\tilde{\sigma}$, indicating that σ_i can be a useful estimate of $\tilde{\sigma}$, particularly when the range of true rms spreads in an environment is much larger than T/σ. Thus, for example, suppose that the true rms multipath spread in the

Table 13.5 Normalized Mean and Standard Deviation of 100 Samples of "Instantaneous" RMS Multipath Spread vs. Normalized Pulse Width

Normalized Probing Pulse Width T/σ	Norm. RMS Spread of Pwr Delay Profile $\tilde{\sigma}/\sigma$	Normalized Sample Mean m_{100}/σ	Normalized Sample Standard Deviation s_{100}/σ
.051	1.00	.99	.047
.102	1.00	1.01	.074
.204	1.00	1.00	.101
.307	1.00	1.01	.108
.409	1.01	1.01	.142
.511	1.01	1.00	.150
.613	1.02	1.01	.169
.818	1.03	1.02	.176
1.022	1.04	1.07	.176
2.556	1.24	1.22	.258

environment measured varies from 20 to 100 ns and the probing pulse used was 10 ns. Then T/σ varies from .5 (at 20 ns) to .1 (at 100 ns). According to Table 13.5, at $T/\sigma=.5$ the normalized rms error in rms multipath spread measurement is approximately .15 while at $T/\sigma=.1$ it is approximately .074. It follows that the rms value of error introduced by the instantaneous rms multipath spread estimator will range approximately from 3 ns (at 20 ns multipath spread) to 7.4 ns (at 100 ns multipath spread).

Considering the nonstationarities involved in the measurements, these small errors are not significant and will result in a small spread of the measured range of multipath spreads. Thus it appears reasonable to use instantaneous rms multipath spread measurements in lieu of rms multipath spreads based on average magnitude squared impulse responses as long as the effective[13] probing pulse duration is small compared to the range of multipath spreads measured.

Table 13.6 presents a summary of rms multipath measurements from references [73], [74], and [76]-[80]. Where possible an attempt has been made to select data from these references dominated by unresolved paths rather than direct paths and large resolvable discrete paths. In Table 13.6 the range of measured rms multipath spreads is given in column 2. The next three columns present the 10, 50, and 90 percentiles of the measurements taken from graphs in the corresponding references. Thus, for the data from Ref [80], for 10% of the time the rms multipath spread was less than 40 ns, for 50% of the time the rms multipath spread was less than 125 ns, and for 90% of the time the rms multipath spread was less than 185 ns. The sixth column presents the effective pulse duration or resolution of the channel probing method and the last column is reserved for comments. We now elaborate on the comments presented.

[13] There are a variety of channel measurement approaches in addition to simply transmitting a probing pulse. However, in all cases one may define an effective probing pulse. Thus in pseudo random BPSK probing the effective pulse is the autocorrelation function of the probing signal, and in transfer function measurement, it is the Fourier Transform of the frequecy domain window.

As noted in Table 13.6, average magnitude squared pulse responses were used to estimate the Delay Power Spectrum, and the rms multipath spread was based upon this estimate. Pulse responses for either the transmitter or receiver located at 8 equally spaced points along a 1.2 m square were used for the Delay Power Spectrum estimate. Assuming an independent measurement every half wavelength, there were approximately eight

Table 13.6 Summary of Indoor RMS Multipath Spread Measurements

Data from Ref.	RMS Multipath Spread Range (ns)	10% (ns)	50% (ns)	90% (ns)	Eff. Pulse Duration (ns)	Comments
[80]	30 - 250	40	125	185	25	315×110 m bldg outside dimens. Incl: 4 145×36 m bldgs of 6 floors each.Vertical paths and horizontal paths. 850 MHz .Some LOS meas. Averaged magnitude squared pulse responses used.
[79]	20 - 218	25	60	140	25	Bldg in form of H, 118×48 m, with 20×23 m projection. Worst case rms spread due to hill behind building. Some LOS meas. 850 MHz. . Averaged magnitude squared pulse responses used.
[78]	10 - 45 10 - 55	16 17	26 30	35 45	25	Meas. for two buildings at 910 MHz. One bldg has 60 m and 45 m wings and other 35 m square. Some LOS meas. Instantaneous magnitude squared pulse responses used.
[77]	20 - 200	20	67	95	10	Office building 50×27 m with mostly soft partitions. Obstructed LOS. 1.5 GHz operation. Instantaneous magnitude squared impulse responses used.
[76]	12 -50	15	25	42	4	Same bldg as in [79] at 1.5 GHz . However, excluded paths with direct LOS as well as discrete paths with long delays. Frequency averaged magnitude squared pulse responses.
[74]	25 -150	45	105	130	10	Factory bldg's with square footages of 74,100,150,28, and 21 thousand sq. meters. Obstructed paths only. 1.3 GHz operation. Instantaneous magnitude squared pulse responses used.
[73]	8 - 42	19	26	34	5	Two office bldg's - can infer only that one dim. is ≥ 30m. 1.1 GHz operation. Data presented here for 30m transmit-receive sep. to minimize LOS path contr..Inst. mag. sq. pulse responses used.

independent pulse responses. This should reduce the rms error in estimating the rms multipath spread relative to the "instantaneous" method by $\sqrt{8}$. The 315×110 m building actually consisted of four 6-floor buildings, each 145×36 m in plan with a large central cavity 31 m wide running through the whole complex. The statistics on rms multipath spread presented are a combination of measurements for a cut along the fourth floor of one building and a vertical cut through building 2 utilizing floors 2 - 6. There was not a significant difference in the statistics of rms multipath spread for the horizontal and vertical cuts. We only used the combined data in Table 13.6 to minimize the percentage of cases having a direct LOS path.

Ref.[79] compares rms multipath measurements already presented for the building described in [80] with those for a much smaller building using the same operating frequency and probing equipment. Surprisingly, the worst multipath spread is almost as large as for the large building and the percentiles are quite large. It was felt that a hill behind the building contributed to the large spreads.

In [78] rms multipath results are presented for two buildings and two different frequencies, 910 MHz and 1.75 GHz using a 40 Megachip/sec pseudo-random probe. Table 13.6 arbitrarily presents results only for 910 MHz since the results at the two frequencies differ a small amount. Experiments were conducted at the Communications Research Center and at Carleton University, both at Ottawa. Instantaneous rms multipath spread measurements were used. Since the effective probing pulse duration is 25 ns and the range of measured rms multipath spreads are relatively small (say 10 - 50 ns) the error in using the instantaneous rms multipath spread needs to be examined. From Table 13.5 it is determined that the rms error is 7.5 ns when the rms spread is the maximum measured of 50 ns.and less than 3 ns at the minimum measured spread of 10 ns. Even in this extreme case the use of instantaneous spreads does not have a severe impact if the channel were truly WSSUS.

In [77] channel measurements were obtained with a 100 to 500 Megachip/sec pseudorandom probe at 1.5 MHz. Three buildings were measured, but in only one of these buildings were there any paths with the direct path obstructed. We present results only for the obstructed direct paths. Only instantaneous rms multipath spread measurements were
obtained. From Table 13.5 with a 10 ns probing pulse the rms error introduced is around 10 ns at the maximum measured rms spread and around 3 ns at the low end of the measured range. These errors are not significant compared to the range of rms spreads measured. It is interesting to note that this modest sized building produced the same size spreads as in the somewhat larger building in [79] and the much larger building in [80].

The building examined in [76] is the same as the small building in [79]. Note that the spreads are considerably less than were reported for the same building in [79]. This discrepancy was noted in [76]. The reason for the discrepancies was explained on the basis of the path loss under which the large spread was measured. In the case of [80], the large rms spreads occurred only when the received signal levels were extremely low, e.g., 100 -140 dB of path loss. When Devasirvatham [79] truncated the data to a path loss of less than 100 dB, as was the situation with the paper being reviewed, comparable results were said to be obtained. Of course, the reduced SNR of the channel measurements in [76] relative to [79], obscured the tails of the pulse response and limited the measured multipath delays to 200 ns. This limitation could have reduced the measured spreads in [76].

The measurement procedures used by Rappaport in [74] have already been discussed in detail above. Due to our interest in the unresolved paths the rms multipath spread statistics presented in Table 13.6 are for the cases of obstructed direct path measurements. Instantaneous rms multipath measurements were used. Using Table 13.5 it is determined that the rms error is around 8 ns at the largest rms spread measured and less than 3 ns at the low end.

The measurements procedures by Hashemi in [73] have already been discussed above. Instantaneous rms spreads were measured covering a range close to those measured in [76] and [78]. With the 5 ns effective pulse width, we see from Table 13.5 that the rms error is only 3.4 ns at 42 ns, the largest rms spread measured, and 1.4 ns at the smallest spread measured. For Table 13.6 we selected statistics only for the path lengths of 30 m in the hope that this would lead to mostly paths without a significant direct path component.

The measurements reviewed in this section so far have been restricted to both the transmitter and receiver located in the same building. However there is interest in situations wherein one terminal is outside and the other is inside the building. We have only one reference [83] in which such measurements were made. These measurements are now reviewed.

The measurements were carried out by Devasirvatham using the same equipment and measurement procedures as were used by him for the measurements in [79] and [80] discussed previously. All measurements were made with the transmitter located inside the buildings around 1.8 m above the floor. The receiver was outside in the Bellcore radio research van representing a possible base station.

Measurements were taken for two residences and one office building. We have encountered the office building in [76] and [79]. Residence 1 is an apartment on level 2 of a two-floor condominium complex consisting of groups of three buildings surrounding 40×30 m courtyards. The receiver was positioned at three possible locations, 8 and 31 m in front of Residence 1, and 82 m away in an adjacent courtyard, in all cases with the receiver slightly above roof level. For the 82 m distance there was no line-of-sight to Residence 1. As in [79] and [80], average power delay profiles were used to calculate rms multipath spreads.

The first row of data in Table 13.7 presents the min, max, 10%, 50%, and 90% values of measured rms multipath spread for the two receiver LOS positions in the near courtyard of Residence 1. The second row in Table 13.7 presents the measured rms multipath spreads for the receiver located in the non-LOS position in the adjacent courtyard. Note the striking increase in rms multipath spread for the non-LOS position. The most likely explanation is the existence of a direct path in the first two receiver positions. Another possibility is the existence of resolved and unresolved reflections from other buildings in the third receiver position. In fact the worst case averaged power delay profile presented in Fig.3 of [83] for the third receiver position shows a strong reflection from another building complex arriving 1 microsec after the first arriving energy. This profile had an rms multipath spread of 420 ns. If the strong reflection component is removed the profile may be approximated by an exponentially decaying profile with an rms spread of 390 ns. It is interesting to note that the rms spreads are significantly larger than those measured for the largest buildings of the strictly indoor channels shown in Table 13.6. Resolved and unresolved reflections from other houses are undoubtedly the cause of the increased spread.

Table 13.7 Indoor-Outdoor Channel Measurements from [83]

RMS Multipath Spread Range (ns)	10% (ns)	50% (ns)	90% (ns)	Comments
30 -90	34	62	88	Residence 1 is unit on second floor of a two floor condominium complex. Receiver situated 8 and 31 m from transmitter in courtyard in front of Residence 1 and at roof level. Averaged power delay profiles used to calculate rms multipath spreads.
220 -420	225	270	350	Receiver situated 82 m from Residence 1 behind buildings in an adjacent courtyard from Residence 1 and at roof level. Buildings block line-of-sight. Averaged power delay profiles used to calculate rms multipath spreads.
40 -310	60	145	250	Residence 2 is a two story house at the edge of a one-acre zoned development. Receiver positioned 46 and 168 m from the front and 114 m from back of Residence 2. Some obstruction of LOS by houses. Averaged power delay profiles used to calculate spreads.
20 -320	40	100	270	Same office building as in [76] and [79] of Table 13.6.Built against the side of a small hill behind it. Receiver positioned 69 m in front and 15 m in back of building. Averaged power delay profiles used to compute rms multipath spreads

Residence 2 is a two story house at the edge of a one-acre zoned development. The receiver van was positioned at three locations: 46 and 168 m from the front of Residence 2 on a road running parallel to the house, and 114 m from Residence 2 on a road running past houses located behind Residence 2. There was some obstruction by houses in the last two locations, so that both LOS and non-LOS channels were measured. The rms multipath spreads listed in row 3 of Table 13.7 show that large and small rms multipath spreads were measured. Most likely, the large ones are due to the non-LOS channels and the small ones to the LOS channels. Fig.4 of [83] presents the worst case averaged delay profile. This profile is similar to the worst case for Residence 1 mentioned above, in that one relatively strong resolvable path can be identified (at .7 microsec) and the remainder can be approximated by an exponentially decaying profile (with an rms spread of around 360 ns).

The fourth row in Table 13.7 presents measurements for the office building which we have encountered before (see the [76] and [79] measurements listed in Table 13.6) for strictly indoor measurements. The receiver van was positioned in the driveway , both 69 m in front of the building and 15 m behind it. The worst case averaged power delay profile was shown in Fig.5 of [83] corresponding to the position behind the building where a hill was situated. It consisted of two scatter paths separated by .6 microsec, each with approximately the same delay constant of around 139 ns, plus a small direct path.

13.2.2 Default Scenarios

Section 13.2.1 reviewed the multipath measurements and models presented in references [72] - [80]. It was found that the Mixed model, i.e. a model consisting of a mixture of complex Gaussian WSSUS " scatter paths" and a set of discrete paths (including a possible direct path) models the short term or local area fluctuations of the channel. An exponentially decaying Delay Power Spectrum appears to be the best shape to use for the scatter paths. There is in fact some basic theory on electromagnetic field decay in lossy cavities that leads directly to the exponential decay and actually has been used to predict well the time constant of this decay in indoor channel probing [82].

Admittedly there is some disagreement between experimenters as to whether the short term fluctuations in amplitude of multipath components are modeled best with lognormal or Rayleigh statistics, the former conflicting with the complex Gaussian model. However, an examination of the experiments reveals that for those experimenters arriving at lognormal statistics as a better model, the number of samples used to form the empirical distribution functions is inadequate to develop reliable enough statistics to allow choosing either lognormal or Rayleigh statistics.

Having settled on the Mixed model, we still have the task of proposing ranges of parameter values. Specifically we need to specify

1) the rms multipath spreads, Doppler spreads, relative strengths, locations, and number of scatter paths, and

2) delays, Doppler shifts, relative strengths, and number of the discrete paths, including the direct path, and

3) the relative strengths between the discrete and scatter paths.

We have included the Doppler effects in the above list because we assumed that one terminal is moving.

Unfortunately, as in the case of the Outdoor Channel, experimenters have made no attempt to extract the structure parameters outlined above. The primary effort has been devoted to the collection of the rms multipath spread and path loss. In some cases [74],[77] there were attempts to classify data according to whether an LOS path existed or not, which is a step in the right direction. Also Saleh and Valuenzela [76] excluded measurements with a physical LOS path as well as discrete paths at long delays. Presumably this procedure enhanced the likelihood of having scatter paths only. However, the fact that a physical LOS does not exist does not mean that an electrical, albeit weakened, LOS component does not appear in the impulse response.

Although a weaker second scatter path was sometimes noted in [76] we have decided to simplify the model and use a single scatter path to model the unresolved paths as was done in the default scenarios for the macrocell channels. Based upon the reported measurements, Table 13.8 presents proposed small, medium, and large values of the rms multipath spread for four environment classifications: Indoor Small Office, Indoor Large Office, Indoor Commercial, and Indoor-Outdoor Microcell (Residential or Office).

Table 13.8 RMS Delay Spreads of Scatter Path for Four Environments

Environment	Small rms delay spread-ns	Medium rms delay spread-ns	Large rms delay spread-ns
Indoor Small Office	20	60	90
Indoor Large Office	40	120	180
Indoor Commercial	40	110	140
Indoor-Outdoor Microcell (Resid. or Office)	40	150	300

As for the JTC model, for default scenarios it is assumed that the ray arrival angles are uniformly distributed in both elevation and azimuth, and the antennas are non-directive, which yields the uniform Doppler power spectrum, Eq. (13.2), for one terminal moving. The computer program is more general, allowing the additional choices of the Clarke and Jakes Doppler spectrum, Eq. (7.30) (also called the Classic spectrum by the JTC), and an arbitrary 32'nd order IIR Doppler spectrum[14].

The preceding discussion has provided data from which the unresolved paths of the Indoor channel may be modeled as Complex Gaussian WSSUS channel. A complete specification of the Mixed channel requires that we specify the parameters of the Discrete Non-Fading Paths model also. As for the Outdoor Channel default scenarios, four special "structure" cases are defined:

1) unresolved paths only, i.e., no discrete paths including no direct path

2) unresolved paths plus a direct path only

3) unresolved paths plus discrete paths with no direct path

4) unresolved paths plus discrete paths plus a direct path

We have already considered structure 1). Selection of a value of rms delay spread for the scatter path from Table 13.8 will specify the assumed exponential shaped Delay Power Spectrum (the exponential "delay constant" equals the selected rms spread). Specification of the mobile velocity and carrier frequency will fix the Doppler Power Spectrum via Eq.(13.2).

When structure 2) occurs, in addition to selecting the rms delay spread of the scatter path from Table 13.8, it is necessary to allocate the relative power of the channel between the scatter path and the direct path. Three choices are given in Table 13.10, below.

Table 13.9

Choices for Power Allocated to Scatter Path relative to Total Power

	Low Scatter Power	Medium Scatter Power	High Scatter Power
Relative Power	-10 dB	-3 dB	-.5 dB

In addition to the choice of delay spread for the scatter path from Table 13.8 and the allocation of relative power to the scatter path from Table 13.9, it is necessary to choose the number of discrete paths, allocate relative power to these paths, and select the delays of these paths, when structure 3) is selected. Considering the paucity of data this is a big order and we must make arbitrary choices. The small amount of data on discrete paths that can be squeezed from [73]-[80] shows 1 path usually, so we assume only one path for the default scenario. We consider two delay positions for this discrete path: *near* at 1/2 the maximum rms spread and *far* at 3 times the maximum rms spread for whichever environment is selected. The strength of the scatter path power relative to the total channel power is selected as *low scatter*, *medium scatter*, or *high scatter* in accordance with Table 13.9, i.e., the same way as for structure 1), since there is a single discrete path in both cases.

Structure 4) is the most general situation. A choice is first made as to the power of the scatter path relative to the total (including the direct path) discrete paths' power using Table 13.9 as for structures 2) and 3). The last step is to select the fraction of the

[14] C.M.Keller, Generic Channel Simulator Software, MIT Lincoln Lab. Project Memo 44PM-AST-0046, 7 June 1996.

total discrete paths' power to be devoted to the direct path. The choices of *low direct, medium direct ,* and *high direct* are listed in Table 13.10.

Table 13.10

Choices for Direct Path Power Relative to Total Discrete Paths' Power for Structure (4)

	Low Direct Power	Medium Direct Power	High Direct Power
Relative Power	-10 dB	-3 dB	-.5 dB

To complete the channel specification it is necessary to choose the Doppler shifts for the discrete paths (including the direct path). This will be done the same way as was done for the outdoor channels. The Doppler shift as a fraction of the magnitude of the maximum Doppler shift, V/λ, is given by

$$f_k = \frac{\nu_k}{V/\lambda} = \mathrm{Cos}(\alpha_k) \qquad (13.12)$$

where α_k is the angle between the velocity vector of the mobile and the line-of-sight to the reflecting object (or to the transmitter in the case of the direct path), and ν_k is the Doppler shift of the k-th discrete path. For the LOS path the Doppler shift is V/λ. Due to the apriori arbitrary angular directions $\{\alpha_k\}$, for the non-LOS discrete path the fractional Doppler shifts can lie anywhere in the interval (-1,1). For this reason the program will select the Doppler shift of the discrete path randomly in this interval.

14 GENERIC CHANNEL SIMULATOR

The Generic Channel Simulator (GCS) is a companion software package designed to implement the channel models developed under the present contract and two prior related contracts, DAAB07-93-C-N651 and DAAB07-94-C-H601. Initially the modeling and simulation was confined to the HF Ionospheric channel. The tapped delay line models and associated statistical channel models employed were of a generic nature and it was found that much of the software could be employed directly or modified slightly to model other radio channels, particularly the mobile cellular and non-cellular channels in the higher frequency bands. Thus under subsequent contracts the repertoire of simulated channels has expanded considerably. This section presents tree diagrams showing the directory structure of the program at this time and the names of individual programs. A brief discussion of the individual programs and the parameter inputs is presented. Currently, the GCS software is under development by the MIT Lincoln Laboratories.

For each channel the intent is to provide separate programs which simulate distortion (e.g. time variant multipath), and additive disturbances (e.g., interference) in addition to programs that allow estimation of path loss. Channel model and additive disturbance programs are normalized so any desired SNR can be achieved by adjustment of scale factors after simulator output files have been generated. The software has been programmed in ANSI C and developed in a Unix environment on a SUN workstation. Both Motif Windows and command -line scripts can be used for entry of parameters.

Fig.s 14.1-14.5 present the directory structure. As Fig.14.1 indicates, there are three initial subdirectories: GenChanSim/HF, GenChanSim/MobileChan, and GenChanSim/Sat. The latter subdirectory is intended for conventional geostationary satellite channels. At the present time the subdirectory is empty and reserved for future use. Each of these subdirectories has three further subdirectories /PropChan, /AddDist, and /PathLoss, to include the simulation of propagation channel distortion, additive disturbances, and estimation of path loss.

Fig.14.2 continues with the directories and programs below the /HF subdirectory. The program **propchan** is located in the /HF/PropChan subdirectory. This program provides for the simulation of both normal and disturbed ionospheric propagation channels. The normal channel, which corresponds to the case of a typical quiet mid-latitude ionosphere, is modeled as a set of paths with specified delays, Doppler shifts, linear group delay distortions, and relative amplitudes. The disturbed channel, which corresponds to a disturbed ionosphere as occurs frequently at the high latitudes and near the equator, is modeled as a set of complex Gaussian factorable WSSUS channels, one for each propagation mode. Theoretical shapes are used for the Doppler and Delay Power Spectra. The model requires specification of the Doppler spread, Delay spread, relative strength, delays, and Doppler shifts for each propagation mode. In all the programs the user must select a sampling rate. [84] presents details on these channel models and proposes ranges of parameter values. Also Dean [85] has presented ranges of propagation channel parameters suitable for testing modems.

In the /HF/AddDist/ subdirectory are three programs: **atmosphere**, **narrowband**, and **gaussnoise**. **Atmosphere** simulates lightning induced noise (usually called atmospheric noise), **narrowband** simulates the narrow band interference contributed by various narrowband HF communication signals, and **gaussnoise** simulates a complex Gaussian noise stream to model receiver noise.[86] provides a users manual for the HF programs. Since the directory structure has changed some updating is required, although there has been no change in the HF software per se. However during the current contract, default scenarios have been developed for the HF channel based upon results in [84] and [85]. These are incorporated in the GCS. The Appendix to this report documents the HF scenarios. In the /HF/PathLoss subdirectory a program pathloss is shown ,without boldface, to denote the fact that such a program has not yet been finalized. The intention here is to incorporate an existing program, e.g. IONCAP, to realize the path loss estimation. Use of IONCAP will also provide automatic calculations of individual path

strengths and delays for normal ionospheric paths when terminal location and ionospheric conditions are specified.

Fig.14.3 shows some directories below the /MobileChan subdirectory. The /MobileChan/PathLoss subdirectory shows a number of programs for path loss estimation. Details on these programs may be found in [2], Section 3.1 and 4.1. **qkarea** is the Institute for Telecommunication Sciences Irregular Terrain Model [87] (updated version of the well

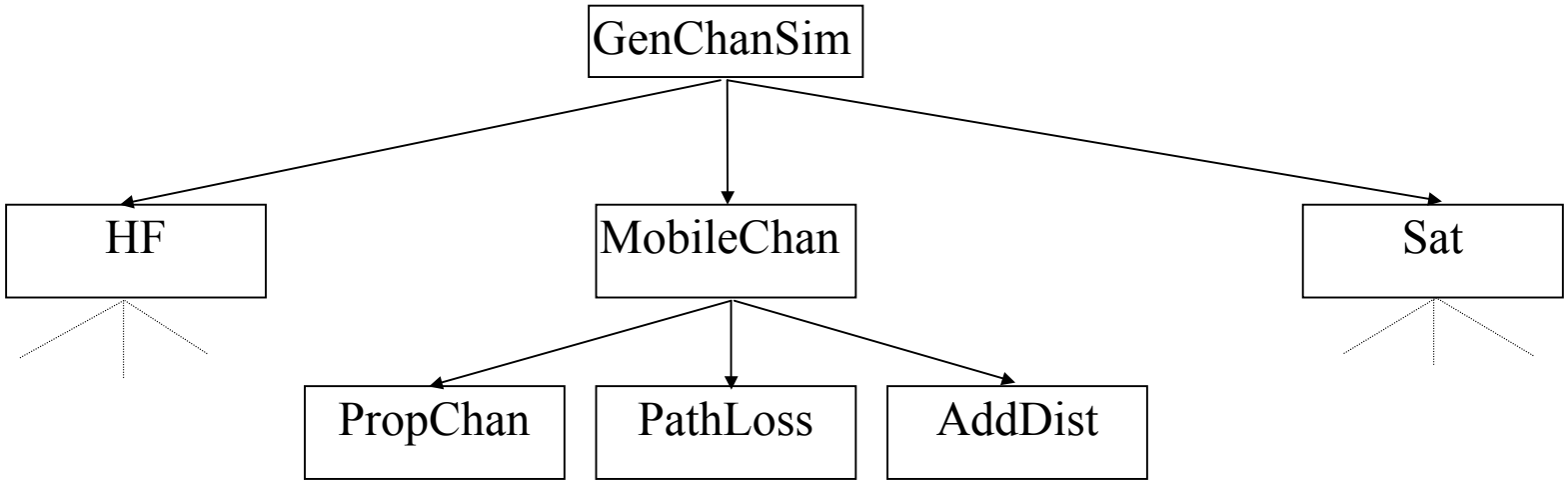

Fig. 14.1 Generic Channel Simulator: First Two Directory Levels

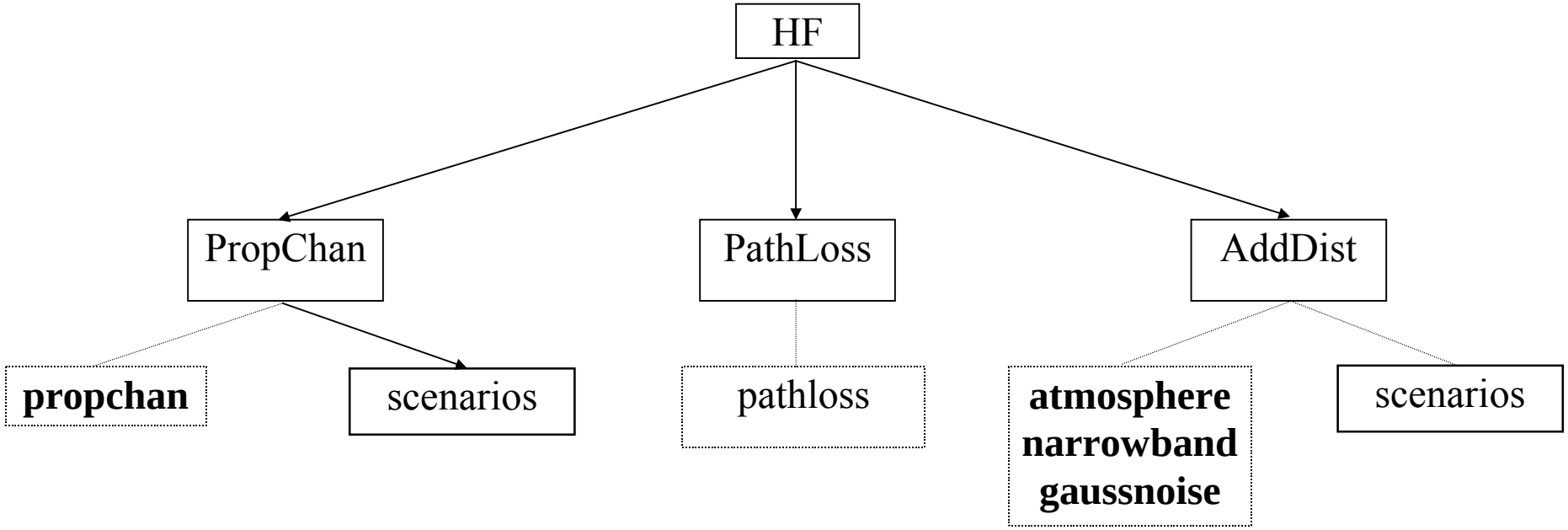

Fig. 14.2 HF : Subdirectories and Programs

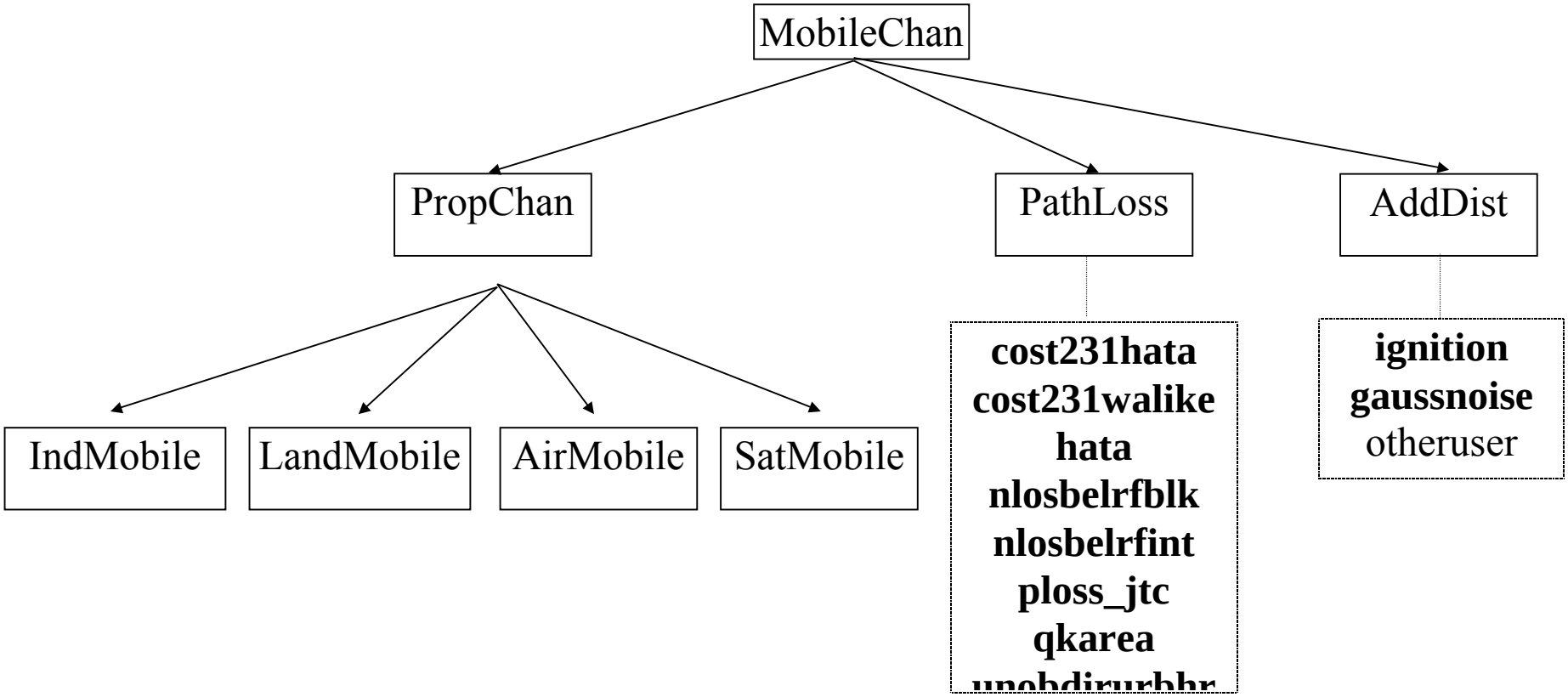

Fig. 14.3 MobileChan: First Two Subdirectory Levels and Programs

known Longley-Rice model) applicable primarily to non-urban situations. **hata** is the well known empirical Okomura-Hata model [88] appropriate to flat urban and suburban environments but limited to base heights greater than 30 meters and antennas above the roof line. The Euro-COST 231 Working Group on UHF Propagation extended the Okomura-Hata model from an upper frequency limit of 1500 MHz to 2000 MHz. This is the **cost232hata** program. COST 231 [89] also developed another model for the flat urban environment based on separate work by Walfisch and Ikegami. This model allows the base antenna to be somewhat below the roof line. However the performance is poor if the base antenna drops very far below the roof line because wave guide effects of street "canyons" and corner diffraction are not considered.**Cost231walike** is an implementation of this model.

The routines **nlosbelrfblk**, **nosbelrfint**, were formulated in [2] to extend **cost231walike** so that a low base antenna could be used, i.e., so that macro and micro cells could be handled in the same formulation. **nlosbelrfblk** and **nosbelrfint** apply to path losses when there is no line-of-sight between transmitter and receiver, the former applying when the receiver is not at an intersection and the latter when it is. In [2] the terminology used for these programs is "Walfisch/Ikegami with 2D Road Guiding". **unobdirurbhr** computes path loss when there is a line-of-sight between between transmitter and receiver in a non-rural environment**. ploss_jtc** is an implementation of path loss models proposed by the JTC [90] plus the modified exponential distribution (MED [91]) to accommodate path loss through vegetation.

The subdirectory /MobileChan/AddDist/ has the program **ignition** which realizes the ignition noise model described in Section 11. **gaussnoise** is the same receiver noise program mentioned previously and is accessible to all /AddDist/ subdirectories. A program **otheruser**, not yet implemented, will model other user interference.

Fig.14.4 expands the directory structure below the /MobileChan/PropChan/ LandMobile/ subdirectory . First the Land Mobile channels are subdivided into cellular

channels under the /LandMobile/cellular/ subdirectory and VHF/UHF non-cellular channels under the /LandMobile/VHFUHF/subdirectory. This subdivision parallels the subdivision of channels as in Sections 7 and 10, respectively. Thus the /LandMobile/cellular subdirectory is divided into a /JTCmod/ subdirectory dealing with the JTC multipath models of Section 7.1 and into a /mixedmod/ subdirectory dealing with the improved mixed models proposed in Section 7.2.

jtcchan is the program that implements the Discrete Complex Gaussian Factorable WSSUS channel model discussed in Section 7.2. Thus input parameters are the strength and delay of each path together with the Doppler Power Spectrum and carrier frequency. Here one may choose the following shapes: Classic (Jakes/Clarke) spectrum, a flat spectrum, or an arbitrary spectrum specified by an appropriate file. The default scenarios proposed by the JTC and listed in Section 7.1 are implemented via **jtcchan**.

mixedchan is the program that implements the generic mixed model consisting of a Discrete Non-Fading Paths model used to model the resolved paths and the Complex Gaussian Factorable WSSUS model, or scatter model, for short, used to model the unresolved paths. Each isolated group of unresolved paths is represented by a separate scatter path. Thus the strength, delay, and fractional Doppler shift (relative to maximum) of the resolvable paths and carrier frequency are input parameters. For each scatter path it is necessary to specify the rms delay spread and strength in addition to selecting a Doppler Spectrum shape with the same choices as in **jtcchan**: classic, flat, or data input. The default scenarios listed are implemented by **mixedchan**. In addition to the default scenarios a set of 9 channels is given with parameters closely modeling those of 9 measured channels presented by Cox and Leck [10][11].

Referring to Fig.14.4, we see that the other major subdirectory, /LandMobile /VHFUHF/ contains the program **vhfuhfmixedchan**. This program differs from **mixedchan** in having the velocities of both terminals specified and allowing the specification of an additional Doppler Power Spectrum shape called Classic2 appropriate

to the case of two moving terminals (see Section 10). As is clear from Section 10, the scenarios selected for the /LandMobile/VHFUHF/ subdirectory are the same as for the /Land Mobile/cellular/mixedmod/ subdirectory with the exception of the use of the Classic2 spectrum and the selection of one of five values for the ratio of the minimum to maximum terminal velocities.

Fig.14.5 presents the /AirMobile/ subdirectory structure. Two subdirectories are shown /AirMobile/airtoair/ and /AirMobile/airtoground/ corresponding to channel models discussed in Sections 8 and 9, respectively. The program **airairchan** in the /airtoair/ subdirectory simulates the Air-Air VHF/UHF channel discussed in Section 8. To run this

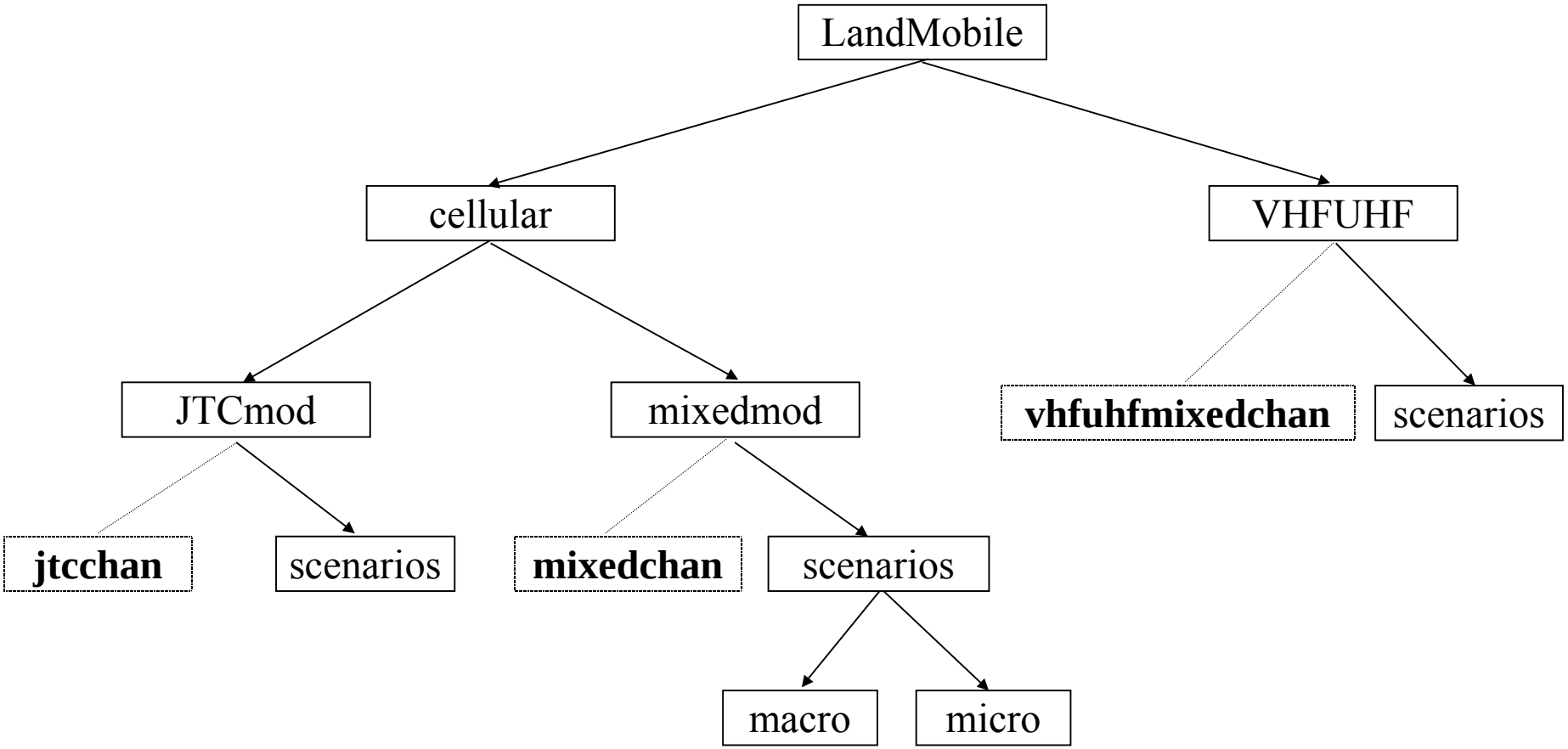

Fig. 14.4 MobileChan/PropChan/LandMobile: Subdirectories and Programs

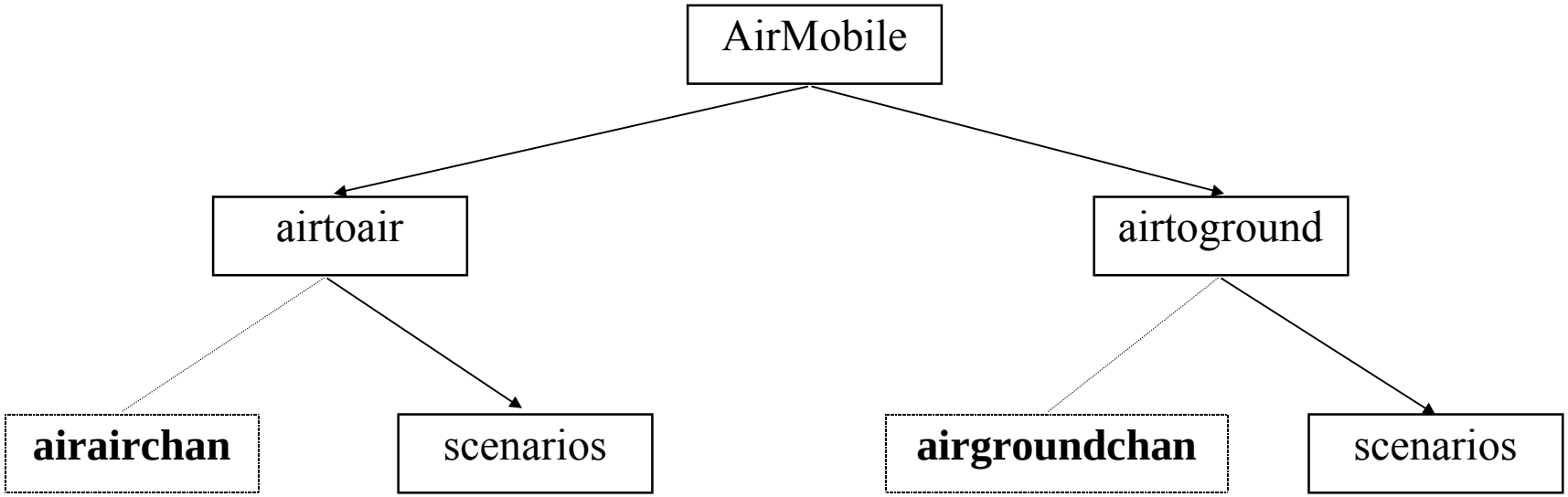

Fig. 14.5 MobileChan/PropChan/AirMobile: Subdirectories and Programs

program it is necessary first to select sample rate, carrier frequency, velocity components of each aircraft (zero vertical velocity components assumed), the ground separation and heights of the aircraft, and the rms surface slope. A choice is then made as to whether the user wants to specify the strengths of the specular and scatter path components relative to

the direct path or to use the theoretical channel model developed in Section 8. If the latter choice is made, it is then necessary to specify the rms surface height, transmit-receive antenna gain product in the specular direction relative to the LOS direction, conductivity and dielectric constant of surface, and polarization of transmitted signal. The default scenarios given in Section 8 are implemented with **airairchan.**

The program **airgroundchan** in the /airtoground/ subdirectory simulates the Air-Ground VHF/UHF channel discussed in Section 9. Since the air-ground channel is a special case of the air-air channel one would expect the parameter inputs for **airgroundchan** to simply be a special case of those of the **airairchan**. In large part this is true. However an additional option has been added based upon observed measurements, namely the case of multiple specular components as discussed in Section 9. Thus after the selection of sample rate, carrier frequency, velocity components, aircraft ground separation and altitude, and rms surface slope, there are three choices: 1) for the single specular component case enter the strengths of the specular and scatter components relative to the direct path components directly, or 2) use the parameters for the theoretical model as discussed in the previous paragraph, or 3) select the multi-specular case and choose the strengths and elevation angles of the specular components. The default scenarios are implemented with **airgroundchan**.

There are two more subdirectories under /MobileChan/PropChan/ in Fig.14.3 dealing with programs and scenarios under development at the time this report was being generated./MobileChan/PropChan/SatMobile will contain programs and default scenarios for Land Mobile Satellite channels as presented in Section 12. These programs would be used in simulating PCS communication links implemented by the several proposed land

mobile satellite systems. /MobileChan/PropChan /IndMobile will contain programs and default scenarios for Indoor and Indoor-to-Outdoor channels as detailed in Section 13. These programs would be used in simulating the links of wireless local area networks.

15 REFERENCES

[1] P. A.Bello, "Characterization of Randomly Time-Variant Linear Channels", *IEEE Trans. on Comm.*, Vol. CS-11, December 1963, pp. 360-393.

[2] P.A.Bello, C.A.Nissen, andJ.J. Blanchard, Generic Channel Simulator, Draft Final Report on Project 8632L,Mitre Corp., September 30, 1994

[3] William C. Jakes, Ed., Microwave Mobile Communications, John Wiley, 1974

[4] R. H. Clarke, "A Statistical Theory of Mobile Radio Reception", *BSTJ*, Vol. 47, 1968, pp. 957-1000.

[5] Jeffrey A. Wepman, J. Randy Hoffman, and Lynette H. Loew, "Impulse Response Measurements in the 1850-1990 MHz Bands in Large Outdoor Cells", U. S. Department of Commerce, *NTIA Report 94-309*, June 1994.

[6] Jeffrey A. Wepman, J. Randy Hoffman, Lynette H. Loew, and Vincent S. Lawrence, "Comparison of Wideband Propagation in the 902-938 and 1850-1990 MHz Bands in Various Macrocellular Environments", U. S. Department of Commerce, *NTIA Report 93-299*, September 1993.

[7] Scott Y. Seidel, Theodore S. Rappaport, Sanjiv Jain, Michael L. Lord, and Rajendra Singh, "Path Loss, Scattering, and Multipath Delay Statistics in Four European Cities for Digital Cellular and Microcellular Radiotelephone", *IEEE `Transactions on Vehicular Technology*, Vol. 40, No. 4, November 1991.

[8] Theodore S. Rappaport, Scott Y. Seidel, and Rajendra Singh, "900-MHz Multipath Propagation Measurements for U. S. Digital Cellular Radiotelephone", *IEEE Transactions on Vehicular Technology*, Vol. 39, No. 2, May 1990.

[9] Robert J. C. Bultitude, "Measurement, Characterization, and Modeling of 800/900 MHz Mobile Radio Channels for Digital Communications", Ph.D dissertation, Carleton University, Ottawa, Ontario, Canada, copyright February 1987.

[10] Donald C. Cox and Robert P. Leck, "Distributions of Multipath Delay Spread and Average Excess Delay for 910-MHz Urban Mobile Radio Channels", *IEEE Transactions on Communications,* Vol. COM-23, No. 11, November 1975.

[11] Donald C. Cox and Robert P. Leck, "Correlation Bandwidth and Delay Spread Multipath Propagation Statistics for 910-MHz Urban Mobile Radio Channels", *IEEE Transactions on Communications,* Vol. AP-23, No. 2, March 1975.

[12] Donald L. Nielson, "Microwave Propagation Measurements for Mobile Digital Radio Application", *IEEE Transactions on Vehicular Technology*, Vol. VT-27, No. 3, August 1978.

[13] Jan Van Rees, "Measurements of the Wide-Band Radio Channel Characteristics for Rural, Residential, and Suburban Areas", *IEEE Transactions on Vehicular Technology*, Vol. VT-36, No. 1, February 1987.

[14] J. P. de Weck, P. Merki, and R. Lorenz, "Power Delay Profile Measured in Mountainous Terrain", 38th IEEE Vehicular Technology Conference, Philadelphia, Pennsylvania, June 15, 1988.

[15] Andreas Zogg, "Multipath Delay Spread in a Hilly Region at 210 MHz", *IEEE Transactions on Vehicular Technology*, Vol. VT-36, No. 4, November 1987.

[16] G. L. Turin, F. D. Clapp, T. L. Johnston, S. B. Fine, and D. Larry, "A Statistical Model of Urban Multipath Propagation", *IEEE Transactions on Vehicular Technology*, Vol. VT-21, pages 1-9, February 1972.

[17] W. R. Young, Jr., and L. Y. Lacy, "Echoes in Transmission at 450 Megacycles from Land-to-Car Radio Units", *Proceedings of the IRE*, Vol. 38, pages 255-258, 1950.

[18] Robert J. C. Bultitude and G. Keith Bedal, "Propagation Characteristics on Microcellular Urban Mobile Radio Channels at 910 MHz", *IEEE Journal on Selected Areas in Communications*, Vol. 7, No. 1, January 1989.

[19] Phillip A. Bello, "Aeronautical Channel Characterization", *IEEE Transactions on Communications*, Vol. COM-21, No. 4, May 1973, pp. 548-563.

[20] A.J. Mallinckrodt, "Ground multipath in satellite-aircraft propagation," presented at the Symp. Application of Atmospheric Studies to Satellite Transmissions, Boston, Mass., Sept. 1969.

[21]S. H. Durrani and H. Staras, "Multipath problems in communication between low altitude spacecraft and stationary satellites," RCA Rev., pp. 77-105, Mar. 1968

[22] P. Beckmann and A. Spizzichino, *The Scattering of Electromagnetic Waves From Rough Surfaces*. New York: Pergamon, 1963.

[23] Wind Waves at Sea, Breakers and Surf U.S. Hydrographic Office Publication, H.O.602, 1947

[24] M. J. Feuerstein, K. L. Blackard, T. S. Rappaport, S. Y. Seidel, and H. H. Xia, "Path Loss, Delay Spread and Outage Models as Functions of Antenna Height for Microcellular System Design", *IEEE Transactions on Vehicular Technology*, Vol. 43, No. 3, pages 487-498, August 1994

[25] H. H. Xia, H. L. Bertoni, L. R. Maciel, A. Lindsey-Stewart, and Robert Rowe, "Microcellular Propagation Characteristics for Personal Communications in Urban Suburban Environments" , *IEEE Transactions on Vehicular Technology*,Vol. 43 No. 3, pages 743-752, August 1994.

[26] Phillip A. Bello, "Dielectric Building Channel Model for Lineal Microcells," MITRE
Technical Report *MTR 94B0000084*, September 1994.

[27] Robert J. C. Bultitude and G. Keith Bedal, "Propagation Characteristics on Microcellular Urban Mobile Radio Channels at 910 MHz", *IEEE Journal on Selected Areas in Communications*, Vol. 7, No. 1, January 1989

[28] J.-P. Rossi and A. J. Levy, "A ray model for decimetric radiowave propagation in an urban area", *Radio Science*, Volume 27, No. 6, Pages 971-979, November-December 1992.

[29] Robert J. C. Bultitude and G. Keith Bedal, "Propagation Characteristics on Microcellular Urban Mobile Radio Channels at 910 MHz", *IEEE Journal on Selected Areas in Communications*, Vol. 7, No. 1

[30] A.R.Paradis, L-Band Air -Air Multipath Measurements, Lincoln Laboratory Report ATC-77, September 6, 1977.

[31] C.Cox and W. Munk,"Statistics of the Sea Surface Derived from Sun Glitter", Journal
of Marine Research, Vol. 13, No.2, pp195-227,1954.

[32] J.Austin, "Low-Grazing Angle Propagation Measurements for the MK-XV Q/A IFF System", MIT Lincoln Laboratory Report IFF-18,16 November 1983.

[33] D.F. Sun, "Experimental Measurements of Low-Angle Ground-Reflection Characteristics at L- and C-Bands for Irregular Terrain", MIT Lincoln Laboratory Report ATC-107, 1November 1982.

[34] A.S.Akki and F.Haber, "A Statistical Model of Mobile -Mobile Land Communication

Channel", IEEE Trans. on Veh. Tech., Vol. VT - 35, No. 1 February 1986,pp 2-7.

[35] I.S.Gradshteyn and I.M. Ryzhik, Tables of Integrals,Series, and Products, Academic Press, 1980

[36] A. D. Spaulding, "Man-Made Noise: the Problem and Recommended Steps toward Solution," Office of Telecommunications Report 76-85, April 1976.

[37] J. Liu, et al., "Survey of Multipath and Noise Measurements in Cities," ICC'71 Conference Record, June 14 -161 1971.

[38] P. Bello and C. Boardman," Software VHF/UHF Radio Channel Simulator", Final Report by CNR Inc on Contract No. MFA904-80-C-0443, November 1981.

[39] W. Johnson, "Technique for Correlating Radiated Noise with Individual Spark Events in an Automotive Ignition System," IEEE Trans. on Vehicular Technology, Vol. VT-27, No.3, August 1978.

[40] R. A. Shepherd and J. C. Gaddie, "Ignition Noise of Foreign and Domestic Vehicles in Use in the United States," IEEE 29th Vehicular Technology Conf., Chicago, IL, March 1979.

[41] R. A. Shepherd, Private Communication, circa 1981.

[42] G. L. Maxam, et al., "Radiated Ignition Noise due to the Individual Cylinders of an Automobile Engine," IEEE Trans. on Vehicular Technology, Vol. VT-25, No. 2, May 1976.

[43] W. Weibull, "A Statistical Distribution Function of Wide Applicability," J. Mech., Vol. 18, No. 1, September 1951, pp. 293 -297.

[44] A.D. Spaulding and J.S. Washburn, "Atmospheric Radio Noise: Worldwide Levels and Other Characteristics, NTIA Report 85-173, U.S. Dept. of Commerce, April 1985.

[45] P.A. Bello, "Wideband HF Propagation, Narrowband Interference, and Atmospheric Noise Models for Link Perfomance Evaluation", MITRE Technical Report MT 93B0000086, July 1993.

[46] R. B. Schulz, et al., "Amplitude Probability Distribution Measurements of V-8 Ignition Emanations," ICC'74 Conference Record, June 17 -19, 1974.

[47] D. L. Nielson "Microwave Propagation and Noise Measurements for Mobile Digital

Radio Application,," SRI Packet Radio Note, January 1975.

[48] A. D. Spaulding, et al., "Urban Residential Man-Made Radio Analysis and Predictions," U.S. Dept. of Commerce Telecommunications Research and Engineering Report 14, June 1971.

[49] R. A. Southwick, et al., "A Method to Evaluate the Degradation Effects of Impulsive Interference," ICC'74 Conference Record, June 17 -19, 1974.

[50] C.R. Freeman, " Trends in Urban Noise in the 200 to 950 Mhz Band over the Past 40 Years," Proceedings of the COMMSPHERE "01" Symposium, Herzliya, Israel, pp 6.3.1-6.3.6, Dec 16-18,1992

[51] A.D.Spaulding, "The Natural and Man-Made Noise Environment in Personal Communication Services Bands," unpublished NTIA report received by publication office November 1994. Also, " The Roadway Natural and Man-Made Noise Environment", generated in the same time frame. The latter document contains more material than the former.

[52] G. Anzac, " Radiofrequency Noise Measjrements in Urban Areas at 480 and 950 MegaHertz," NASA Technical Memorandum X-1972, March 1970.

[53] A.D. Spaulding and R.J.Disney ,"Man-made Radio Noise, Part 1: Estimates for Business, Residential,, and Rural Areas," Office of Telecommunications Report OT 74-38, June 1974.

[54] E.N. Skomal, " Man-made Radio Noise", Van Nostrand Rheinhold Company, New York, 1978

[55] E.N. Skomal, " A Long-term Trend in Urban Zone Man-made Radio Noise and the UHF automotive ignition resonance," Symposium Record, IEEE 1985 International Symposium on EMC, August 20-22, Boston, MA, 1985.

[56] R. Rusch, "The Market and Proposed Systems for Satellite Communications," Applied Microwave and Wireless, PP 10-34, Fall 1995.

[57] G.M. Comparetto, N.D.Hulkower, "Global Mobile Satellite Communications: A Review of Three Contenders, " American Institute of Aeronautics and Astronautics, pp 1-11, 1994.

[58] E. Lutz et al," The Land Mobile Satellite Communication Channel - Recording,

Statistics, and Channel Model", IEEE Trans. on Vehic. Tech., Vol. 40, No. 2, May 1991, pp 375 -386.

[59] W. Vogel and J.Goldhirsh," Extended Empirical Roadside Shadowing Model from ACTS Mobile Measurements", Proceeings of the NASA Propagation Experiments Meeting and ACTS Propagation Studies Workshop, Colorado State University, Fort Collins, Colorado, June 14 - 16, 1995.

[60] C.Loo, "A Statistical Model for a Land Mobile Satellite Link" , IEEE Trans. on Vehic.
Technology, Vol. VT-34, No.3, August 1985.

[61] S.O.Rice, "Mathematical Analysis of Random Noise", Bell Syst. Tech. J., vol23, pp 282-332, July 1944 and vol. 24, pp 46-156, Jan. 1945.

[62] H.Bischl, Markus Werner, and Erich Lutz, "Elevaton-dependent Channel Model and Satellite Diversity for NGSO S-PCNs" Proceedings of the Vehicular Technology Conference, Atlanta GA, April, 1996 pp 1038 - 1042.

[63] W.Smith and W.Stutzman, " Statistical Modeling for Land Mobile Satellite Communications," Virginia TechReport EE Satcom 86-3, Aug. 1986.

[64] W. J. Vogel and U.S.Hong, " Measurements and Modeling of Land Mobile Satellite Communications at UHF and L-Band," IEEE Trans. AP Vol 36, pp 707-719,May 1988.

[65] W.J.Vogel and J.Goldhirsh, " Fade Measurements at L-Band and UHF in Mountainous Terrain for Land MobileSatellite Systems, " IEEE Trans. AP Vol 36 pp 104-113, May 1988.

[66] H.Bischl, Markus Werner, Erich Lutz, "Elevation-dependent Channel Model and Satellite Diversity for NGSO S-PCNs," IEEE VTC Conference Record, Atlanta GA, April, 1996, pp 1038-1042.

[67] H. Lin, R. Akturan, W. Vogel, "Photogrammetric Satellite PCS Channel Modeling using Markov Chain Approach," preprint of paper to be given at the 1996 International Communication Conference.

[68] B.Vuketic and J.Du, "Channel Modeling and Simulation in Satellite Mobil Communication Systems", Journal on Selected Areas on Communication Systems," Vol. 10, No.8,October 1992, pp 1209-1218.

[69] H.Kobayashi, Modeling and Analysis: An Introduction to System Performance Evaluation Methodology, Addison-Wesley, 1978.

[70] J.Goldhirsh and W. Vogel, Propagation Effects for Land Mobile Satellite Systems: Overview of Experimental and Modeling Results, NASA Reference Publication 1274, February, 1992.

[71] A.Jahn and E. Lutz, "Wideband Channel Characterization for LMS Systems: Experimental Results and Modeling", Proceedings of the Interrnational Communication Satellite Systems Conference, pp 313-321, 1995.

[72] L.Dossi, G.Tartara, and F. Tallone, "Statistical Analysis of Measured Impulse Response Functions of 2.0 Ghz Indoor Radio Channels", IEEE Journal on Selected Areas in Communcations, V.14, No.3, April 1996, pp 405-410.

[73] H.Hashemi," Impulse Response Modeling of Indoor Radio Propagation Channels", IEEE Journal on Selected Areas on Communications, Vol. 11, No. 7, September 1993, pp 967-978.

[74] T.S. Rappaport, "Characterization of UHF Multipath Radio Channels in Factory Buildings", IEEE Transactions on Antennas and Propagation, Vol.37, No.8, August 1989, pp. 1058-1069.

[75] T.S.Rappaport, S.Y.Seidel, and K.Takamizawa. "Statisical Channel Impulse Response Models for Factory and Open Plan Building Communication System Design", IEEE Trans. on Communications, Vol. 39, No.5, May 1991, pp 794-807.

[76] A.Saleh and R.A. Valenzuela, "A Statistical Model of Indoor Multipath Propagation", IEEE Journal on Selected Areas in Communications, Vol., SAC-5, No.2, Feb. 1987, pp 128-137.

[77] P.Papazian et.al., "Wideband Propagation Mesurements for Wireless Indoor Communication", NTIA Report No.93-292, January 1993.

[78] R.J.C.Bultitude, S.A. Mahmoud, W.A. Sullivan," A Comparison of Indoor Radio Propagation Characteristics at 910 MHz and 1.75 GHz", IEEE Journal on Sel.Areas on Comm., Vol. 7, No.1, January 1989, pp 20 - 30.

[79] D.M.J. Devasirvatham, "A Comparison of Time Delay Spread and Signal Level Measurements within two Dissimilar Office Buildings" IEEE Trans. on Antennas and Propagation, AP-35, March 1987, pp 319 - 324.

[80] D.M.J. Devasirvatham, " Time Delay Spread Measurements of Wideband Radio Signals within a Building", Electronic Letters, Nov. 8, 1984, Vol.20, No.23, pp 950-

951.

[81] P.A. Bello,"Some Techniques for the Instantaneous Real-Time Measurement of Multipath and Doppler Spread", IEEE Trans. on Comm. Tech., Vol.13,No.3 ,Sept. 1965, pp 285 -292.

[82] C.L. Holloway, "A Simplified Model for Calculating the Delay Spread of the Impulse Response for Indoor Wireless Communications", Proceedings of the National Radio Science Meeting, Jan. 9-13, 1996, Boulder, Colorado p. 167.

[83] D.M.J. Devasirvatham, " Time Delay Spread and Signal Level Measurements of 850 MHz Radio Waves in Building Environments", IEEE Trans. on Antennas and Prop., Vol.AP-34, No.11, November 1986, pp 1300-1305.

[84] P.A. Bello, "Wideband HF Propagation, Narrowband Interference, and Atmospheric Noise Models for Link Perfomance Evaluation", MITRE Technical Report M93B0000086, July 1993.

[85] R.A. Dean, "Wideband HF Channels: a Strategy for Channel Simulation", IEEE MILCOM Conference Record, Boston MA, October 1993.

[86] R. Coutts, "Software Wideband HF Channel Simulation", *MITRE Report MTR93B0000122*, The MITRE Corporation, Bedford, Massachusetts, October 1993.

[87] G.A.Hufford, A.G.Longley, and W.A.Kissick, *A Guide to the Use of the ITS Irregular Terrain Model in the Area Prediction Mode*, Institute for Telecommunications Sciences (ITS), NTIA Report 82-100, April 1982

[88] M. Hata, "Empirical formula for propagation loss in land mobile radio services", *IEEE Trans. on Vehicular Technology*, VT-34, No. 4, pp. 149-153 (1985).

[89] Euro-Cost 231, "Urban transmission loss models for mobile radio in the 900- and 1800-MHz bands", (revision 2), European Cooperation in the Field of Scientific and Technical Research (EURO-COST), Working Group 2, "UHF Propagation", COST 231 TD(91)73, The Hague, September 1991.

[90] *Draft Technical Report on RF Channel Characterization and Deployment Modeling,* Joint Technical Committee (Air Interface Standards), JTC(AIR)/94.08.01-065R4, August 1994.

[91] M. A. Weissberger, “An Initial Critical Summary of Models for Predicting the Attenuation of Radio Waves by Trees”, *ESD-TR-81-101*, DOD Electromagnetic Compatibility Analysis Center, Annapolis, MD, July 1982.

APPENDIX. WIDEBAND HF DEFAULT SCENARIOS

The Wideband HF Channel simulation uses three sets of parameters: *propagation* channel parameters, *atmospheric noise* parameters, and *narrowband interference* parameters. We consider these sets of parameters in order, following a brief review of the HF channel characteristics. Numerical values for Default Scenarios are taken from [84] and [85].

A.1 Propagation Scenarios

The HF propagation medium can be represented as a linear, randomly time-variant operation. From innumerable measurements and propagation analyses, it is known that the received HF signal can be expressed closely as the sum of contributions from one or more propagation modes. Single hop and multiple hop paths, high rays, low rays, and magneto-ionic components may each be regarded as separate propagation modes for modeling purposes. The received signal is then modeled as the sum of the outputs of all propagation modes of sufficient strength. Because of the frequency dependence of the refractive index, the relative importance of different propagation modes will vary with operating frequency. In fact, below some frequency (called the Lowest Usable Frequency (LUF)) absorption prevents any significant propagation, and above another frequency (called the Maximum Usable Frequency (MUF)) no reflection occurs and ground communication stops. Both the MUF and LUF depend on path length and ionospheric conditions.

Each propagation mode itself may be regarded as a time-variant linear operation. This linear operation will have different statistical structures depending upon the ionospheric conditions in the propagation path. Thus if the percentage change in electron density is small enough, the propagation is called quiet or normal, and a mode acts over a MHz bandwidth approximately like an all-pass filter with a somewhat nonlinear group

delay vs. frequency, a slowly-changing mean time delay, complex amplitude, and Doppler shift.

When the electron density fluctuations become sufficiently large, the mode acts like a scatter-type channel with an associated Doppler spread, Doppler shift, and a multipath spread caused by random fluctuations of received energy over a range of path delays. The mode may then be called disturbed, *or* scattered.

The propagation channel parameters consist of three groups: *quiet path* parameters, *disturbed path* parameters, and *slow fading* parameters. For the quiet ionospheric condition, it is necessary to select the *number* of quiet paths, the *amplitude* of each path in dB relative the largest path, the *Doppler shift* of each path in Hz, the *bulk delay* of each path in milliseconds, and the (linear group) *delay distortion* of each path in microsec/MHz. Table A.1 lists quiet path parameters.

Note that only single path and double path cases are shown. The single path case in turn is broken up into *short* paths and *long* paths. For both the short and long paths three values of Doppler shift are given in Hz.: *small* (.1), *medium* (.4), and *large* (2). For the short paths, three linear group delay distortion values are given in microseconds/MHz: small (50), medium (100), and large (300). For the long paths these numbers change to 10, 50, and 100 for the small, medium, and large values, respectively.

Three double-path cases are shown corresponding to the combination of a ground wave path with a near vertical incidence path (GW/NVI), reflections from a two-hop E layer and a single- hop F layer (2E/1F), and reflections from a two-hop F layer and a 3-hop E layer.

As pointed out above, a propagation path traversing the disturbed ionosphere may be modeled as a WSSUS channel. Theoretical Doppler and Delay Power Spectral shapes presented in [84] are used in the channel simulations. in Table A.2 presents single path

selections of the three disturbed path parameters *Doppler shift*, *rms Doppler Spread*, and *rms Delay Spread* needed by the GCS to completely specify the channel. For each case small, moderate, and large values of the parameters are given.

Table A.1 Scenario Parameters for Quiet Wideband HF Channels

Number of Paths	Path Length	Doppler Shift (Hz)	Group Delay Distortion (microsec/MHz)	Relative Delay (millisec)	Relative Amplitude (dB)
1	Short	.1, .4, 2.0	50, 100, 300	NA	NA
	Long	.1, .4, 2.0	10, 50, 100	NA	NA
2	GW/NVI	0	0	0	0
		.1	100	1.5	-6
	2E/1F	0	0	0	0
		.3	50	.03	0
	2F/3E	.2	40	0	-6
		.3	60	.25	0

The long term or slow fading can be modeled as a stochastic process by exponentiating a Gaussian process with an exponential autocorrelation function [84]. To completely specify this process requires only the rms value of the Gaussian process and the time constant of the exponential autocorrelation function. Table A.3 presents small, moderate, and large selections of each of these parameters.

Table A.2 Scenario Parameters for Disturbed Wideband HF Channels

Doppler Shift (Hz)	RMS Doppler Spread(Hz)	RMS Delay Spread(microsec)
.1, 2, 10	1, 4, 14	50, 200, 650

Table A.3 Scenario Parameters for Slow Fading

RMS Path Fluctuations (dB)	Time Constant (sec)
.5, 1, 3.25	2, 12, 64

A.2 Atmospheric Noise Scenarios

Atmospheric burst noise perceived at any point in space is due to the superposition of received signals from lightning flashes arriving from storms around the world. Most of the noise is received as over-the-horizon (OTH) flashes rather than line-of-sight (LOS) flashes. Flashes are arrive randomly in time and each flash is assumed to consist of a random number of strokes with random interarrival times based upon empirical distributions.

A necessary condition for choice of the statistics of the stroke strengths is that the resulting atmospheric noise process generated be consistent with the many years of measurements of the envelope statistics of atmospheric noise codified by a family of curves adopted by the CCIR. This family of curves is indexed on a single parameter V_d which is
the ratio of the rms value of the envelope to the mean value of the envelope, expressed in dB. The value of V_d varies with bandwidth occupied and operating frequency.

The analysis presented in [84] reduces the specification of the atmospheric noise model to only two free parameters λ_A, the rate of occurrence of lightning flashes worldwide in flashes/second and the CCIR parameter V_d. Values of λ_A range from 50 to 200 flashes/sec and values of V_d vary from 3 to 11. We arbitrarily select 50, 100, and 200 flashes/sec as *small, moderate*, and *large* flash rates, respectively, for the default scenarios. Table A.4 (from Table 3.3 of [84]) presents estimated values of V_d as a function of operating frequency for a 1 MHz bandwidth. Since the default scenarios are presented only for a 1 MHz bandwidth, *operating frequency*, rather than V_d is specified in the default scenario.

Table A.4 Estimates of V_d vs. Operating Frequency for a 1 MHz Bandwidth

Operating Frequency (MHz)	V_d
5	**10.7**
10	**9.5**
20	**7.0**
30	**3.5**

A.3 Interference Scenarios

Any attempt to process received signals with wide bandwidths, e.g., 1 MHz, at HF frequencies, must confront the large number of strong narrowband interferers present. Strictly speaking, the information that is needed to model narrowband interference is:

1) distribution function for strength of interferers

2) arrival time statistics for interferers

3) statistics for frequency location of interferers

4) statistics for interferers as stochastic processes including statistics for bandwidths of transmitted interferers

5) fading statistics for interferers

Unfortunately the measurements actually taken provide information far short of this ambitious list. Nonetheless, it is necessary to model items l)-5). This has been done in [84] by using available measurements, heuristic reasoning, and sometimes arbitrary assumptions.

We next summarize the various parameters used to specify the interference model and provide default scenarios To keep the number of simulations reasonable, it is necessary to minimize the number of combinations of parameter values listed. Table A.5 lists selections of parameter values for the interference which are applicable to either the random interferer arrival case, or the persistent interferer case. Table A.6 presents arrival parameters dealing specifically with persistent or random-arrival interference.

The top entry in Table A.5 is needed to set the interference power relative to the ambient noise power. We give *large* and *moderate* estimates, respectively, for Europe (70, 50 dB) and North America (30, 10 dB).

Table A.5 Parameters for Interference Scenarios

Parameter	Category	Numerical Values
Ratio of Interference Pwr. to Noise Power in 1 MHz Band	Europe	70, 50
	CONUS	30,10
Maximum RMS Doppler Spread Superimposed on Interferer by Channel (Hz)	Non-Fading	0
	Quiet Channel	.1,2
	Disturbed	20
Maximum Interference Bandwidth (Hz)	Non-Fading	0
	Low	200
	SSB Voice	3,000
	High	10,000
Truncated Pareto Distribution Parameters D(dB), α	Dynamic Range D	30, 60, 90
	Slope Parameter α	.3, .45, .6

The second entry suggests values to be assigned to the maximum Doppler spread inserted on the received interference by the propagation media. Since LOS transmission with minimal sky wave transmission is possible, the first entry is the non-fading case. The next entry is for the quiet or normal WBHF channel. In this case, the *large* Doppler spread listed, 2 Hz, corresponds to the maximum Doppler shift difference between multiple propagation modes, while the *low* value listed, 0.1 Hz, corresponds to the case of a single propagation mode. When the interferer radio waves propagate through auroral or equatorial disturbances, much larger Doppler spreads exist and 20 Hz has been selected.

Although possible interferers can have a large range of bandwidths, measurements seem to indicate that the largest interferers are unmodulated carriers. This corresponds to the first entry in the maximum interferer rms bandwidth category. We have arbitrarily selected three other bandwidths to cover the range of possibilities (200 Hz, 3 kHz, 10 kHz).

The last category is parameters for the truncated Pareto distribution used to model average strengths of received interferers. *Small*, *medium*, and *large* values are given. Two parameters are needed here, D, which specifies the ratio of the largest to the smallest interferer (30, 60, 90 dB) and *a* which specifies the slope of the (untruncated) Pareto distribution. Specific values have been selected based upon available data (0.3, 0.45, 0.6).

Table A.6 presents arrival parameters for the interference. The first category is for an assumed random arrival of interferers in time and frequency. Here the average number of coexisting interferers is assumed to be one of three values (30, 200, 1000) and the average duration of an interferer is assumed to be one of three values (1, 10, 100 seconds), which correspond to *small, moderate*, and *large* values of the parameters, respectively . The next two categories are for persistent interferers. These have been included to handle cases where the duration of the interferers are much larger than the simulation time. Two cases are considered: random assignment of frequencies for interferers, and periodic

assignment. For the random frequency assignment case, the number of interferers selected are 30, 200 and 1000, corresponding to *small, moderate*, and *large* values, respectively. We consider the case of uniform or periodic spacing of interferers in the frequency band due to the existence of frequency allocations. For the periodic assignment, it is necessary to specify the spacing between interferers and the total bandwidth occupied by the interferers. In Europe the spacing between carriers was observed to be 5 kHz, but other spacings should be considered corresponding to any government regulations. The percentage of the band occupied by the uniformly spaced interferers is assumed to be 20% , 50%, or 100%, corresponding to *small, medium*, or *large* values, respectively.

Table A.6 Arrival Parameters for Interference Scenarios

Parameter	Category	Numerical Values
Average Number of Coexisting Interferers - N_I	Random Arrival and Random Frequency Assignment	30,200,1000
Average Lifetime of Interferer - T_I		1, 10, 100
Average Number of Interferers - N_I	Persistent Interferers, Random Frequency Assignment	30,200, 1000
Spacing of Interferers in Frequency - (kHz)	Persistent Interferers, Periodic Frequency Assignment	5
% of Band		20, 45, 100